THE APPLICATION OF OPTICAL FIBRE TECHNOLOGY TO THE RAMAN SPECTROSCOPY OF POLYMERS

A Thesis submitted to the
UNIVERSITY OF SOUTHAMPTON
in support of candidature for the
degree of
Master of Philosophy

by

Gary Ellis, B.Sc., P.G.C.E.

"Saber es saber a qué atenerse"

Ortega y Gasset (1933)

Dedicated to my parents, Jean and Eric.

ACKNOWLEDGMENTS

I wish to express my gratitude to the following people, without whom this thesis would not have been possible ...

Dr. P.J. Hendra, for his supervision, support, and constant encouragement,

Dr. D.J. Cutler, Dr. H.A. Willis and Prof. M. Fleischmann for fruitful discussions and helpful advice,

the technical staff in the department,

my colleagues, past and present, for their support, friendship and above all their sense of humour,

Lynn Jones, for her valuable time, and her care in the preparation of the typescript,

and my parents, for their love.

Financial assistance for this work was provided by the Royal Institution, through Applied Photophysics Limited.

CONTENTS PAGE

Dedication ii
Acknowledgments iii
Contents iv
Abstract vii

Chapter 1 : INTRODUCTION 1

1.1 Introduction 2
1.2 Vibrational Spectroscopy 2
1.2.1 Molecular Vibrations 3
1.2.2 Raman Spectroscopy 7
1.3 The Development of Raman Spectroscopy 9
1.3.1 Detectors 12
1.3.2 The Laser Raman Concept 16
1.3.3 Stray Light and the Multiple Monochromator 18
1.4 Rapid Scanning and the Multiplex Advantage 21
1.5 Practical Raman Spectroscopy 26
1.5.1 Sampling Systems 26
1.5.2 Residual Problems 26
1.6 Fibre-Optics 29
1.6.1 Fibre-Optics Theory 30
1.6.2 Waveguide Properties of Fibres 36
1.6.3 Optical Properties 36
1.6.4 Manufacture of Optical Fibres 38
1.7 Aim 44

Chapter 2 : INSTRUMENTATION AND EXPERIMENTAL TECHNIQUES 49

2.1 Raman 50
2.1.1 Raman Instrumentation 50
2.1.2 Experimental Technique 52
2.2 Fibre-Optic System Design for Raman Spectrophotometry 54
2.2.1 Preparation of the Fibre 57
2.2.2 Illumination of the Fibre 61
2.2.3 Throughput 63
2.2.4 Collection 63
2.2.5 Refractive Index of Liquids 67
2.2.6 Solids 67
2.2.7 Probe Design 77

PAGE

Chapter 3 : RAMAN SPECTROSCOPY OF FLOWING MOLTEN POLYETHYLENE 79

3.1 Introduction 80
3.2 Extrusion and Polymer Flow 81
3.3 Experimental 84
3.3.1 The Extruder 84
3.3.2 System Design 85
3.3.3 The Die 85
3.3.4 The Fibres 89
3.4 Method 90
3.4.1 System Testing 90
3.4.2 Recording Raman Spectra 92
3.5 Results 92
3.5.1 Die Swell 94
3.5.2 Raman 94
3.6 Discussion of Results 103
3.7 Conclusions 106

Chapter 4 : EFFECTS OF A SWELLING AGENT ON THE LOW FREQUENCY RAMAN SPECTRUM OF POLYETHYLENE 108

4.1 Introduction 109
4.1.1 Lamellar Structure 109
4.1.2 The Longitudinal Acoustic Mode (LAM) 110
4.1.3 Swelling of Polymers 113
4.2 Experimental 114
4.2.1 Sample Preparation 114
4.2.2 Raman Spectroscopy 115
4.2.3 Differential Scanning Calorimetry (DSC) 115
4.2.4 Density Column Measurements 118
4.2.5 Swelling 118
4.3 Results 119
4.3.1 Raman Method 119
4.3.2 Longitudinal Acoustic Modes: Effects of Swelling 119
4.3.3 Raman Internal Modes 122
4.3.4 DSC/Density Crystallinity 122
4.4 Discussion 123
4.5 Conclusions 125

PAGE

Chapter 5 : CONCLUSION 129

Appendix 136

UNIVERSITY OF SOUTHAMPTON

ABSTRACT

FACULTY OF SCIENCE

CHEMISTRY

Master of Philosophy

THE APPLICATION OF OPTICAL FIBRE TECHNOLOGY TO THE RAMAN SPECTROSCOPY OF POLYMERS.

by Gary Ellis

The laser was successfully developed as a light source for Raman spectroscopy in the early 1960's. At that time it seemed likely that Raman spectroscopy would compete favourably with its vibrational counterpart - infrared spectroscopy. However, it is now clear that, in its applications, Raman is far behind its competitor. It is accepted that fluorescence is a major drawback, but another serious discouragement to potential users exists, vis. sample alignment. The use of fibre-optics as a solution to this problem is investigated.

The experimental section describes the design and construction of a fibre-optic sampling system compatible with existing Raman technology. It considers some practical aspects of the use of optical fibres, and compares the performance of a simple fibre-optic probe system, in a variety of samples, with conventional excitation techniques. The positioning of the optical fibres at the sample is also investigated, with a view to the development of a versatile and efficient probe.

Two aspects of the morphology of polyethylene were studied, to demonstrate the value of fibre-optics.

1. Observation of flowing molten polyethylene: A fibre-optic probe was placed in an extruder system at the tapered entrance of a capillary die. At high pressure and temperature the polymer was forced through the die and the Raman spectra recorded. Over a range of temperature and shear rates it was observed that the Raman spectra remained invariant.

2. Swelling effects in solid linear polyethylene: The polymer was exposed to the effects of a non-solvating agent (xylene). The low-frequency Raman active longitudinal acoustic mode (LAM) was monitored using a fibre-optic probe embedded in the polymer sample. It was clearly shown that the LAM moved to lower frequency and broadened on the addition of xylene, and that this effect was reversible.

CHAPTER I

INTRODUCTION

1.1 Introduction

A molecular system can execute a number of energetic transitions, through translational, rotational, vibrational and electronic processes. The nature of such processes have become well understood, and consequently when attempting to determine molecular structure a large number of experimental techniques are available.

Research in the Chemistry Department at Southampton University has long been involved in the elucidation of molecular structure. In particular, Raman spectroscopy (which investigates the vibrational characteristics of molecular systems) has been enthusiastically developed. The research group has considered many chemical systems including deeply coloured inorganic molecules and complexes, gases/vapours adsorbed to catalysts, and polymers (1), and a particular interest in improving spectroscopic technique has always been maintained. Much specialised apparatus has been developed and applied in the study of adsorbed species (2, 3), electrochemical processes (4, 5), the concentration of molecular species in flames (6), samples under conditions of high and low temperature and high pressure, and more recently the Raman spectra of flowing polymers (7, 8). The continuing improvement of experimental technique and efficiency regarding the design and construction of specialised sampling apparatus is very much an ongoing concern within the group.

1.2 Vibrational Spectroscopy

Spectroscopy is frequently, but not exclusively, defined as the study of the interaction of electromagnetic radiation with matter.

Electromagnetic radiation can be considered as a wave-train, propagated in a straight line from a source, such that

$$y = A \sin \frac{2\pi x}{\lambda} \qquad \text{e.q. 1.0}$$

where y = the displacement of the light reactor with a maximum value A, x is the distance travelled and λ is the wavelength, given by $\nu = c/\lambda$ where ν = the frequency and c = the velocity of the light (see figure 1.1).

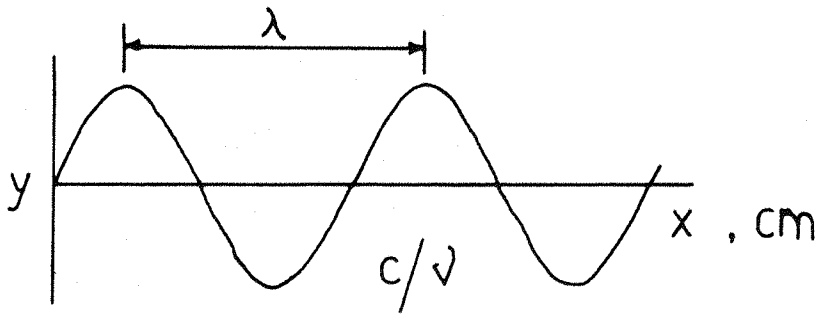

Figure I.I

Representation of a travelling wave.

The energy of a molecular oscillator is non-continuous, and any energy change occurs as a distinct jump between one energy level and another, i.e. the energy is quantised. Transitions may take place between the two vibrational energy levels provided that the appropriate amount of energy, ΔE, separating the levels can be either absorbed or emitted. This energy can take the form of electromagnetic radiation of a particular frequency, where

$$\nu = \frac{\Delta E}{h} \qquad \text{e.q. I.I}$$

where h = Planck's constant.

The spectroscopist considers the frequency, wavelength and wavenumber notionally, as if they were units of energy, and relates this to the vibrational structure of the molecular system under consideration.

I.2.I Molecular Vibrations

For a molecular system of 'N' atoms, there are 3N independant degrees of freedom corresponding to 3 translations, 3 rotations (2 in linear molecules), and the balance of 3N-6 (3N-5 for linear molecules) give rise to vibrations. These vibrations are referred to as "normal modes" of vibration and may be defined precisely for each individual

molecule. For carbon dioxide, CO_2, there are 3x3-5 = 4 normal modes of vibration and these are illustrated as Noctor diagrams in figure I.2.

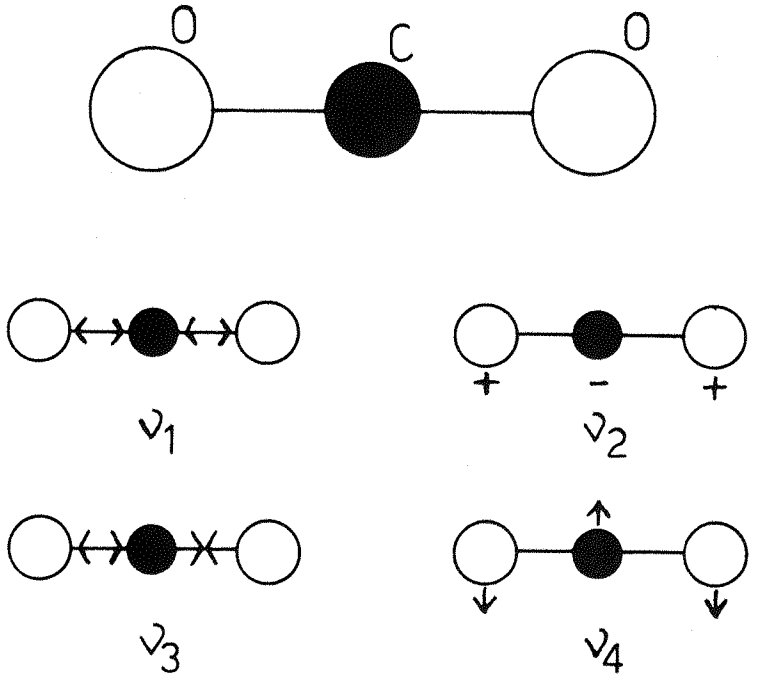

Figure I.2

Normal modes of vibration for a molecule of carbon dioxide.

In a polymer containing 20,000 atoms we would expect to find 59,994 normal modes. If they were all to occur, the resulting spectrum would be an unintelligible jumble. However, if we were to consider polyethylene, for example, it is apparent that whole classes of vibrations have almost identical frequencies. In the symmetric CH-stretch a vast number of vibrations can occur along the length of the chain. The totally in-phase and a slightly out-of-phase variation are illustrated in figure I.3. If the frequency of vibration is plotted against the phase shift, δ , between each CH_2 unit for any mode, a 'dispersion curve' is obtained (figure I.4). The number of values is dependent on molecular weight, and for an infinite chain only the values where $\delta = 0, \pi$ are spectroscopically active.

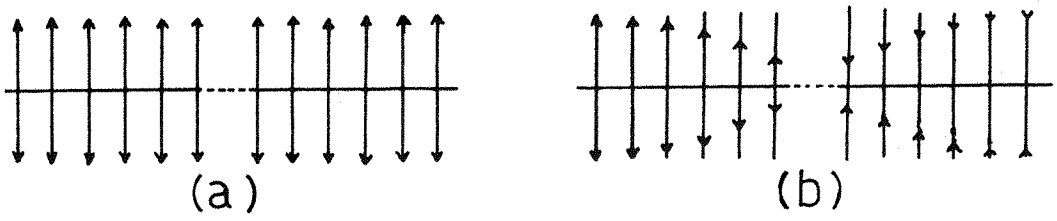

Figure 1.3

Phase relationships along a polyethylene chain for the $-CH_2$ symmetric stretch; (a) totally in phase, (b) slightly out of phase.

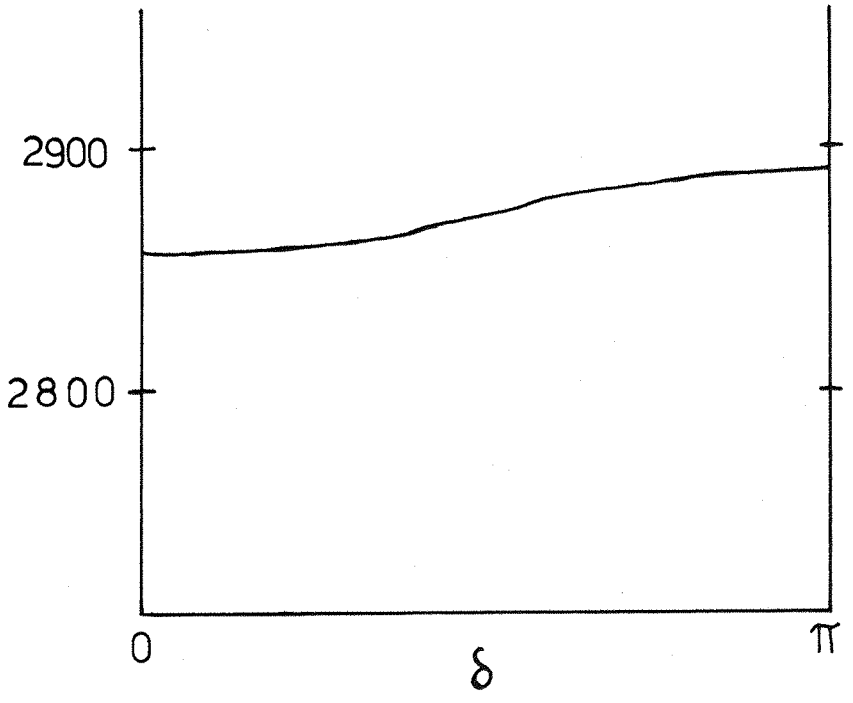

Figure 1.4

Dispersion curve for the $-CH_2$ symmetric stretch

A classification of the normal modes of vibration for polyethylene was prepared by Krimm in 1956 (9) using symmetry analysis. (See figure 1.5).

A further complication of the spectrum can arise when the molecule is placed in a crystal field. In polyethylene the unit cell incorporates two chains. As a consequence the individual modes of each have the option

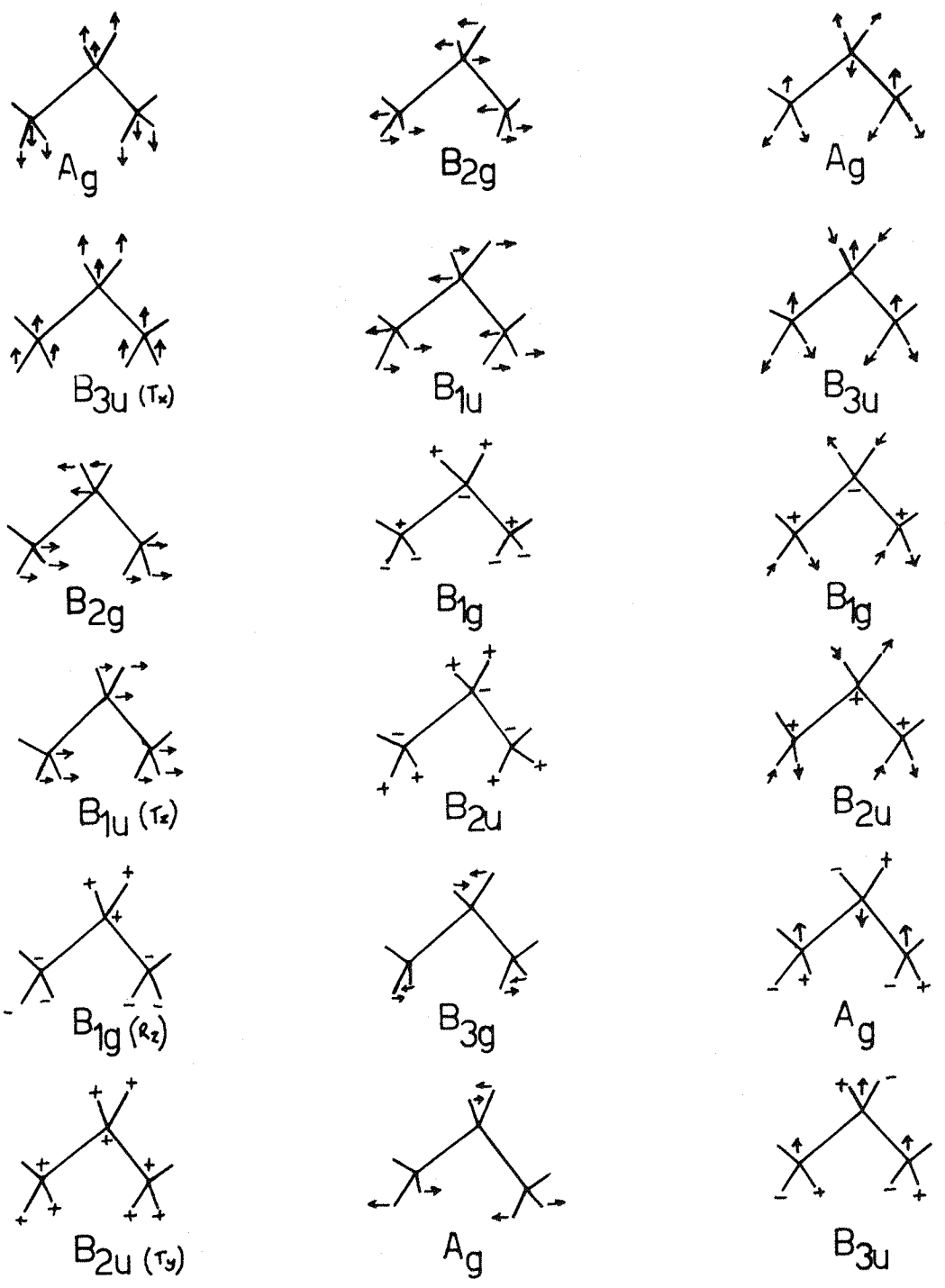

Figure I.5

Normal modes of vibration of a single polyethylene chain (9).

of vibrating in phase or out of phase, resulting in each mode exhibiting two frequencies, depending on the phase. This is called correlation splitting.

Not all of the normal modes of vibration are spectroscopically active. The spectroscopic activity is governed by the selection rules of the vibrational technique employed.

I.2.2 Raman Spectroscopy

In 1928 C.V. Raman (10) observed what had been predicted by Smekal (11), vis. inelastic light scattering.

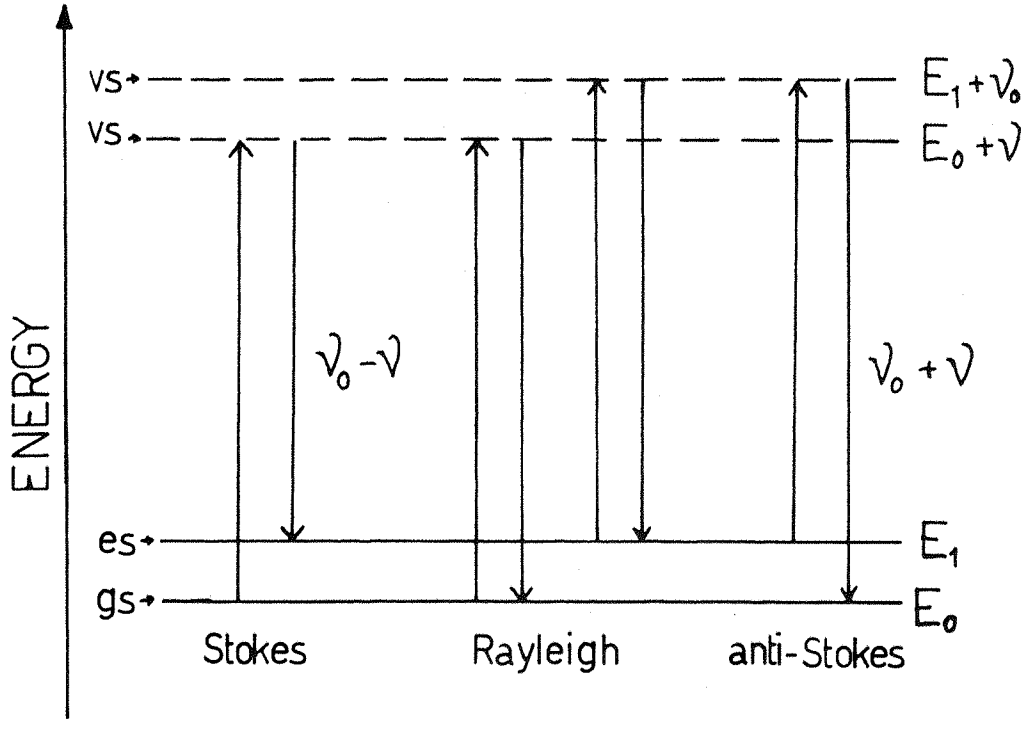

Figure I.6

Energy level diagram showing the transitions induced in the Raman experiment; gs = groundstate, es = excited state, vs = virtual state, ν_0 = exciting frequency, ν = vibrational frequency.

Absorption of a photon from the electromagnetic field excites the molecule into a virtual state, characterised by a different polarisation,

which re-emits a photon to fall into a different vibrational level (figure 1.6). Although this quantum mechanical explanation introduces the concept of virtual states, the half-life of the polarised species is approximately 10^{-14} seconds, thus it is safe to approximate the effect as the inelastic scattering of the incident photon. The "stokes" lines are those usually considered since they are the strongest. This arises from the Boltzmann distribution; a larger number of molecules always exists in the lower energy, or groundstate. Elastic scattering is a much more efficient process and the overall intensity of the Raman scattered radiation is typically 10^{-6} that of the Rayleigh scatter. However, the energy difference between the exciting frequency and that of the scatter is measurable, and is equivalent to the energy difference between vibrational states of the molecule.*

Classically, the Raman effect is based upon the polarisability of the molecule. If a sample is either to scatter or absorb an incident beam it must interact with the oscillating electric field of the electromagnetic radiation, such that an induced dipole is created resulting in a 'polarised' molecule, with a dipole moment related to the field strength, E, by

$$\rho = \alpha E \qquad \text{e.q. 1.2}$$

where α = the polarisability of the molecule. α, which can be thought of as the ease with which the electron cloud may be deformed, is not constant. It is altered about a mean value, α_o, by vibrations (and rotations). If the change in the vibrational coordinate is small then α may be expanded...

$$\alpha = \alpha_o + \left(\frac{d\alpha}{dQ}\right)_{Q=Q_O} \cdot Q + \tfrac{1}{2}\left(\frac{d^2\alpha}{dQ^2}\right) Q^2 + \ldots \qquad \text{e.q. 1.3}$$

... where Q = the vibrational coordinate and $\left(\frac{d\alpha}{dQ}\right)_{Q=Q_O}$ = the polarisability change which varies with time given by ...

$$Q = Q_O \sin 2\pi\nu t \qquad \text{e.q. 1.4}$$

... where ν = the vibrational frequency. If the applied field is due to the electric vector of electromagnetic radiation (for example a laser beam) which also varies with time, given by ...

$$E = E_O \sin 2\pi\omega t \qquad \text{e.q. 1.5}$$

* Rotational and electronic states can give rise to Raman lines.

... where ω = frequency of incident monochromatic radiation, substitution for α and E in e.q. 1.2 gives us the induced dipole moment.

$$\rho = \alpha o Eo.\sin 2\pi\omega t + \frac{EoQo}{2}\left(\frac{d\alpha}{dQ}\right)_{Qo}\left[\cos 2\pi(\omega-\nu)-\cos 2\pi(\omega+\nu)\right] \qquad \text{e.q. 1.6}$$

Three component frequencies can be observed, which can be related to the energy level diagram in figure 1.6.

ω	Rayleigh line	
$\omega + \nu$	anti-stokes	(shift towards blue)
$\omega - \nu$	stokes	(shift towards red)

If a vibration produces no change in the sign of the polarisability then it will be silent in the Raman effect. The selection rule is thus given as

$$\left(\frac{d\alpha}{dq}\right)_{q=qo} \neq 0 \qquad \text{e.q 1.7}$$

A plot of the polarisability versus the normal coordinate for carbon dioxide (figure 1.7) illustrates the selection rule, showing that for this molecule only the symmetric stretching mode is Raman active. The effect of each vibration on the shape of the polarisability ellipsoids, which are the plot of the loci $\left(1/\sqrt{\alpha}\right)_{\theta}$ for the molecule, are also shown.

1.3 The Development of Raman Spectroscopy

Once discovered, the Raman effect was rapidly developed as a means of investigating molecular vibrations, particularly in the years up to the Second World War. A comprehensive series of organic and inorganic substances had been well characterised by 1943 (12).

In early experiments the source was provided by a mercury discharge lamp, and the scattered light collected by a spectrograph and detected photographically. A typical arrangement is shown in figure 1.8. A wide range of sources were considered (13, 14), but the mercury discharge remained the most popular with its relatively uncluttered blue line at 4358Å.

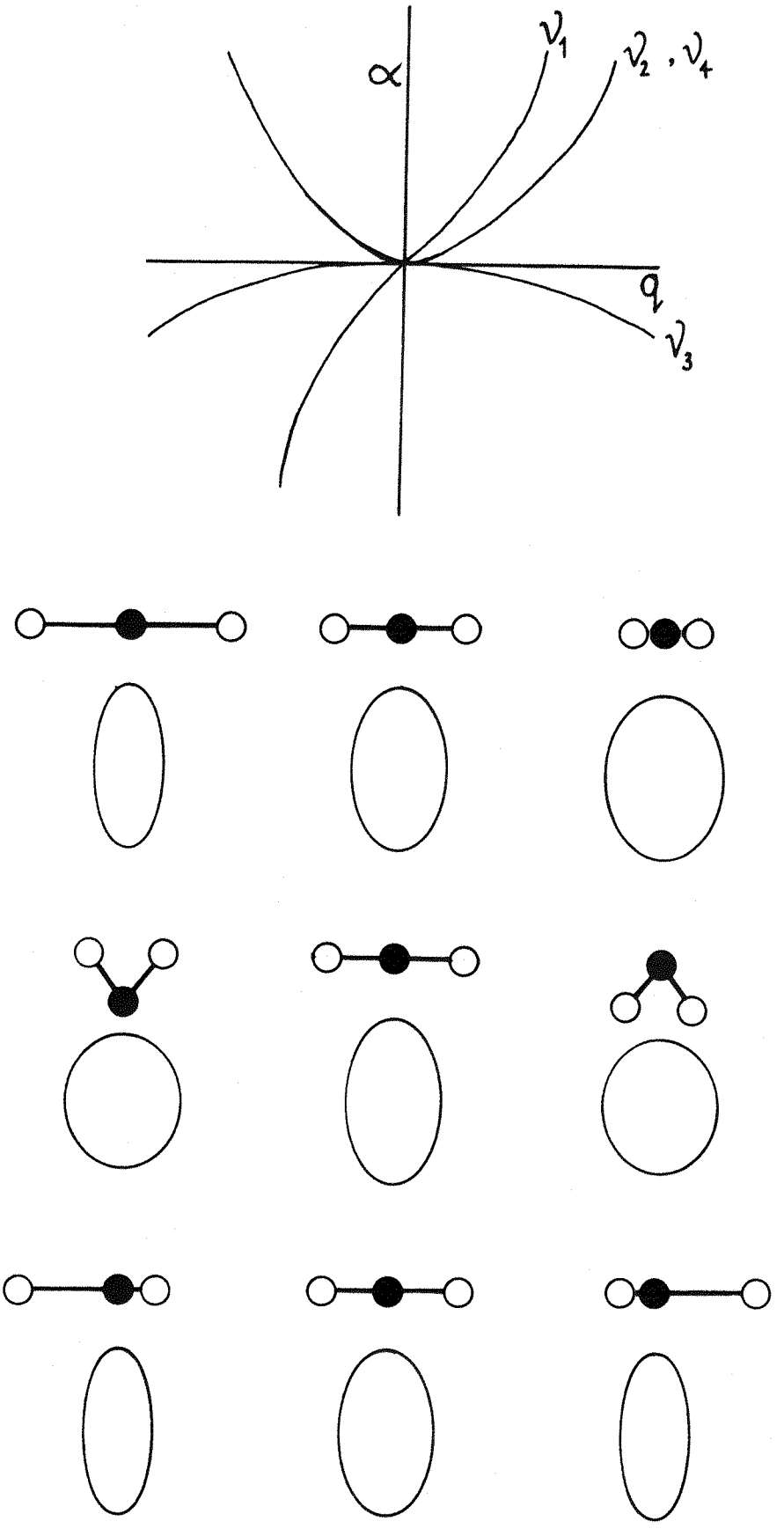

Figure 1.7

Changes occurring in the polarisability, α, and polarisability ellipsoid with displacement, q, during the symmetric stretch (ν_1), anti-symmetric stretch (ν_3), and bending (ν_2,ν_4) vibrations of CO_2.

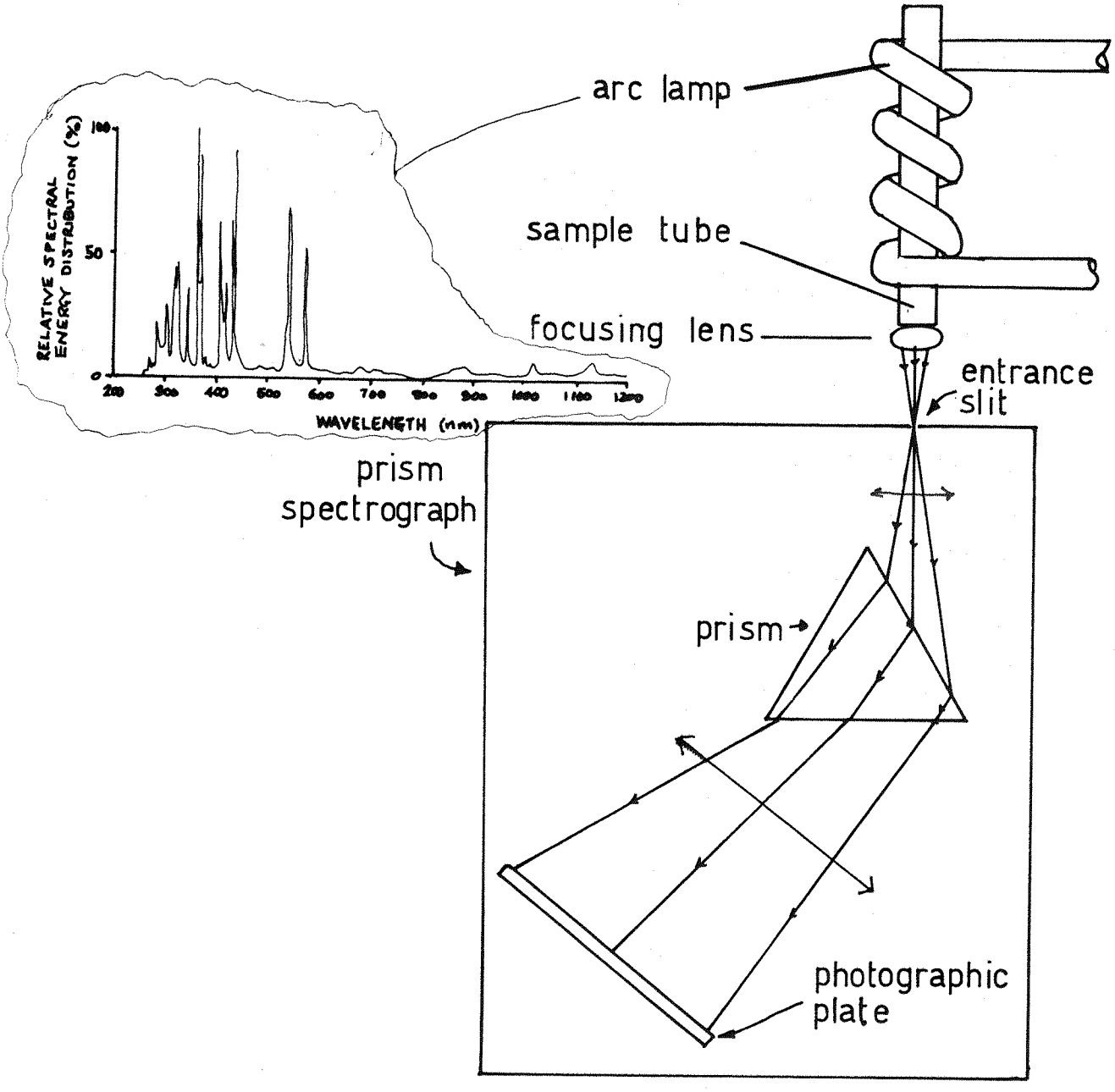

Figure 1.8

Typical arrangement for Raman spectroscopy in its early days of development.

However, a number of experimental limitations were apparent;

i) the source is not truly monocromatic, and a number of discharge lines are excited (figure 1.8);

ii) the emission between the discharge lines is sensitive to pressure, and although later the Toronto Arc was developed (15) (it operated at much lower pressures than the original lamps), there was

always a continuous measurable background in the region of the spectrum where the Raman lines were found.

iii) the discharge lines commonly occur as close spaced multiplets with a finite half-width - for example, the mercury 4358Å 'line' is in fact a number of emissions falling within a band of half-width $\sim 0.4 cm^{-1}$. This limits the resolution possible in the scattered spectrum.

iv) the spectrograph has relatively poor stray light performance. Limited and varying dispersion in Cornu (prism) spectrographs makes grating spectrographs more favourable. However, even with careful masking, spurious lines, internal scattering due to the grating and grating "ghosts" (double images) still limit the measurements.

v) photographic techniques to record the spectral data were slow. Inaccuracies occurred because of the log character of the emulsion response, fluctuations in background on the densitometric tracing caused by the granularity of the emulsion, fluctuations of the standard light source during emulsion calibration exposure, and local variations in the sensitivity and the degree of development of the photographic plate. At best a precision of ±14% in intensity was estimated by Reitz (16), although later films proved to be a little better. The real problem with photographic detection was that for weak scatterers, there was inevitable failure in emulsion response (the "reciprocity failure", known to photographers).

Considered alongside competition by processes such as fluorescence, photodecomposition, and elastic scattering for the incident excitation energy, it was difficult to achieve great success. However useful as a structural determinant, the advent of high speed infrared spectroscopy led to a rapid fall in the popularity of the Raman experiment.

1.3.1 Detectors

A spectrometer collects light from a source, disperses it, and selects a small spectral region to pass onto a detecting and measuring device. The amount of energy in this spectral interval is usually very small (Raman scattered radiation is $\sim 10^{-6}$, the intensity of the elastically

scattered radiation). This can be problemmatic, hence, the general requirements for a detector are:

i) High sensitivity - the detector should produce a large output signal for a small radiation input.

ii) Low Noise - in the absence of radiation a detector will produce some signal, i.e. 'noise'. This limits the smallest genuine signal that can be detected.

iii) Linearity - the output of the detector should be proportional to the radiation input, so that accurate photometric measurements can be made. The constant of proportionality (gain) should be independent of the wavelength of the radiation. (Most detectors are wavelength dependent).

Photoelectric detection was envisaged for Raman spectroscopy as early as 1940 (17), and with the advent of the photomultiplier tube (18, 19) the first Raman spectrometer to employ PM tube detection was developed (20). However, up until the late 1940's the principal means of recording radiation was still the photographic plate. Its chief characteristics are a low quantum efficiency (i.e. a large number of radiation quanta are needed to make one grain of the emulsion developable) and a very large information storage capacity. Thus, a photographic plate can simultaneously record the information in a large number of spectral channels. This 'multiplexing' can be advantageous for some applications. Accurate photometry is difficult because the response of the photographic plate is non-linear and wavelength dependant.

The Photomultiplier (PM) Tube

If sufficiently energetic photons fall onto the surface of a photocathode, electrons are emitted. Their number is a measure of the incident light. These electrons are accelerated towards a second electrode by a positive potential. The surface of this second electrode is treated such that a high secondary emission ratio for electron impact is achieved, and these secondary electrons are then accelerated by a similar voltage to a third electrode, and so on. There may be as many as eighteen multiplication stages, or 'dynodes'. Two PM tubes are illustrated in

figure I.9. Thus, a single photoelectron can produce a substantial current pulse at the final electrode. This high quantum efficiency is the strength of the PM tube detector. Careful selection of the photoemissive surface material allows a broad linear spectral response over the region of interest (figure I.9).

Noise

The smallest radiation signal that can be seen is determined by random fluctuation at the output of the complete detection system (detector + amplifier + ... + recording device). This 'noise' is made up of a number of contributions, some or all of which may be present in any specific system.

i) Photon noise: statistical fluctuations in the number of quanta received by a detector in a given time interval (can be reduced by increasing the intensity of the source or by observing over a longer time interval).

ii) Johnson noise: voltage produced by thermal fluctuation of electrons in a resistance.

iii) Current Induced (C.I.) noise: this is due to the polarising current (present in nearly all semiconductor detectors). The noise power per unit bandwidth is proportional to the reciprocal of the frequency - I/f noise. (Can be reduced by using a high chopping frequency in the amplification stage (see later)).

iv) Dark Current noise: random events in the detector can produce a signal even in the absence of illumination. This signal, or 'dark current' is statistical noise which becomes serious at very low levels of illumination. (Can be reduced by cooling the detector).

v) Electronic noise: it is possible, by careful design, to make noise produced by the electronic amplifying system small compared with photon and detector noise.

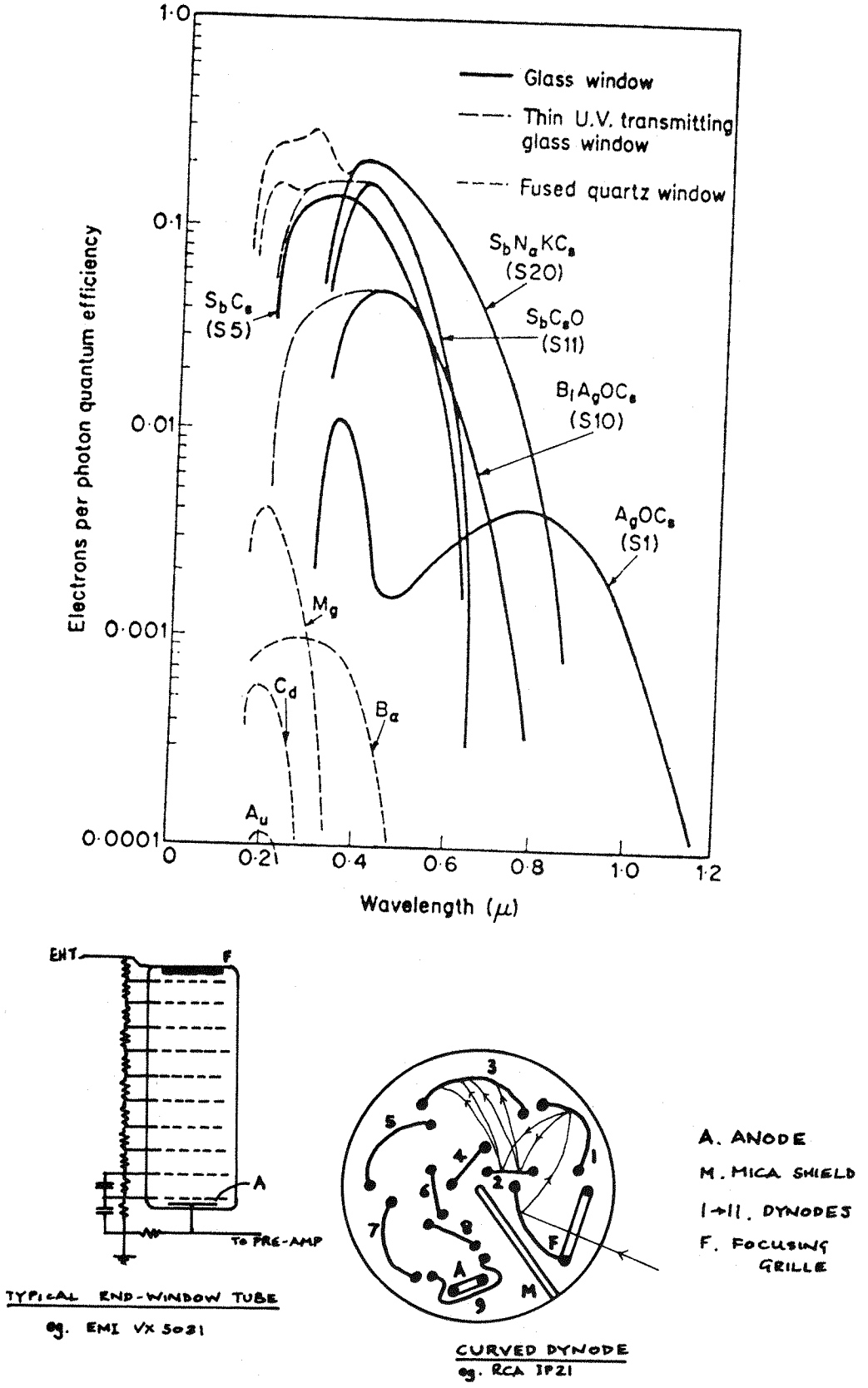

Figure 1.9

Photomultiplier detectors, and graph to show the spectral response characteristics of various commercially available systems. (Type of photocathode surface indicated on each curve).

Signal Processing

The electrical signals emerging from the detector are amplified. Because of the difficulty in amplifying a steady d.c. signal, some device is nearly always used which interrupts the incident radiation periodically (a 'chopper') and so produces an a.c. signal at the detector output. This is amplified, rectified (filtered) and finally recorded in some convenient form - usually on a chart recorder.

This and later methods such as photon counting (21) are used to process the signal coming from the detector. The processing techniques employed can improve the signal-to-noise (S/N) ratio, although no significant difference in performance is achieved using any particular individual amplification system.

1.3.2 The Laser-Raman Concept

Interest in Raman Spectroscopy was regenerated with the advent of the laser, conceived in the mid 1950's (22).

Laser action arises from a population inversion which occurs due to the excitation of molecules in some way, held in an optical resonant cavity (a cavity with a mirrored surface at each end). In the early stages of the lasing process photons are emitted in all directions, spontaneously, by some molecules in the medium. However, all of these, save those emitted along the cavity axis are lost through the side walls. When a molecule emits spontaneously it stimulates other molecules to emit. These stimulated emissions are of the same frequency*, and hence highly quasi-monochromatic radiation is produced. (Since the resonant modes of the cavity are considerably narrower in frequency than the bandwidth of the normal spontaneous transition, it is those modes that are sustained.) The effective bouncing of photons back and forth across the active medium along the cavity axis results in an amazing degree of collimation of the laser beam. This is emitted through a partially reflecting/partially transmitting end window, and can be effectively thought of as a coherent plane wave (since all the electric fields of the photons are in phase).

* as the original emission. Laser emissions at a number of different frequencies can be sustained. A prism is placed inside the cavity in order that a particular 'line' may be selected. (Fig 1.10)

The first practical demonstration of laser action was the stimulated emission by ruby (23) in 1961. Raman spectra were successfully recorded in 1962 (24, 25). Development of the helium-neon continuous laser device (26, 27) as a source was successful (28), although original experiments were restricted to transparent samples, which were placed inside the laser cavity. Any other samples tended to extinguish the laser.

Various studies (29, 30) supported the view that the laser source was far superior to that of the discharge lamp.

Later, developments of far more useful Raman sources such as the argon-ion (31) with a power output of 1Watt at each of the strongest emissions (5145Å, 4880Å), and the krypton-ion (32), with a useful red emission at 6328Å emitting approximately 0.5Watts, increased the potential of Raman spectroscopy further. In these systems the energy is deposited into a mixture of gases by an electric discharge. The amount of energy that can be extracted depends on a variety of factors including the composition of the mixture, the size of the tube, the manner in which the energy is deposited and the internal kinetics of the atoms/molecules involved. Most of these lasers contain a hermetically sealed mixture of gases that is interchanged during the laser tube's lifetime; generally the amount of light emitted can be controlled only by adjusting the tube voltage or the optics outside the laser tube. A typical continuous wave (CW) gas laser is illustrated in figure 1.10.

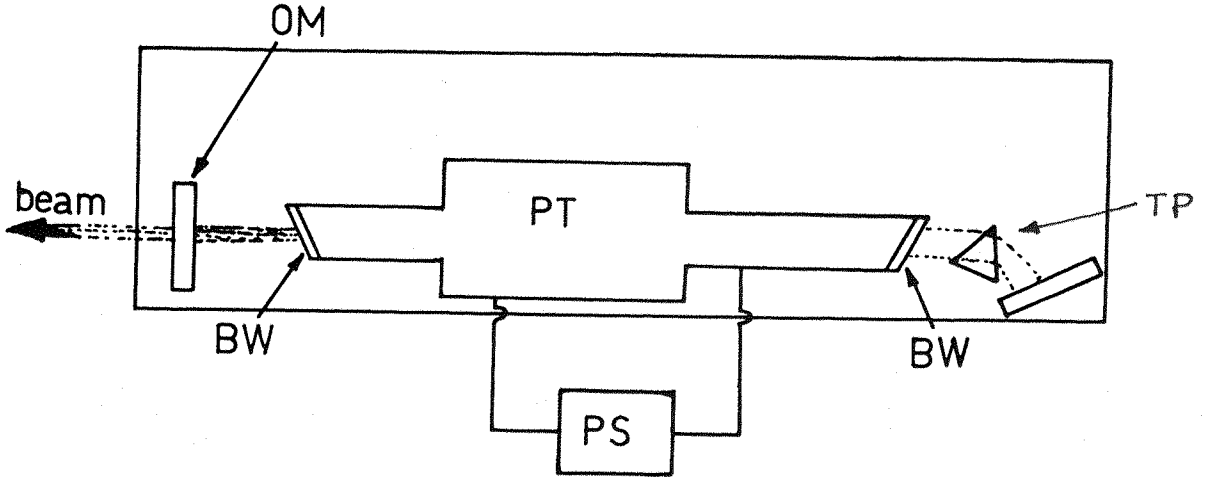

Figure 1.10

A typical gas laser. OM = output mirror, PT = plasma tube, BW = Brewster end-windows, PS = power supply, TP = tuning prism.

In the ion lasers the active species is the ion of a rare gas. The gas lasers have multiline outputs spanning the visible and near ultraviolet. Typical lines at which the three principal gas lasers can be operated are shown in table I.I (33). The values are expressed as wavelength (λ) and wavenumber (cm^{-1}) in air. (The difference between $\Delta\nu$ (air) and $\Delta\nu$ (vac) is usually less than $1cm^{-1}$ and can be effectively ignored in Raman spectroscopy).

The halfwidth of a commercial argon ion laser is $\sim\frac{1}{3}cm^{-1}$, compared to the He-Ne $\sim 0.5cm^{-1}$. These values can be reduced, but for most routine Raman work, the linewidth is not too important, and a resolution of $1cm^{-1}$ is completely acceptable.

Plasma lines generated by the discharge can be problemmatic if proper filtering techniques are not employed. Figure I.II shows the plasma lines emitted by an argon-ion laser. Filtration can be achived using simple pre-sample optical bandpass filters. However, dependant on the efficiency of these systems, spurious lines can still appear in the Raman spectrum.* These are easy to detect, since they are typically very sharp when compared to normal Raman bands.

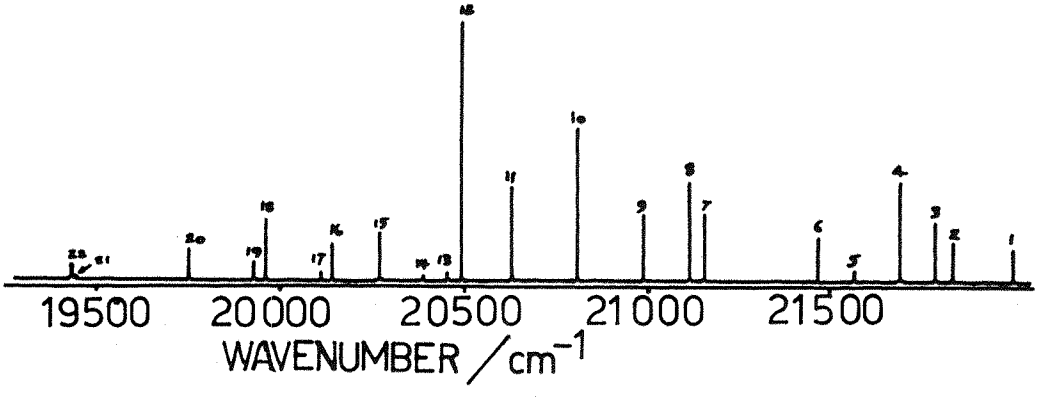

Figure I.II

Spectrum of plasma lines emitted by an argon-ion laser.

I.3.3 Stray Light and the Multiple Monochromator

Stray light occurs through phenomena such as errors in the grating, dust on the mirrors, imperfect coatings, blemishes, etc. ... (figure I.I2).

*Fluorescent lighting spikes can appear at $\Delta\nu \sim 2180cm^{-1}$ for the 4880Å line, and $\Delta\nu \sim 1125cm^{-1}$ for the 5145Å line in argon-ion.

Laser	λ (nm)	ν air (cm^{-1})	colour	Typical power (mW)
Ar^{+} (1)	457.9	21838.8	violet	300
	465.8	21468.4		130
	472.7	21155.1		250
	476.5	20986.4	blue	600
	488.0	20491.8	blue	1300
	496.5	20141.0		600
	501.7	19932.2	green	300
	514.5	19436.3	green	1700
	528.7	18914.3	yellow-green	300
Kr^{+} (2)	476.2	20999.6		60
	482.5	20725.4		45
	520.8	19201.2		90
	530.9	18835.9		200
	568.2	17759.4		200
	647.1	15453.6	red	500
	676.4	14784.2		120
	752.5	13289.0		100
	795.3	12510.9		30
He-Ne (3)	632.8	15802.8	red	50

Table 1.1

Some lasing lines of typical gas lasers.

Notes:

(1) Spectra Physics Model 164.08,

(2) Spectra Physics Model 164-01,

(3) Spectra Physics Model 125A.

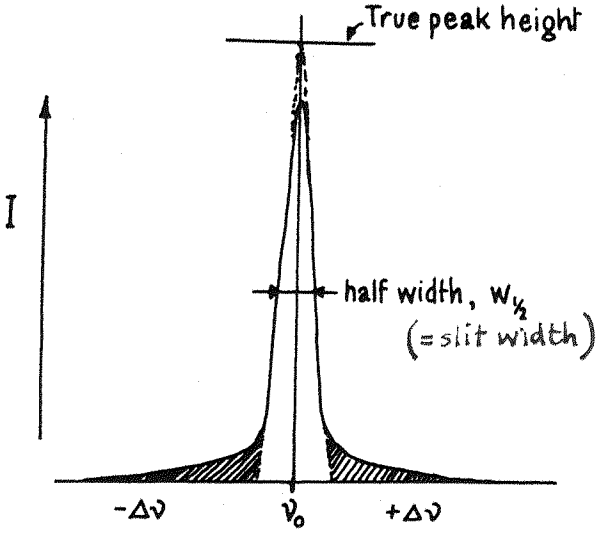

Figure 1.12

Stray light. I = signal intensity as one translates the laser frequency, ν_0. Stray light occurs in the shaded region; in this special case which demonstrates occurrence of stray light.

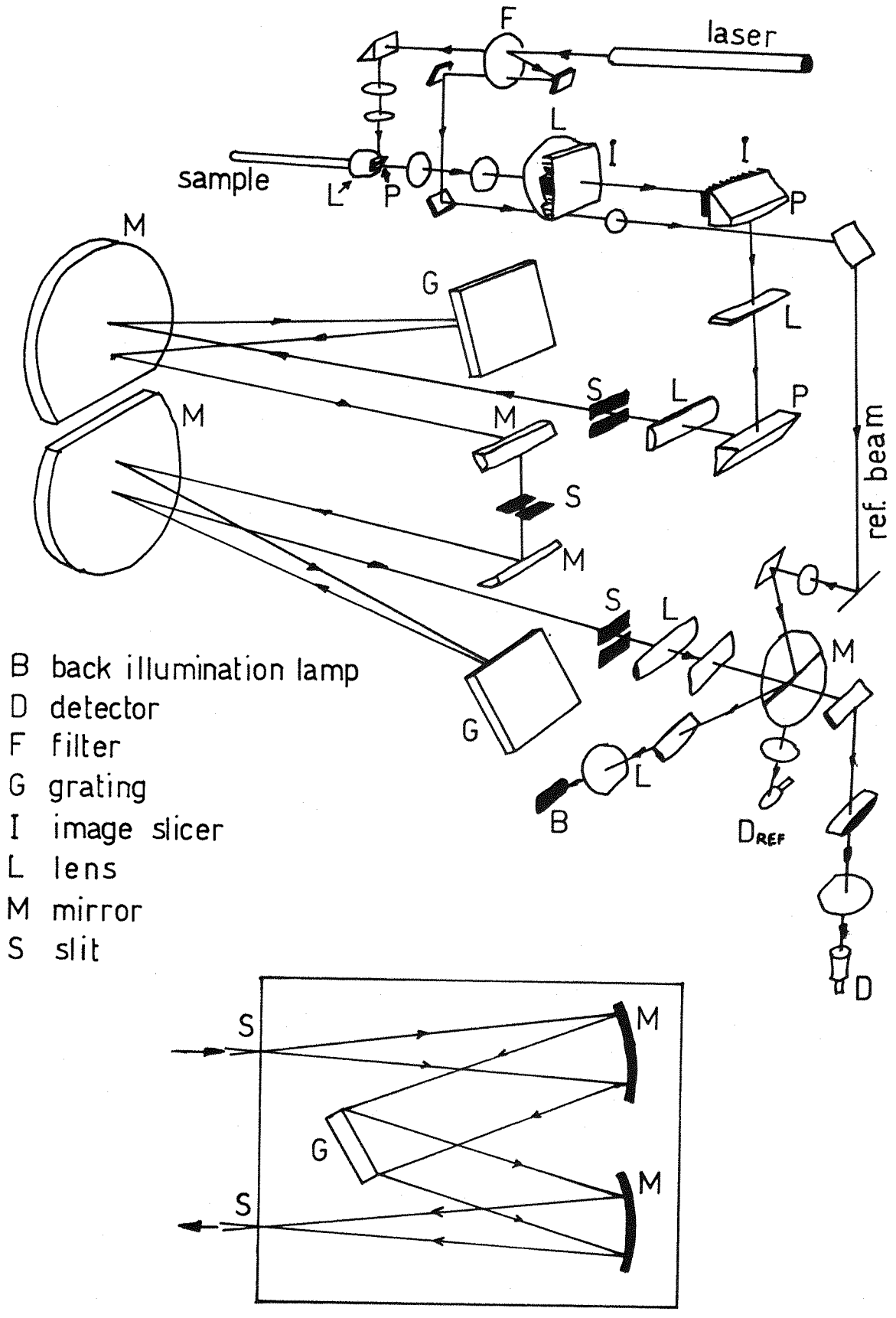

Figure 1.13

(a) Cary 81L Raman spectrometer, and (b) optical arrangement for a Czerny-Turner monochromator system.

This can be reduced by increasing the number of reflections in the system, and carefully masking the optics inside the monochromator. Increasing the dispersion by using multiple monochromators was suggested by Landon & Porto in 1965 (34). However, they overlooked the fact that the Cary 81L Raman spectrometer (at that time powered by a Toronto Arc mercury discharge lamp) had been commercially available as a double monochromator for some time (figure 1.13). In actuality, seventy instruments were produced with the arc source, and a further twenty were modified to accommodate a Helium-neon laser source. It was this combination of the double monochromator and the laser that led to a ressurgence of interest in Raman spectroscopy.

Many different monochromator designs have been used in order to produce non-aberrant images.* The most popular devices for Raman work have been the Czerny-Turner type (figure 1.13), which are used in over 50% of all of the commercial instruments produced.

In Raman spectra, stray light poses no real problems beyond a shift of $100cm^{-1}$. However, if work is intended in the region of the spectrum close to the exciting line, a double-slit/double monochromator or, better, a triple monochromator system is essential (see figure 1.14).

1.4 Rapid Scanning and the Multiplex Advantage

The problem of obtaining good spectra in a short time is basically one of signal-to-noise ratio (S/N) in the photodetector. Any attempt to increase the scanning rate of the monochromator or to decrease the exposure time of the spectrograph will inevitably be accompanied by a lower S/N.

For normal scanning, sufficient time must be allowed at each data collection point for the S/N at the point of acquisition to reach an acceptable level, especially for weak signals. Figure 1.15 shows the effect of scan speed on band contours for a single scan.

* There is a limiting value of the slit width, below which the bandpass is not worth reducing. This is due to the fact that a slit image is not perfectly reproduced, and a larger exit slit is required (see figure 1.14). The limit depends on the amount of aberration.

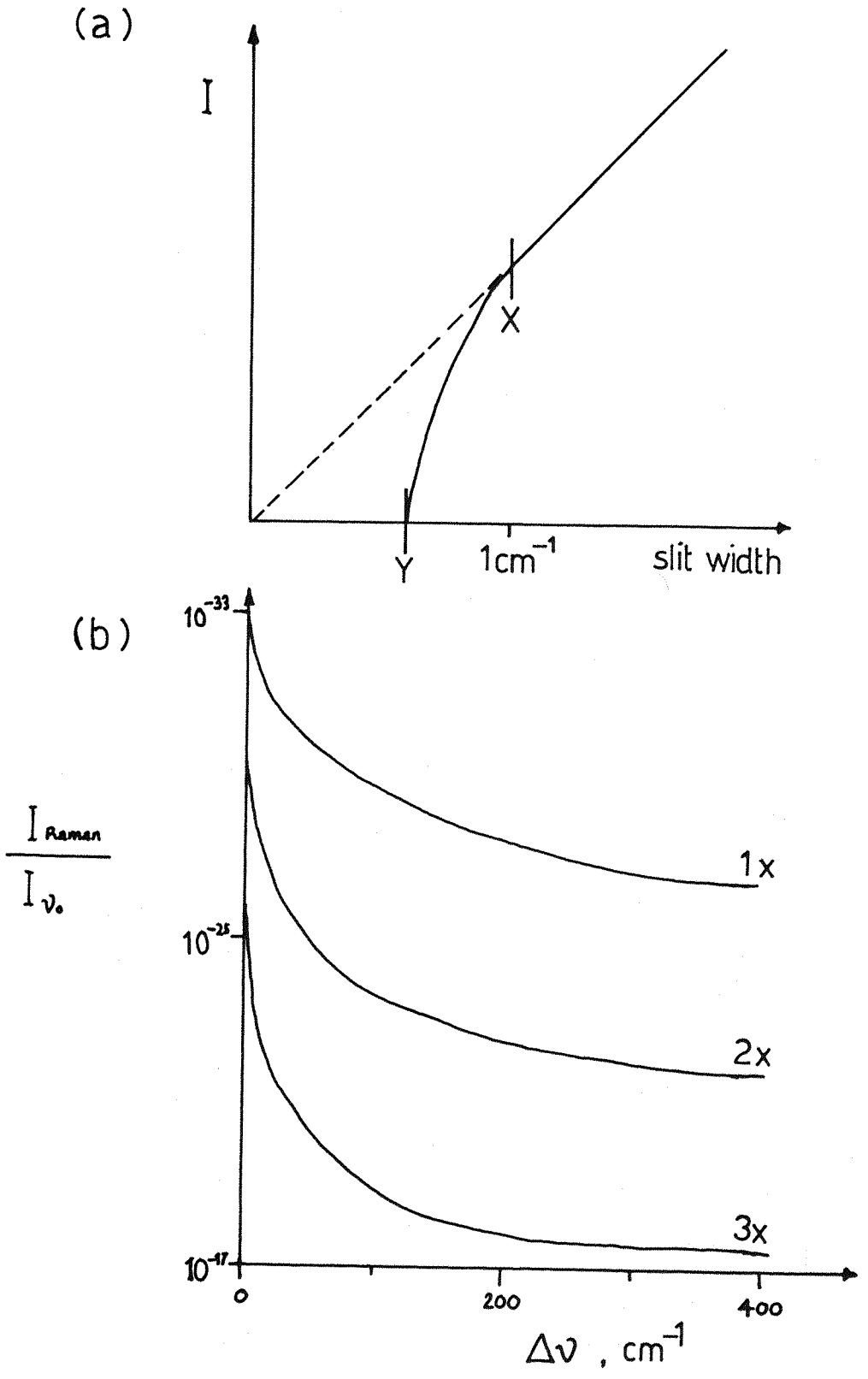

Figure I.14

(a) Plot of intensity of laser line against slit width. X = Raman useful minimum slit width, Y = absolute minimum. (b) Stray light performance of multiple monochromators. 1x = single, 2x = double, and 3x = triple monochromator.

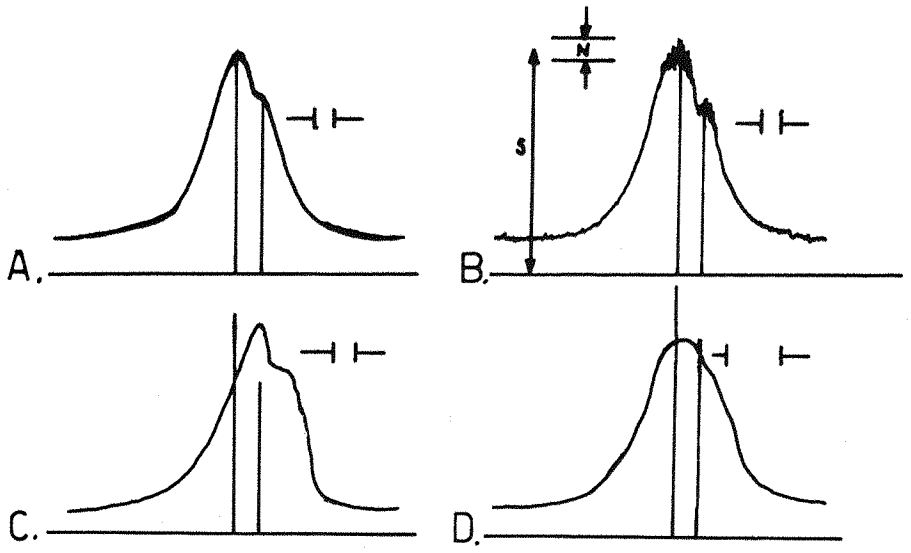

Figure 1.15

Effect of scan speed on band contours. The vertical lines indicate true band position and intensity, and ⟊⟊ = slit width. A = good operating conditions, signal-to-noise ratio (S/N) ~30; B = lower sampling time coupled with a fast scanning rate, S/N = 12; C = too fast a scan, band head shifted dramatically; D = effect of wide slits.

Important developments in the speed of accumulation of Raman data have been made by Delhaye (35). The rapid scanning device consists of a rotating helical cam which linearly moves the existing cosecant bar drive* When engaged, the bar moves up the cam (covering a limited spectral region, e.g. 250cm^{-1}), then drops back to its starting position. The S/N advantage is achieved with repetitive scanning of spectra and accumulation on a signal averager (36). However, the synchronisation of the spectra must be perfect, scanning across the same range at each pass and adding spectra precisely one upon the other.

In spectroscopy, the term 'multiplex' denotes a type of spectrometer in which one detector simultaneously receives signals from different elements of the spectrum, and encodes those signals in such a way that they can be transmitted and recorded by a single information channel.

* Adjustment of the bar is proportional to the cosec of the grating angle i.e. the wavenumber. Therefore, linear in wavenumber.

The advantage of this method is that noise is introduced into the system only by a single detector rather than all the detectors that would be needed for separate simultaneous recording of all the elements of the same spectrum. (If there are 'n' elements in the spectrum, the instrument will show an improvement of the order $\sqrt{n}$ in its S/N).

The multiplex advantage is realised for infrared spectroscopy by the use of the rapidly scanning Michelson interferometer*, as illustrated in figure 1.16. The method is very successful, and has the added advantage that there are no energy limiting slits in the interferometer.

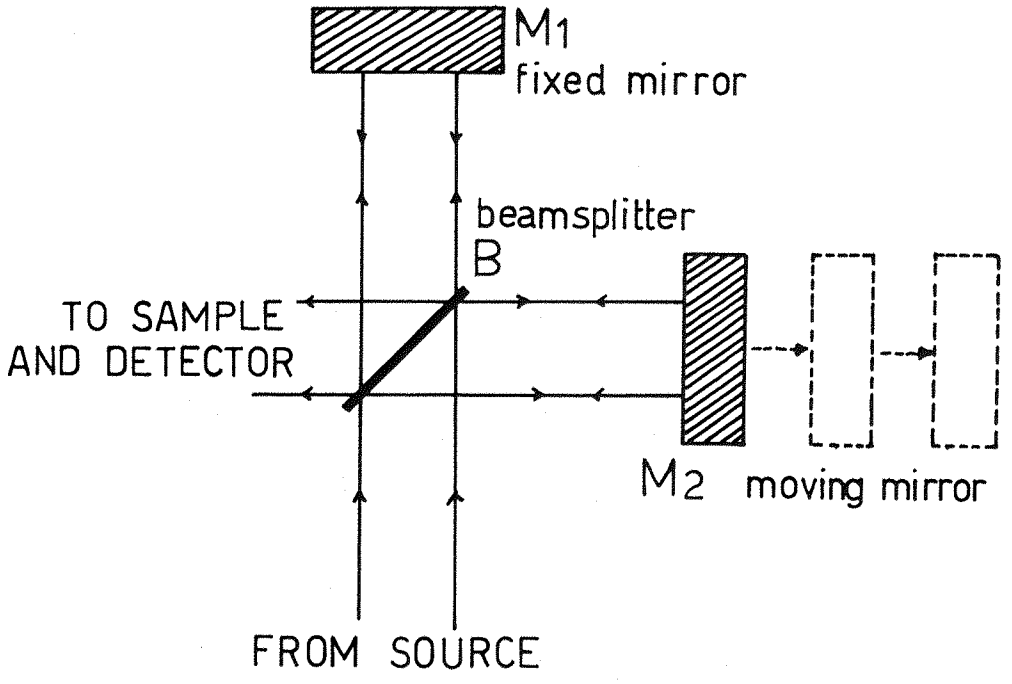

Figure 1.16

The Michelson Interferometer.

In Raman, optical multichannel detectors such as diode arrays or vidicon tubes have been employed in grating spectrometers in an attempt to achieve the multiplex advantage, simultaneously recording a large number of spectral elements - typically ~1000cm^{-1}. However, noise in all but the very latest multiplex detectors is poor, and the sensitivity per channel is

* Raman measurements cannot be made in the visible wing the michelson method, since the noise level is not independant of the signal level at the detector.

less than that of a PM tube.

Systems developed in the last 20 years (37-39) were basically reliant on image intensifiers and low-light-level television (vidicon) cameras. Low dynamic range, image distortion, poor geometric and sensitivity stability limited resolution and a high propensity to overloading of the array excluded the use of such instruments for general purpose Raman work. Consequently, single channel/scanning/recording remained the most widely used method. However, 1000x improvements in the sensitivity of multichannel detection systems over that of conventional techniques have been claimed (40), and further developments in such systems have been reported by Deffontaine (41) utilising the advances in solid-state diode arrays.

A major disadvantage with multiplex Raman is the size of the active region of the detector. It may be only 0.5" long (40) and at best 1" (41). With a typical single monochromator dispersion of $\sim 25 cm^{-1}/mm$, the $\frac{1}{2}$" detector will only "see" $250 cm^{-1}$ of the spectrum ($\sim 0.5 cm^{-1}$ per channel). This may be adequate. However, for Raman work close to the frequency of laser excitation, multiplex spectrometers are impossible to use since the stray light characteristics of single monochromators is very poor. Improving the stray light performance by using multiple monochromator systems negates the advantages of multiplexing. However, single monochromator dispersion can be achieved with the stray light performance of a double monochromator by carefully calculating the monochromator size and using subtractive dispersion. However, problems may arise through aberration of the spectral image, and specially figured correction optics are expensive, and at best can only offer part of the solution.

The use of Fourier Transform spectroscopy (FTS) for the collection and analysis of Raman data has been reported (42). Further, using a slightly modified commercial FT-IR instrument with Raman excitation being provided by a neodymium-YAG laser, FT Raman spectra have been successfully recorded from a number of powdered and liquid samples (43).

In addition to the multiplex advantage, the FT Raman method also achieves the throughput (Jacquinot) advantage, since there are no energy limiting slits in the system. It also acheives the Connes advantage.

These developments are at an embryonic level. Even as such they are generating considerable excitement.

1.5 Practical Raman Spectroscopy

1.5.1 Sampling Systems

A wide range of sampling systems have been developed to access the laser to the sample within the sample compartment, and allow the scattered radiation to be collected in the most efficient way. A number of systems of illumination of samples are illustrated in figure 1.17.

Some sampling arrangements require only simple cells and/or accessories to suit the particular needs of the investigator. For more difficult studies such as high pressure (44), low and high temperature (45, 46), coloured samples (47), surface work (48, 49), biological studies (50), small samples and microscopic studies (51-54), and matrix-isolation studies (55), specialist, and frequently expensive, devices have been developed.

1.5.2 Residual Problems

Even with such a great deal of investment and effort, problems still remain which limit the level of efficiency available from such systems. They are: (a) fluorescence and background, and (b) experimental geometry.

(a) Fluorescence and Background

Although attempts have been made to overcome the problem, the techniques required are complex, expensive and tend to produce only modest improvements.

The intensity of a fluorescent background may be 10^4 times greater than that of the Raman signal. Methods of reduction of fluorescence include purification of the sample (to remove any light-absorbing contaminants), 'burning out', (this involves exposing the sample to

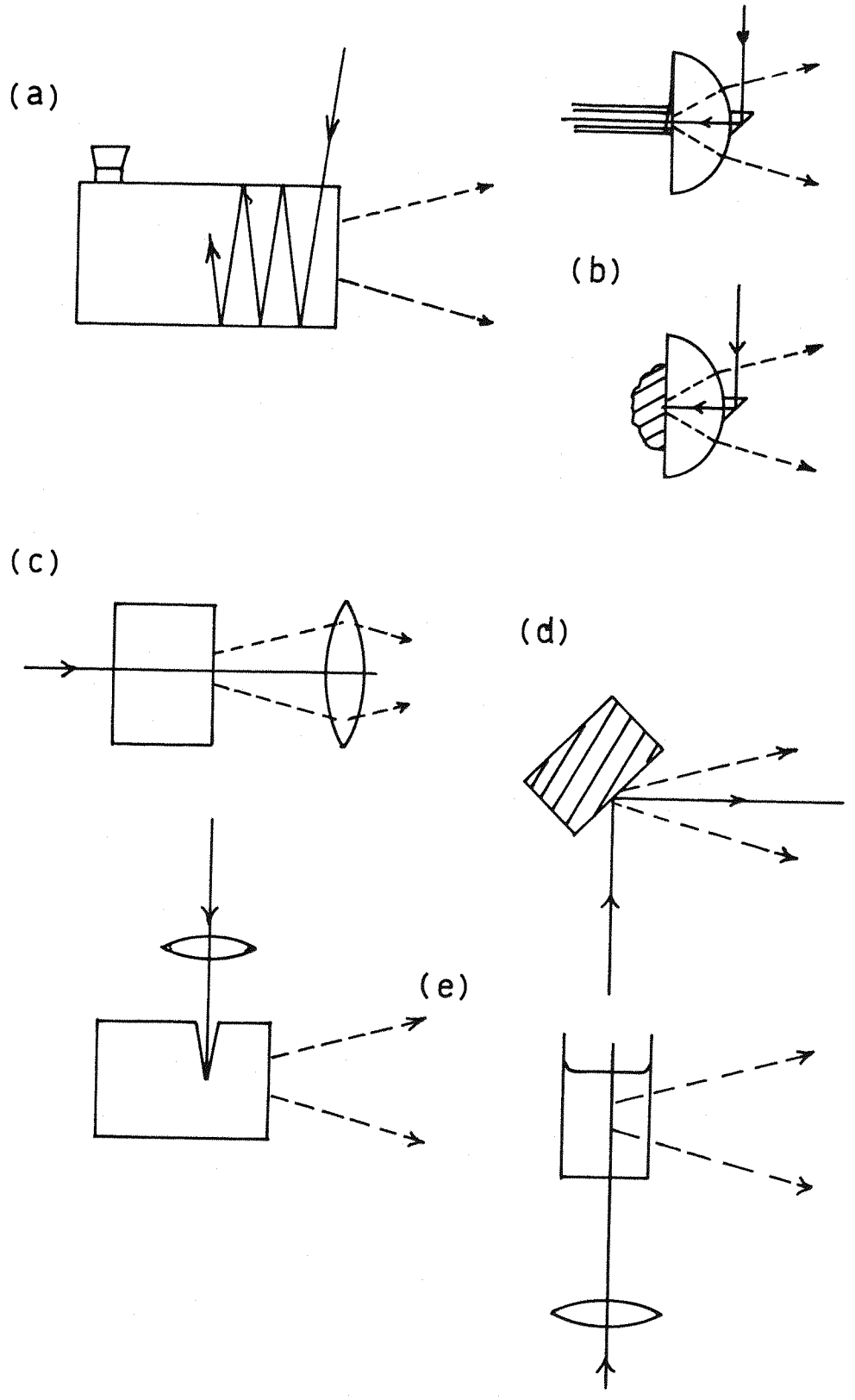

Figure I.17

Raman sampling methods; (a) multireflection cell for transparent liquids, (b) Cary 81L system applied to liquid in a capillary tube and solid samples, (c) 180° sampling, (d) Vessel, and Pellet or block viewed at 45° Reflected beam is "aimed" to just miss entering the slits, (e) 90° system. Block or transparent or liquid in tube.

laser light for long periods of time. The fluorescence 'decays'. However, it is only noticeable given a high initial fluorescence level.), use of quenching agents, repetitive scanning, and the use of a pulsed laser with a box-car detector (56). Most fluorescence encountered in Raman is of short $\frac{1}{2}$ life $\sim 10^{-8}$ secs or lower. Hence, the box-car application requires cavity dumped single-mode lasers, and borders on useless. (It should be noted here that fluorescence is not encountered in F.T. Raman).

(b) Experimental Geometry

At first sight the Raman experiment has a major advantage over its infrared competitor in this respect. In the infrared, filling the sampled aperture with radiation is adequate to observe the absorption. However, inherent limitations such as thin samples, use of windows and recording data from surfaces or other inhomogeneities prove to be problemmatic. Many solutions to these problems have been adopted by i.r. spectroscopists including reflection, emission etc.... Each method has advantages and limitations, but a choice of method to fit a particular system is possible due to the high degree of development in this field.

In Raman first glances suggest that sampling is very satisfactory. As long as the laser is injected into the sample, and the scattered light is collected, any geometry is accessible. Windows provide no real problem. Unfortunately, one major problem persists - alignment.

For a strong scatterer it is trivial to align the imaginary image of the slit with the incoming focused laser beam. Initial location is achieved using a back-illumination system, available on most commercial instruments, and optimisation is achieved by aligning the sample on a known peak. For weak scatterers with no solvent or other supporting assistance, it is almost impossible to find the slit image. Further difficulties arise through high backgrounds and/or fluorescence. These factors raise the limit below which scatterers become in effect, poor ones.

The effect of the alignment problem is that the spectroscopist is tempted to become lazy and not try, (s)he finds it impossible to align

a very weak scatterer and hence cannot use time as a method of increasing sensitivity i.e. using data acquisition to exploit the fact that the signal-to-noise ratio increases as the square root of the exposure time In carbon -13 nmr, for example, it is not unusual to use 48hr scans in order to resolve samples such as low density polyethylene. This is impossible to do in the Raman if automatic and routine alignment cannot be achieved.

The question must be approached optically. Looking back at one of the first commercial laser Raman instruments, the Cary 81L, the sampling method used was in principle undoubtedly the best (see figure 1.17(b)). Scattered light was collected from the lens focus and thrown into the spectrometer.* Simply pushing the sample up against the lens produced an acceptable Raman signal in all cases.

Recent suggestions for overcoming the alignment problem in real scatterers have included the utilisation of the unique properties of fibre-optics.

1.6 Fibre-Optics

In a lecture to the Royal Institution in 1854, John Tyndall first demonstrated the principle of total internal reflection, with a spout of water emerging from an illuminated tank (57). However, practical applications of the phenomenon were not considered until the early twentieth century. The subsequent developments of fibre-optics, principally in the U.S.A., have led to two broad areas of application; the transport of visual information and the transport of light. The most popular commercial exploitation of fibre-optics is in the telecommunications industry, and the vast majority of optical fibres produced are for the transfer of information over large distances. However, their unique properties are increasingly applied to display systems, visual monitoring, contact photography, image-intensifier coupling, and many other uses. A number of more novel applications have included the use of fibres for

* However, the Cary 81L detection system produced a round image at the slit. To fit this to the entrance slit an image slicer was used - an expensive and elaborate solution.

photochemical tumour therapy (58) and the measurement of partial pressures of oxygen in the blood (59).

Spectroscopic applications have been limited in the amount of structural information they can provide. Infrared transmitting fibre technology (60) is not far enough advanced for useful analytical exploitation, but since Raman spectroscopy operates at wavelengths well into the visible, the transmission characteristics of commercially available optical fibres are such that adequate coupling of the two techniques is feasible. Raman experiments involving fibre-optics have been demonstrated (61-63) and work in this laboratory (64) introduced the concept of remote sampling and has led to the development of a viable multi-element probe (65).

1.6.1 Fibre-Optics Theory

An optical fibre can be described as a cylinder of transparent dielectric material of refractive index n_1, whose walls are in contact with a second dielectric material of a lower refractive index n_2. Generally it is assumed that the fibre is immersed in a third dielectric material of refractive index n_0, although this material is normally air ($n_0 \simeq 1.0$).

A. Total Internal Reflection

The passage of light through an optical fibre is achieved by total internal reflection of the light at the cylinder walls. A ray of light is internally reflected at the boundary between the two dielectric media when the ray is incident within the denser medium, and the angle of incidence is greater than a critical value defined by the indices of the media.

Figure 1.18 shows a light beam from within a denser medium, n_1, incident at the boundary with a less dense medium, n_2. The angle of refraction is related to the angle of incidence by Snells law.

$$n_2 \sin \theta_2 = n_1 \sin \theta_1 \qquad \text{e.q. 1.8}$$

As θ_1 becomes larger, it will reach a value where $\theta_2 = 90°$, that is...

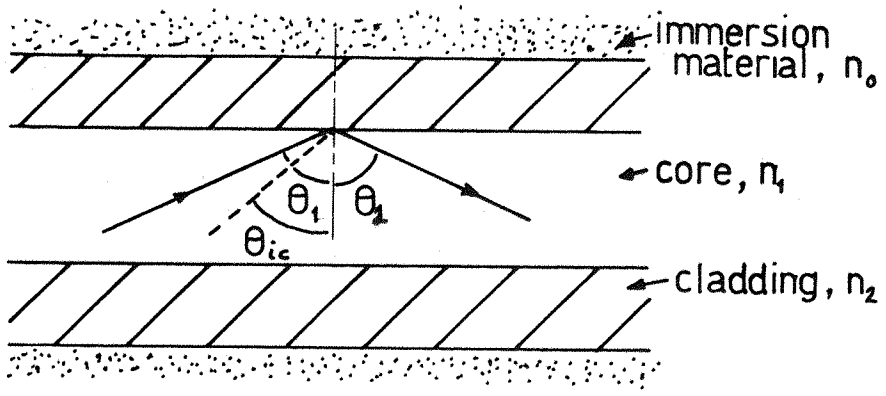

Figure 1.18

Reflection of light at the dielectric interface of an optical fibre; A = core material of refractive index, n_1; B = cladding material, n_2; C = immersion medium, n_o (usually air - n_o = 1.0).

Since $n_1 > n_2$, $\sin\theta_2 > \sin\theta_1$, so that $\sin\theta_2 = 1$ for a value of θ_1 which is less than 90°. The critical angle for reflection θ_{ic} can be derived by setting $\sin\theta_2 = 1$, which gives ...

$$\sin\theta_{ic} = n_2/n_1 \qquad \text{e.q. 1.9}$$

A ray will thus be totally internally reflected for all angles greater than θ_{ic}. Fermats principle; therefore ($\theta_1 = \theta_2$) applies.

The principle of internal reflection has been known for many years, and its use in folded and inverting optical systems is commonplace. Reflectivities of 0.9995 at glass-glass boundaries in optical fibres have been estimated (66), which are several orders of magnitude higher than for example, reflection at an aluminium surface, which exhibits a reflectivity of ~0.9 to 0.96.

B. Ray Propagation

There are two distinct types of ray propagation in optical fibres; meridional rays and skew rays.

In a meridional ray the path through the fibre is confined to a single plane which is normal to the tangent planes at the point of incidence.

For a circular cylinder configuration (a typical optical fibre) the meridional plane is any plane which contains the cylindrical axis.

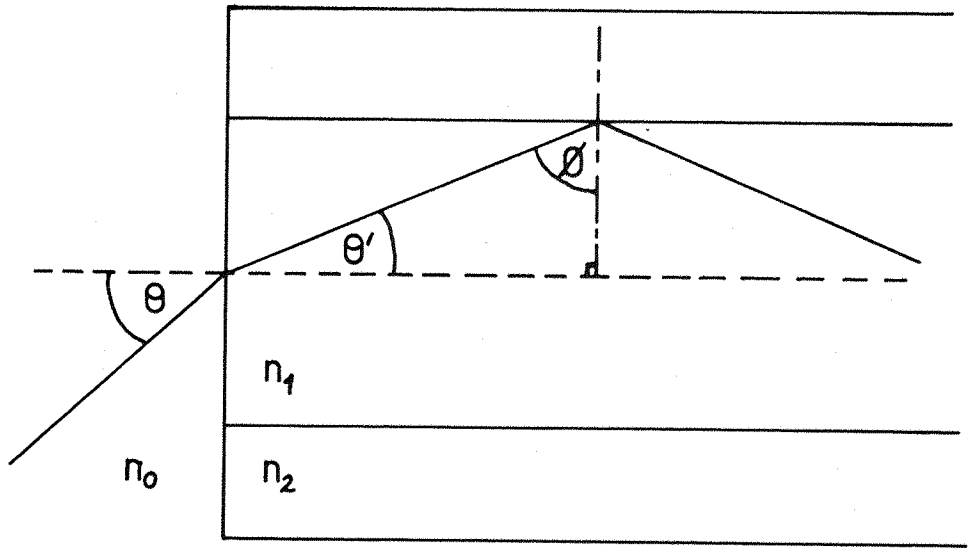

Figure 1.19

Refraction at the end face and reflection at the core/cladding interface of a meridional ray entering an optical fibre.

Figure 1.19 shows a fibre with its end face normal to the fibre axis. A ray entering the system from a medium with refractive index n_o at an angle θ to the normal is refracted at an angle θ' and incident at the dialectric boundary at an angle ϕ. From Snell

$$n_o \sin\theta = n_1 \sin\theta_1 = n_1 \cos\phi \qquad \text{e.q. 1.10}$$

For reflection to occur we must have,

$$\sin \phi > n_2/n_1$$

that is $$\cos \phi < \left[1 - n_2^2/n_1^2\right]^{\frac{1}{2}} \qquad \text{e.q. 1.11}$$

By substituting for inequality 1.11 in equation 1.10 we have,

$$\sin \theta < \frac{1}{n_o} (n_1^2 - n_2^2)^{\frac{1}{2}} \qquad \text{e.q. 1.12}$$

which gives the angular condition which must be satisfied by a meridional ray before internal reflection can occur. The angle of incidence at subsequent reflections is equal to that at the first reflection (considering a straight, parallel cylinder). If the output face lies normal to the cylinder axis, then the emergent rays will lie at an angle θ to the axis. The direction of the rays will depend on the number of reflections experienced by the ray during its passage through the fibre (see figure 1.20). If this number is even, then the ray emerges parallel to its original direction. If the number is odd then the ray emerges at an angle of 2θ to its original direction. Therefore a fibre thus described will accept and propogate a cone of light incident upon its end face provided that the conical half-angle is less than θ_m, where θ_m is defined by the upper limit of the inequality in equation 1.12.

$$\sin \theta_m = (n^2 - n_2^2)^{\frac{1}{2}} \qquad \text{e.q. 1.13}$$

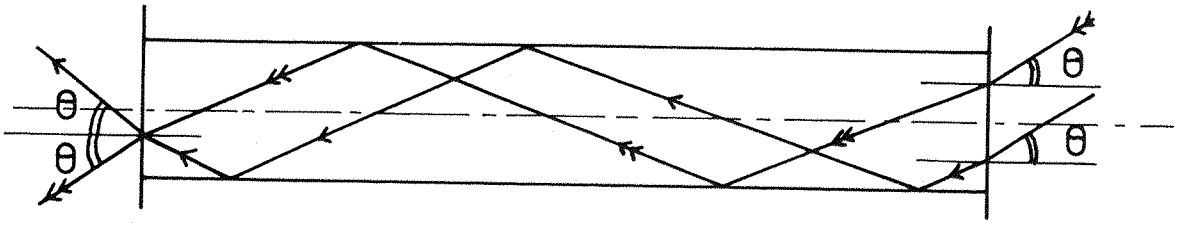

Figure 1.20

The passage of two parallel light rays through an optical fibre, where the number of reflections differs by one.

This is clearly a measure of the light-gathering power of the fibre and the right-hand side of the equation, by analogy with lens optics, is defined as the numerical aperture of the fibre.

The effect of fibre curvature can be seen to have rather a drastic effect on meridional rays; however, these form a much smaller proportion of the flux passing through the fibre, since there is only one meridional plane available (see figure 1.21). A maximum acceptance angle can be calculated for a fibre of diameter, d, with radius of curvature, R, such that

$$\sin \theta_m = \left[n_1^2 - \left(1 + \frac{d}{R}\right) n_2^2 \right]^{\frac{1}{2}} \quad \text{when } R >> d/2 \qquad \text{e.q. 1.14}$$

One of the most important properties of optical fibres is that they are able to retain their light carrying abilities when they are curved.

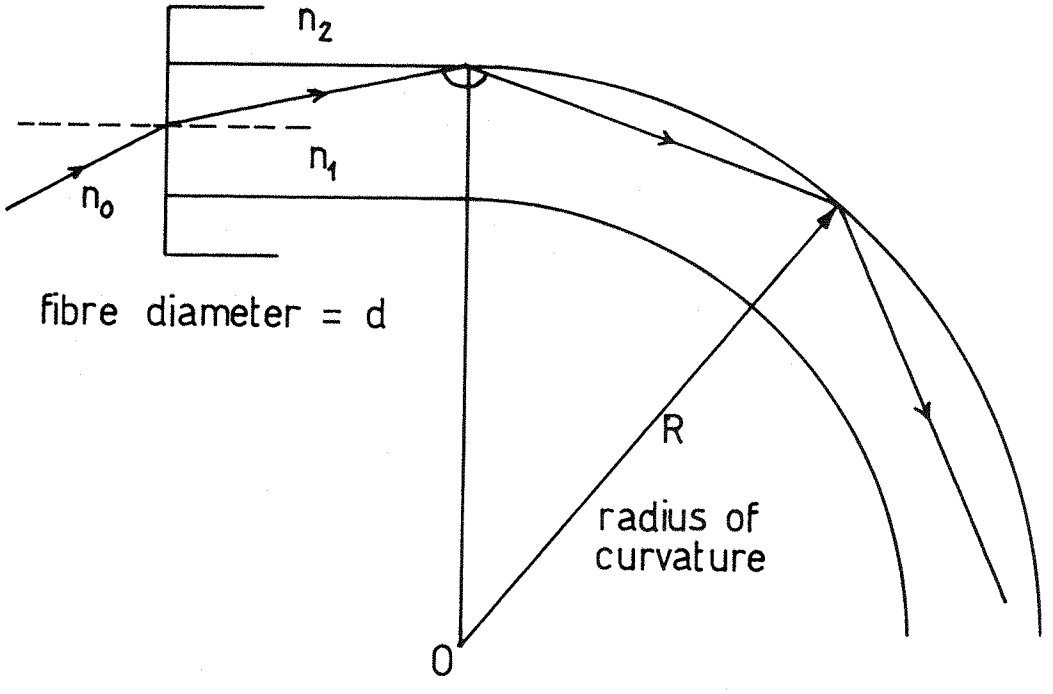

Figure 1.21

Effect of fibre curvature on the path of meridional rays; R = radius of curvature, d = diameter of fibre.

A straight fibre with a core refractive index, n_1 = 1.5 and a cladding index, n_2 = 1.45 would have a numerical aperture equal to $\sqrt{1.5^2 - 1.45^2}$ = 0.38 which would result in a cone semi-angle of $\theta = 22^\circ$. If the fibre was bent to a maximum of R = 10mm then the numerical aperture would be reduced to 0.33, resulting in a half angle of $\sim 19^\circ$.

Such a severe bend would not normally be experienced, but in this condition it would still be equivalent to a perfect lens working at $\sim f/2.5$.

The path of skew rays is not confined to a single plane. A typical skew ray, AB, is shown in figure 1.22 where A and B are points of reflection at the cylinder wall. The azimuthal angle, γ, is defined as the angle between PA and AO where O is the intersection of the cylinder axis with the plan POA normal to the axis. Since PB is parallel to the axis, θ' is the internal axial angle. Thus and $(\pi/2 - \theta')$ define the orientation of the ray AB with respect to the normal OA at A. Thus for the angle of reflection, ϕ, we can write

$$\cos \phi = \cos \measuredangle OAB = \sin \theta' \cos \gamma \qquad \text{e.q. 1.15}$$

For any skew rays the angles γ and θ' are maintained through propagation, and the light travels in a helical fashion. By applying Snells law we can show that the maximum acceptance angle is then

$$\theta_m = \frac{\sin \theta_m}{\cos \gamma} \qquad \text{e.q. 1.16}$$

Thus skew rays will be accepted at larger incident angles than meridional rays where $\cos \gamma = 1.0$, and the meridional numerical aperture is the minimum and thus the quoted figure.

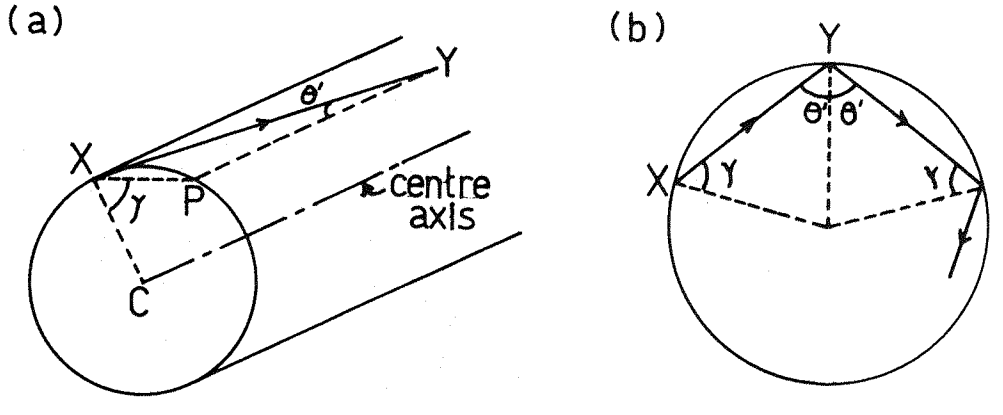

Figure 1.22

Path of a typical skew ray between reflections; (a) along the fibre axis, (b) on a plane normal to the fibre axis.

1.6.2 Waveguide Properties of Fibres

An optical waveguide is a dielectric structure that transports energy at wavelengths in the infrared or visible portions of the electromagnetic spectrum. Optical waveguides can be conveniently divided into two sub-classes called multimode waveguides (with relatively large core diameter) and single mode waveguides (with comparatively small cores). The number of modes of transmission which can be supported in a fibre is proportional to the fibre diameter, d, and the critical angle of reflection, θ_{ic}. Because of diffraction it is impossible to confine the light entirely within the core of waveguides with small diameter and θ_{ic}. Since we are interested in multimode fibres in which both parameters are sufficiently large, thousands of modes are propagated, and all the transmitted light can be assumed to be confined entirely within the fibre core. Thus geometrical optics provide an adequate description of the light carrying properties of the fibres.

1.6.3 Optical Properties

Practical losses are apparent in fibres through several mechanisms.

A. Fresnel Reflection Losses

These losses are incurred at the input and output faces of the fibre and are due to the difference in refractive index between the core and the immersion medium.

The fraction of incident light which is reflected at normal incidence, is sufficiently small ($<5\%$) for a wide range of angles.

B. Absorption Losses

The core is not perfectly transparent and transmission through a length L of the core glass is given by

$$T_{\alpha} = e^{-\alpha L} \qquad \text{e.q. 1.17}$$

where α = the absorption coefficient.

The absorption coefficient of the glass varies with the wavelength of light used (see figure I.23), and it is this which determines the wavelength range over which useful transmission may be achieved. Infrared absorptions (from molecular vibrations) and ultraviolet absorptions (from electronic transitions) faintly impinge upon the visible region of the spectrum, where losses due to impurities such as metal ions are apparent.

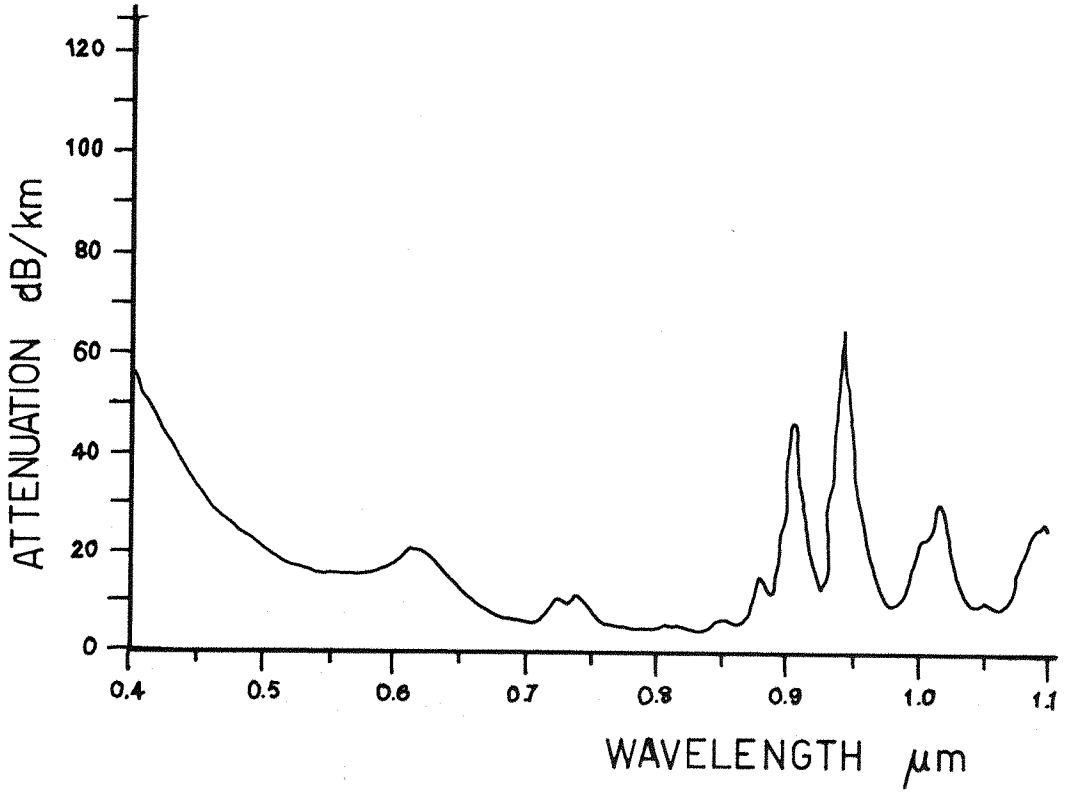

Figure I.23

Graph of absorption versus wavelength for a typical multimode optical fibre.

C. Interface Losses

If there are imperfections in the interface, or if the sheathing is absorbing then the reflection process will tend to fall away from unity.

D. Transmission

The number of reflections suffered by a ray is dependant upon the angle of incidence, and the length of the fibre. The loss per reflection is made up of two parts - energy lost by scattering at an imperfect interface, and absorption or scattering of energy due to its finite penetration into the sheath. The ultimate loss limit however, is set by the Rayleigh scattering which arises from unavoidable fluctuations in the refractive index of the fibre material on a length scale that is small compared to the wavelength of light.

Manufacturers tend to quote losses in optical fibres as an attenuation value, a, which is defined, somewhat arbitrarily, as

$$a = 10 \log \frac{Pi}{Po} \quad \text{dB/km of fibre length} \qquad \text{e.q. 1.19}$$

where Pi and Po are input and output power intensity values respectively. The quoted attenuation value does not generally include Fresnel losses.

1.6.4 Manufacture of Optical Fibres

Optical fibres have been produced from a range of materials. Of these, the most widespread is that used in the first practical applications of the phenomenon (67, 68), silica.*

Until the 1950's, transmission characteristics of light-carrying fibres were poor, because the uncoated core material was exposed to contamination by high-index materials, which resulted in loss of light from the sides of the fibres. In 1954 van Heel (69) coated silica fibres with a solid sheath of plastic with a lower refractive index, and demonstrated the high reflection efficiency required at the glass surface. Basic fibre drawing techniques were developed for the production of glass fibres (70).

Coating glass fibres with glass of lower index (71) led to a resurgence of interest. Since transmission losses were reduced considerably

* Materials other than silica include polymers, non-silica glasses (metal halides and chalcogenides), and crystals. At present research into alternative materials for a variety of applications is widespread.

further development concentrated more on the design of the starting materials, and their efficient, reproducible fabrication.

A. Production of Fused Silica

Large pieces of high quality fused silica have been produced commercially for many years by direct oxy-hydrogen flame (or argon/oxygen plasma torch) soot deposition with simultaneous sintering.

The burners provide enough heat for both the generation of the soot and its immediate sintering to a solid, bubble-free glass when it impacts the hot blank surface. Temperatures on the blank surface must be $\geq 1800^{o}C$ in order to achieve a smooth silica surface which exhibits stable growth. When an oxygen plasma torch is used, the resultant fused silica is both hydroxyl (-OH) free and of high optical quality (see figure 1.24). The glass deposition rate for a single torch is $\sim 0.4g\ min^{-1}$ (72).

B. Efficient Reflection of Light

The refractive index differential between the core and the cladding material can be achieved by one of two methods.

i) Dopants incorporated into the silica can either lower or increase the index of refraction (73). The core material is usually doped with germania (GeO_2) and possibly phosphorus pentoxide (P_2O_3) to enhance n, whereas the cladding may be pure silica, or else it is doped with boron oxide (B_2O_3) at short wavelengths or Fluorine (F) at long wavelengths to depress η . Fibres can also be produced with a pure silica core surrounded by a fluorine-doped silica cladding.

ii) Other coating materials, with lower index, can be used (for example polymers). Plastic clad silica (PCS) fibres, consisting of a high purity, low OH content fused silica core, and high purity silicone rubber cladding were first reported in 1975 (74).

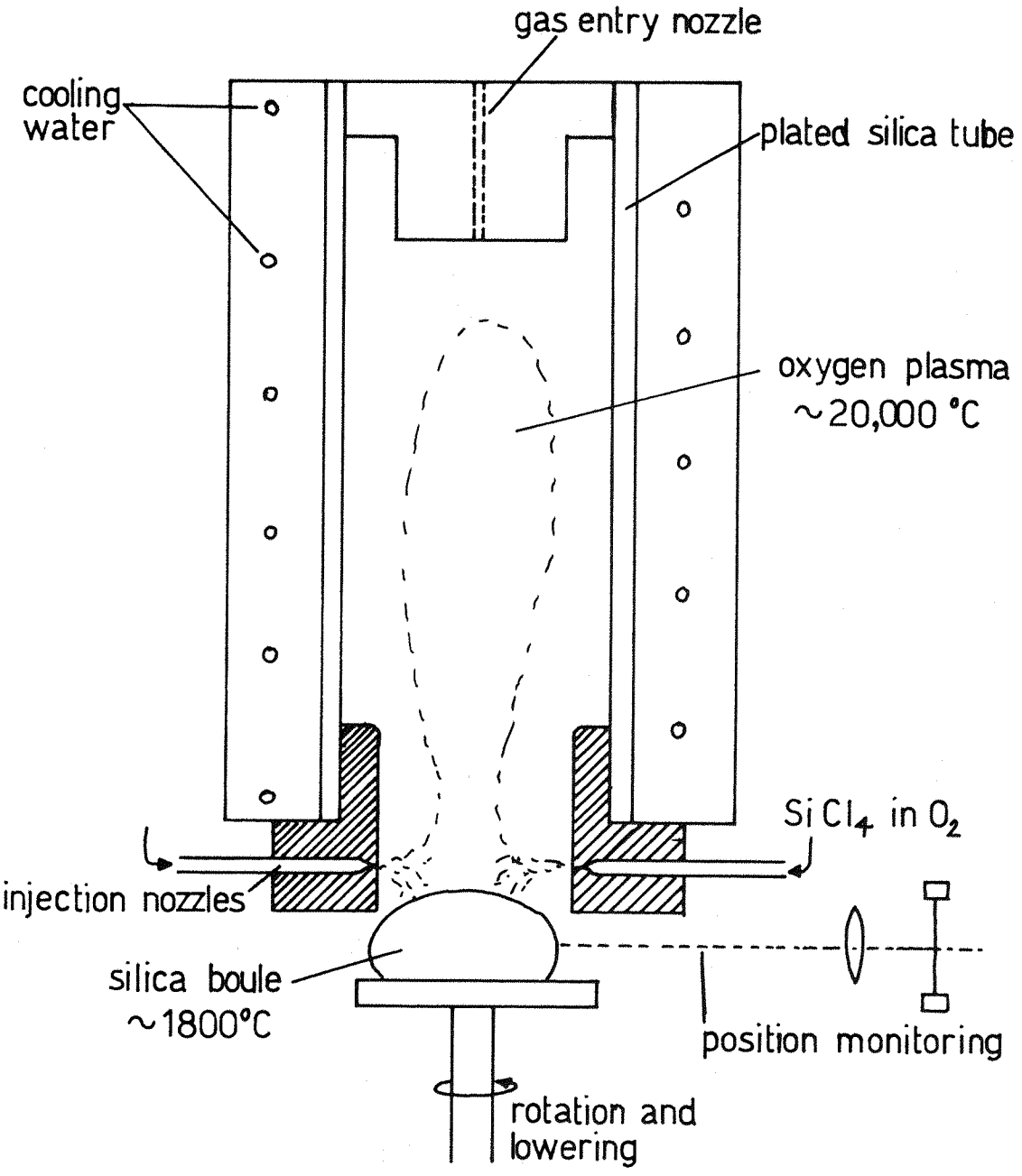

Figure I.24

Production of fused silica using the plasma torch method.

C. Special Techniques of Production

Modified Chemical Vapour Deposition (MCVD)
example; (with Boron as dopant)

A slowly rotating silica tube is heated by a moving burner, and $SiCl_4$, O_2 and BCl_3 gases are fed into the tube (see figure I.25). As the burner moves repeatedly along the tube, SiO_2-B_2O_3 deposits over the entire inner surface of the tube by chemical reaction of the gases. This material becomes the cladding. Next the BCl_3 gas is stopped and the process is resumed. The newly deposited layer consisting of pure silica (SiO_2) becomes the core. The tube is then "collapsed", and a glass rod or "preform" remains. The optical fibre is drawn from the preform. Fused silica "blanks" can also be prepared using an "outside" vapour deposition process.

The Double Crucible Method

This method produces fibres without the need for a preform. A crucible with two compartments, made from platinum, is filled with core and cladding materials. These are melted in a furnace and drawn to produce a fibre (see figure I.25). This simple method is inexpensive and mass reproducible, since the pre-processes required for MCVD are not needed. The fibre is produced at once at fairly high drawing rates ($1-3\ ms^{-1}$) (75).

D. Fibre Coating

The production of PCS fibres uses the same basic coating techniques as those used for the protection of glass-glass fibres, with a pressureless flexible cylindrical die to apply the silicone rubber. Optical monitoring ensures that a constant thickness is maintained throughout the coating procedure.

Practical applications of fibre-optics dictate that the fibres must be able to withstand any physical abuses from their manipulation. Fibres

MCVD (inner deposition method).

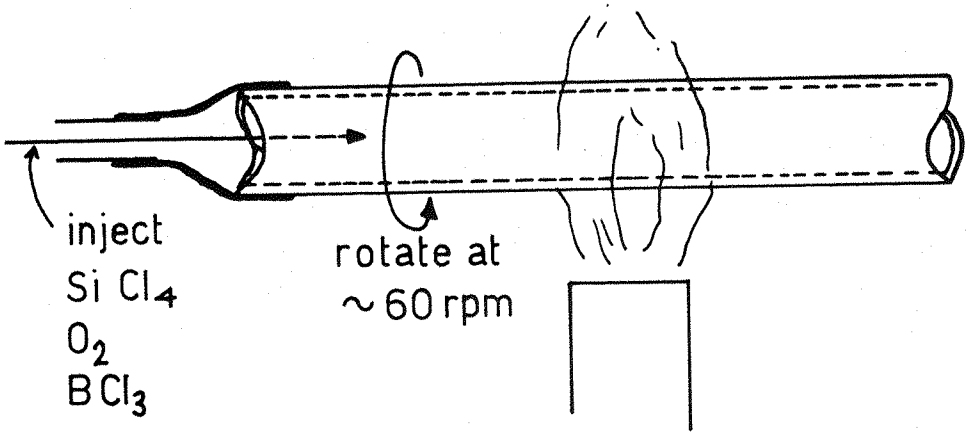

DOUBLE CRUCIBLE METHOD

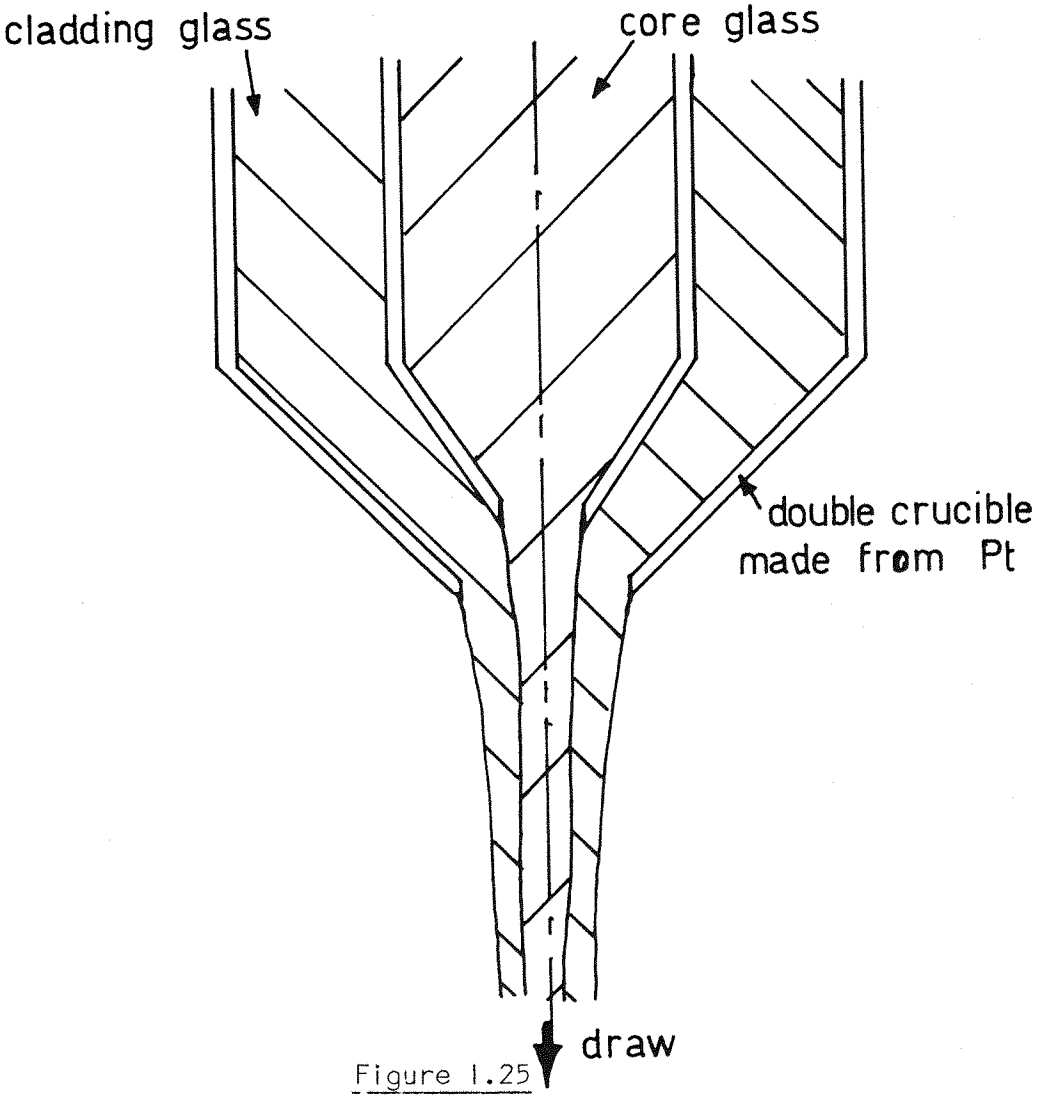

Figure 1.25

Production of optical fibres. (a) Modified chemical vapour deposition (inner deposition method shown), and (b) double crucible method.

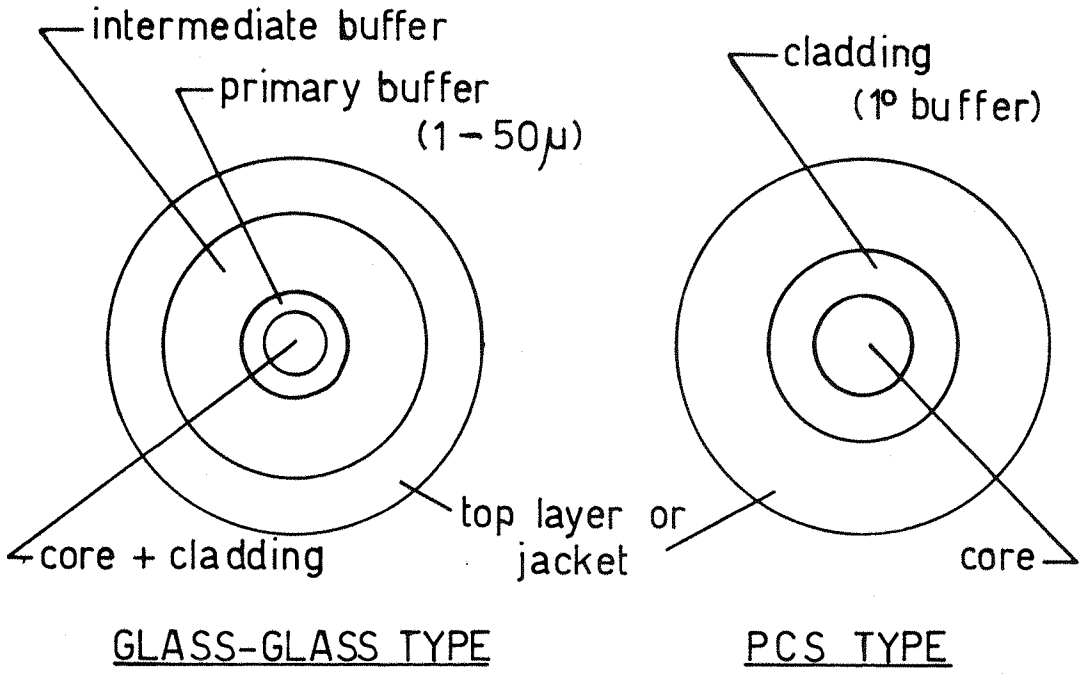

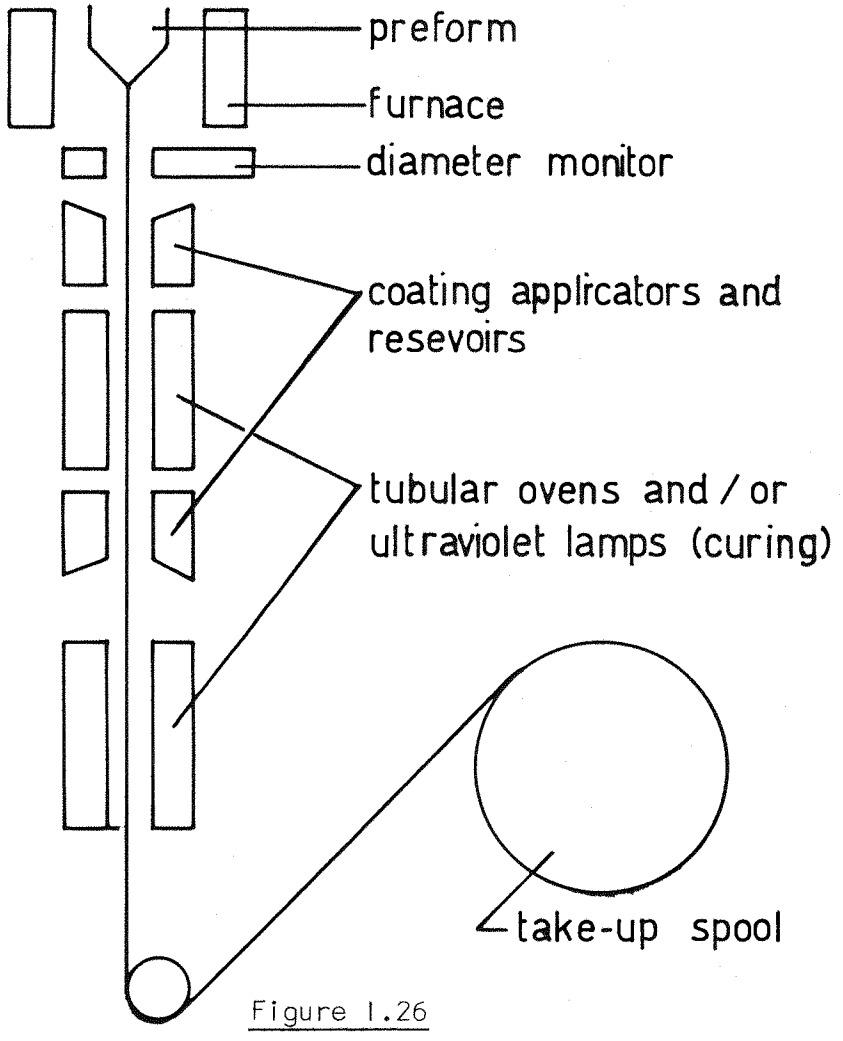

Figure I.26

Typical fibre coating arrangements, and a schematic of the fabrication process.

emerging from any drawing unit will inevitably be flawed (76). The most effective way to protect them, hence maximising their strength and ultimate efficiency limit, is to apply a protective coating immediately after fabrication. A schematic representation of a fibre drawing line is illustrated in figure 1.26.

In the PCS fibre the cladding also acts as the buffer, and there is usually only a single protective coating, for example nylon, needed. This reduces the overall diameter of the PCS system, allowing many fibres to be easily arranged in close proximity.

1.7 Aim

This study directs its attention to the design and construction of a viable fibre-optic system for Raman spectroscopy.

It was intended that, with more understanding of the capabilities of the fibre-optic system, the new method may be used to explore two experimentally demanding problems involving controversial areas in polymer science, namely,

(a) the molecular structure of flowing molten polyethylene, and

(b) low frequency Raman spectroscopy of bulk crystallised polyethylene.

References

1. P.J. Hendra in Vibrational Spectra & Structure, Vol 2 Dekker (1974).
2. P.J. Hendra, I.D.M. Turner, E.J. Loader, M. Stacey, J. Phys. Chem., 31, 300 (1974).
3. I.D.M. Turner, PhD. Thesis, Southampton University (1974).
4. M. Fleischmann, P.J. Hendra, A.J. McQuillan, J. Chem. Soc. Chem. Commun., 80 (1973).
5. M. Fleischmann, P.J. Hendra, A.J. McQuillan, Chem. Phys, Lett., (1973).
6. P.J. Hendra, C.J. Vear, J. Chem. Soc. Chem. Commun., 381 (1972).
7. P.J. Hendra, D.B. Morris, R.D. Sang, H.A. Willis, Polymer, 23, 9 (1982).
8. A.J. Peacock, PhD. Thesis, Southampton (1983).
9. S. Krimm, J. Chem. Phys., 25, 549 (1956).
10. C.V. Raman, K.S. Krishnan, Nature, 121, 501 (1928).
11. A. Smekal, Die Naturwiss, 11, 873 (1923).
12. K.W. Kohlrausch, "Ramanspektren", Leipzig (1943).
13. J. Brandmuller, Naturwiss, 21, 293 (1967).
14. E.R. Lippincott, R.T. Bailey, Spectrochim, Acta., 21, 389 (1965).
15. J.W. Kemp, J.L. Jones, R.W. Durkee, J. Opt. Soc. Amer., 42, 811 (1952).
16. A.W. Reitz, Zeits f. Physik Chemie, B.38, 275 (1937).
17. J.A. Rajchman, R.L. Snyder, Electronics, 13, 20 (1940).
18. D.H. Rank, R. Pfister, D.C. Coleman, J. Opt. Soc. Amer., 32, 390 (1942).
19. R. Pfister, P. Grimm, J. Opt. Soc. Amer, 33, 31 (1943).
20. H.J. Marrinan, J. Opt. Soc. Amer, 43, 1211 (1953).
21. V. Kudrajawzawa, Acta. Physico-Chimica (URSS), 31, 613 (1935).
22. J.P. Gordon, H.J. Zeiger, C.H. Townes, Phys. Rev., 95, 282 (1954).
23. T.H. Maiman, Nature, 187, 493 (1960).
24. S.P.S. Porto, D.L. Wood, J. Opt. Soc. Amer., 52, 251 (1962).
25. B.P. Stoicheff, Proc. 10th Colloq. Spectrosc. Int., Washington 5399 (1963).

26. A. Javan, Phys. Rev. Lett., 3, 518 (1959).

27. A. Javan, W.R. Bennet, D.R. Herriot, Phys. Rev. Lett., 6, 106 (1961).

28. S.P.S. Porto, H. Kogelnik, J. Opt. Soc. Amer., 53, 1446 (1963).

29. R.C. Hawes, K.P. George, D.C. Nelson, R. Beckworth, Anal. Chem, 38, 1942 (1966).

30. M.V. Evans, T.M. Hard, W.F. Murphy, J. Opt. Soc. Amer., 56, 1638 (1966).

31. W.B. Bridges, Appl. Phys. Lett., 128 (1964).

32. W.B. Bridges, Proc. I.E.E.E., 52, 843 (1964).

33. N.C. Craig, Appl. Spectrosc., 33, 475 (1979).

34. D. Landon, S.P.S. Porto, Appl. Opt., 4, 762 (1965).

35. M. Delhaye in Hepple P (ed), 4th Conf. Mol. Spect. Petroleum. Inst. (1968).

36. D.J. Cutler, P.J. Hendra, G.V. Fraser in Developments in Polymer Char. 2., ASP (1978).

37. M. Bridoux, C.R. Heb, Sean. Acad. Sci., 258, 5620 (1964).

38. M. Bridoux, M. Delhaye, Nouv. Rev. Optique, 1, 23 (1970).

39. M. Bridoux, A. Deffontaine, M. Delhaye, F. Grase, K. Reiss, Proc. 5th Int. Conf. Raman Spectrosc., 760 (1976).

40. J.J. Freeman, J. Heaveside, P.J. Hendra, J. Prior, E.S. Reid, Appld. Spectrosc., 35, 196 (1981).

41. A. Deffontaine, M. Bridoux, M. Delhaye, E. Da Silva, W. Hug, Revue Phys. Appl. 19, 415 (1984).

42. T. Hirschfeld, B. Chase, Appl. Spectrosc., 40, 133 (1986).

43. K.P.J. Williams, F.S. Parker, P.J. Hendra, A. Turner, Appl. Spectrosc. (in press)

44. M. Nicol, Developments in Applied Spectroscopy, 10 (1972).

45. J.I. Bryant, Spectrochim. Acta, 24A, 9 (1968).

46. I.R. Beattie, Chem. Britain, 3, 347 (1967).

47. W. Keifer, H.J. Bernstein, Appl. Spectrosc., 25, 500 (1971).

48. J.A. Konigstein. B.F. Gatcher, J. Opt. Soc. Amer., 63, 892 (1972).

49. R.J.H. Clark, P.C. Turtle, Inorg. Chem., 17, 2526 (1978).

50. J.W. Fox, A.T. Tu, Appl. Spectrosc., 33, 647 (1979)

51. S.K. Freeman, D. Landon, Spex. Speaker, 8, 4, (1968).

52. G.J. Long, L.J. Basile, J.R. Ferraro, Appl. Spectrosc., 28, 73 (1974).

53. M. Delhaye, P. Dhamelincourt, J. Raman Spectrosc. 3, 3 (1975).

54. B.W. Cook, J.D. Louden, J. Raman Spectrosc., 8, 249 (1979).

55. M. Moscovits, G.A. Ozin, "Cryochemistry", Wiley, NY (1976).

56. R.P. van Duyne, D.L. Jeanmarie, D.F. Schriver, Anal. Chem., 46, 213 (1974).

57. J. Tyndall, Proc. Roy. Instn., I, 446 (1854).

58. H. Fujii, T. Asabura, S. Jutamulia, S. Kaneko, M. Tsuru, Opt. Laser Tech, 2, 40 (1984).

59. J.I. Peterson, R.V. Fitzgerald, D.K. Buckold, Anal. Chem., 56, 62 (1984).

60. T. Miyashita, T. Manabe, I.E.E.E., J. Quant. Elec., 18, 1432 (1982).

61. G.R. Trott, T.E. Furtak, Rev. Sci. Instrum., 51, 1493 (1980).

62. K. Newby, W.M. Reichert, J.D. Andrade, R.E. Benner, Appl. Opt., 23, 1812 (1984).

63. J.C. Schaeffer, I. Chabay, Opt. Lett., 4, 227 (1979).

64. R.L. McCreery, M. Fleischmann, P.J. Hendra, Anal. Chem., 55, 146 (1983).

65. R.L. McCreery, S.D. Schwab, Anal. Chem., 56, 2199 (1984).

66. R.J. Potter, J. Opt. Soc. Amer., 51, 1079 (1951).

67. J.L. Baird, Brit. Pat., 285, 738 (1927).

68. C.W. Hansell, U.S. Pat., 1, 751, 584 (1930).

69. A.C.S. van Heel, Nature, 173, 39 (1954).

70. H.H. Hopkins, N.S. Kapany, Nature, 173, 39 (1954).

71. B.I. Hirschowitz, L.E. Curtiss, C.W. Peters, H.M. Pollard, Gastroenterology, 35, 50 (1958).

72. K. Nassan, J. Shiever, Am. Ceramic Bull., 54, 11 (1975).

73. S. Tanaka, K. Inada, T. Akimoto, M. Kozina, Electronics Lett., 11, 7 (1975).

74. L. Benbow, C.F. Mitra (eds), "Fibre Optics: Adv. in Research & Development" Plennum (1975).

75. H.F. Wolf (ed), "Handbook of Fibre Optics", Garland (1979).

76. A.K. Banthia, Paintindia, 34, 12 (1984).

CHAPTER 2

INSTRUMENTATION AND EXPERIMENTAL TECHNIQUES

2.1 Raman

2.1.1 Raman Instrumentation

Two spectrometers were used in the course of this study. In both systems the exciting radiation was provided by a Coherent Radiation Innova 90 Argon-ion laser, operating at 5145Å. The plasma lines were removed using an Anaspec Model 300-S pre-monochromator in each case.

ANASPEC LR-36 LASER RAMAN SPECTROPHOTOMETER

In this instrument a short focal length spectrograph defines the spectral region of interest. Its exit aperture is imaged onto a second and larger spectrograph, which runs in subtractive dispersion with its partner. (The second spectrograph has a focal length exactly twice that of the first.) The design of the system is such that it achieves the dispersion of a single monochromator of short focal length, allowing a spectral region[+] of approximately $900cm^{-1}$ to be viewed at any one time by the multiplex detector. The image emerging from the second spectrograph is projected onto an intensified diode array detector containing 1024 elements over an area of $\sim 25mm^2$. The cooled detector head is connected to a Tracor Northern TN1710 data collection unit for information display and manipulation, and a printer for hard copy.

All of the instrumental functions, e.g. bandpass, spectral region, etc. are microcomputer controlled, and the TN1710 provides excellent data handling facilities, including addition/subtraction of spectra, multiplication/division, integration/differentiation, normalisation and Savitzky/Golay smoothing. An optical schematic of the system is presented in figure 2.1.

The instrument has a number of advantages including rapid data acquisition, the ability to use "overnight exposure" techniques, and excellent data storage and plotting facilities. However, the instrument at Southampton was a prototype and as such has suffered numerous teething

[+]wavelength dependant

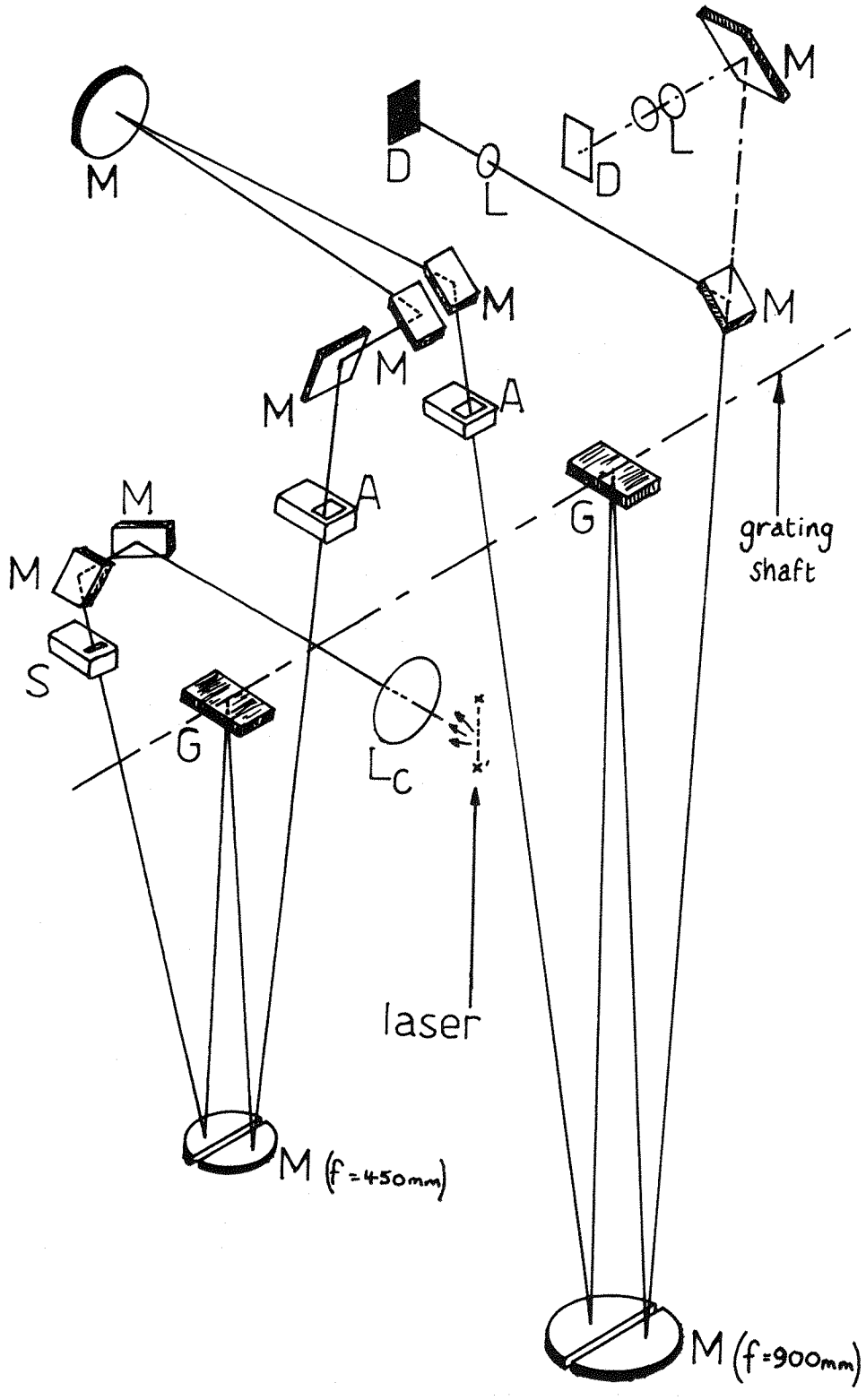

Figure 2.1

Optical schematic of Anaspec LR-36 Laser Raman Spectrograph. M = mirror, L = lens (L_C = collection lens), A = aperture, G = grating, S = slit, D = detector. Sample is in plane x------x.

troubles such as a high incidence of stray light, and some non-linearity in the diode array. The detector had a tendency to overload with high light intensities, and careful monitoring was required when using long time exposures.

The real problem with the LR-36 was the relatively high noise value. Recently, a detector cooling system has been introduced in an attempt to reduce noise. This has been partially successful, but many of the problems mentioned have involved a great loss in user time.

THE CODERG T800 TRIPLE MONOCHROMATOR SPECTROMETER

This is a scanning instrument, employing a triple monochromator running in additive dispersion. Photomultiplier pulses are handled by an Ortec-Brookdeal 5CI pulse counter, and displayed via a digital-to-analogue converter on a chart recorder. Scanning speeds of between 1 and 200cm^{-1} per minute are available. There is also an iterative scanning module available, which has recently been introduced to an IBM-PC, which now allows disc storage and the facility for basic data manipulation.

The stray light performance of the Coderg is excellent, and allows conventional spectra to be recorded to within 6cm^{-1} from the exciting line. An optical diagram can be found in figure 2.2.

The Coderg T800 proved to be by far the superior instrument of the two. The Anaspec LR-36 has value only in routine work on strong Raman scatterers. Although most of the development of the fibre-optic system was performed on the Anaspec, because of its instant display capabilities, the experimental work described in chapters 3 and 4 of this thesis was completed using the Coderg T800.

2.1.2 Experimental Technique

Raman work on the Anaspec is detailed in Section 2.2

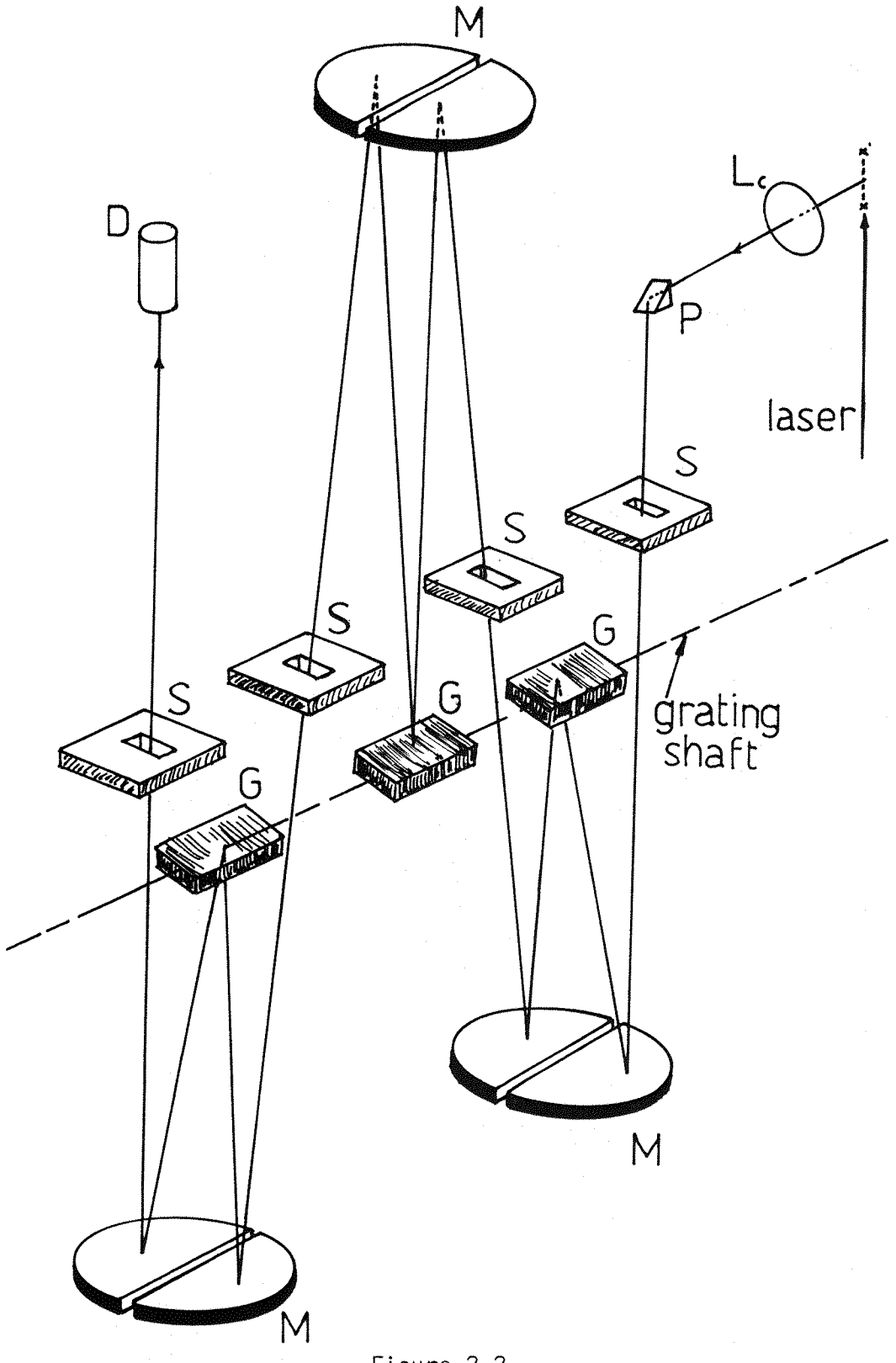

Figure 2.2

Optical schematic of the Coderg T800 laser Raman spectrometer. L_C = collection lens, P = prism, S = slit, M = mirror, G = diffraction grating, D = photomultiplier detection. Sample is in plane x----x'.

The frequency range was calibrated using the exciting line for low frequency work and the fluorescent lighting peaks at $\Delta\nu$ = 1122.2cm^{-1} for the frequency range 1000cm^{-1} - 1500cm^{-1}. Both methods gave the frequency to better than ±0.5cm^{-1}. The intensity of light at the sample was generally set at 100mW, and the high temperature spectra were run at slit widths of 10cm^{-1}, room temperature spectra were recorded at 4cm^{-1} slit width for crystallinity measurements, and low frequency spectra (close to the exciting line) were recorded with a slit width of 1cm^{-1}.

When fibre-optic sampling techniques were not employed, conventional 90° sampling arrangements were used for polymer samples, as shown in figure 1.17(d).

2.2 Fibre-Optic System Design for Raman Spectrophotometry

Based on previous experience the sample is excited by laser radiation emitted from one fibre (the input) and the scattered light collected by a second fibre returning it to the focus of the spectrometer collection optics (see figure 2.3).

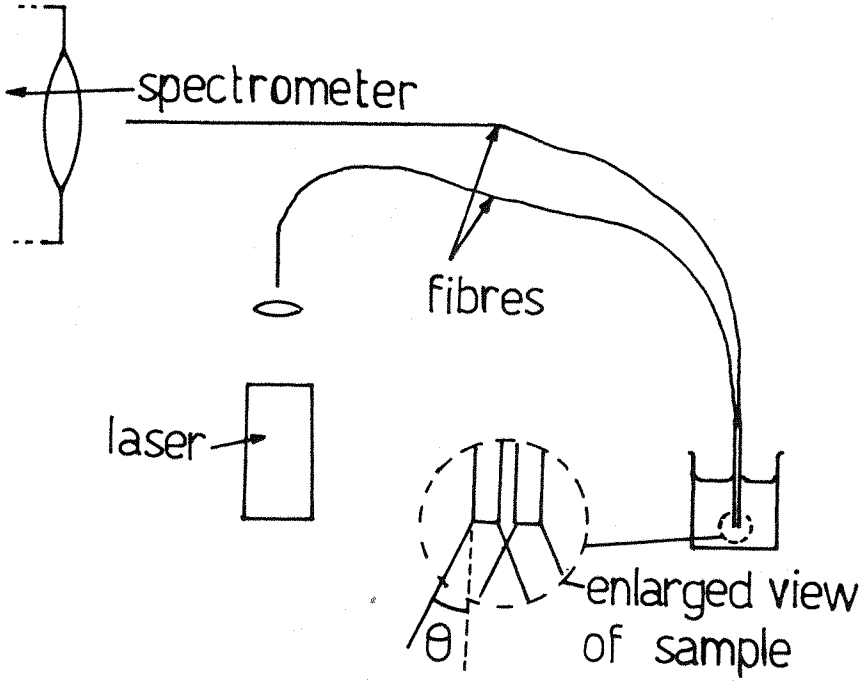

Figure 2.3

Sampling arrangement in McCreery work.

A modified commercial spatial filter collects the laser beam inside the pre-sample optics of the spectrometer. The radiation used is always that filtered by the pre-monochromator, and never the 'raw' laser output. A microscope objective lens (see figure 2.4) focuses the laser beam down onto the end face of the fibre which is securely held in the centre of a pin chuck. The fibre is always gripped by the cladding, not the bared fibre end, and is triaxially adjustable with respect to the microscope objective.

In the subsequent experiments the optical fibre used was of the plastic coated silica (p.c.s.) type; a standard 200μ core telecommunications fibre with a 125μ silicone rubber cladding and a protective nylon overcoating.

The whole system is securely mounted on rails within a specially constructed box, such that the conventional spectrometer optics are not modified in any way. The spatial filter can be reproducibly placed in the exact position for injection of the laser beam into the fibre.

The light is then transmitted to the sample where a second fibre collects some of the scattered radiation. (The arrangement of the fibres at the sample will be considered later.) This is returned to an adjustable mount in the sample compartment of the spectrometer (figure 2.4). Conventional reverse illumination and Raman peak maximisation techniques were used to align the fibre with respect to the spectrometer.

The reverse illumination system is designed to aid alignment of the laser beam with respect to the collection optics of the spectrometer. The slit may be viewed through the collection lens of the instrument when the back illumination light is turned on, and a low-intensity laser beam can be aligned with the imaginary projected image of the slit using the rule of no parallax. Once the beam is in the correct position, the fibre on the adjustable mount may be moved such that the beam glances the tip (see figure 2.5(a). This accurately

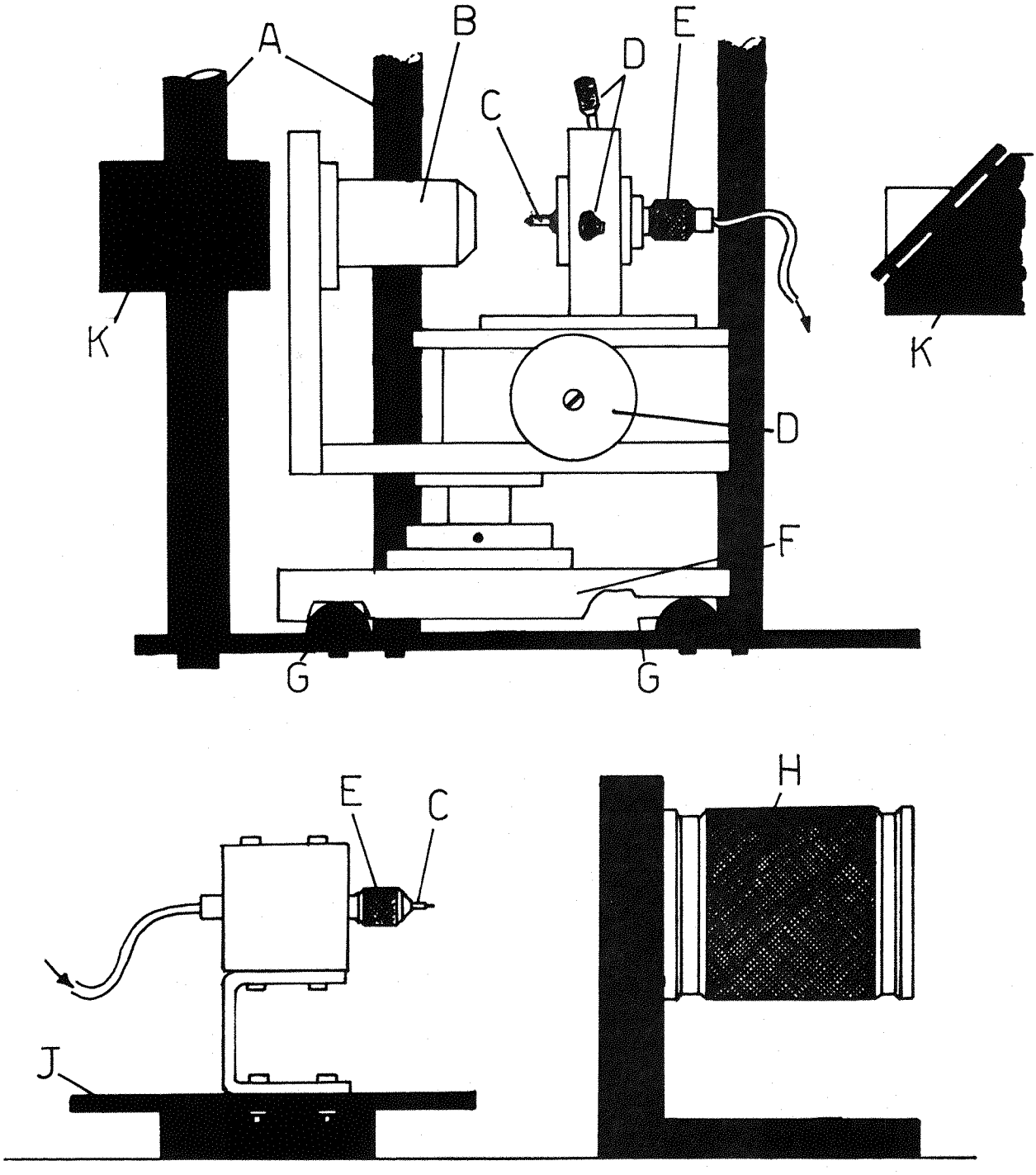

Figure 2.4

Fibre-optic injection and collection system as installed in LR-36 spectrometer sample cabinet. A = support rods, B = objective lens, C = optical fibre, D = adjustment screws, E = pin chuck, F = saddle, G = rails, H = spectrometer collection lens, J = xyz adjustable sample table, K = prism mounting blocks in conventional optical train

locates the end of the fibre in the 'y' and 'z' axis, and the 'x' coordinate can be estimated by eye.

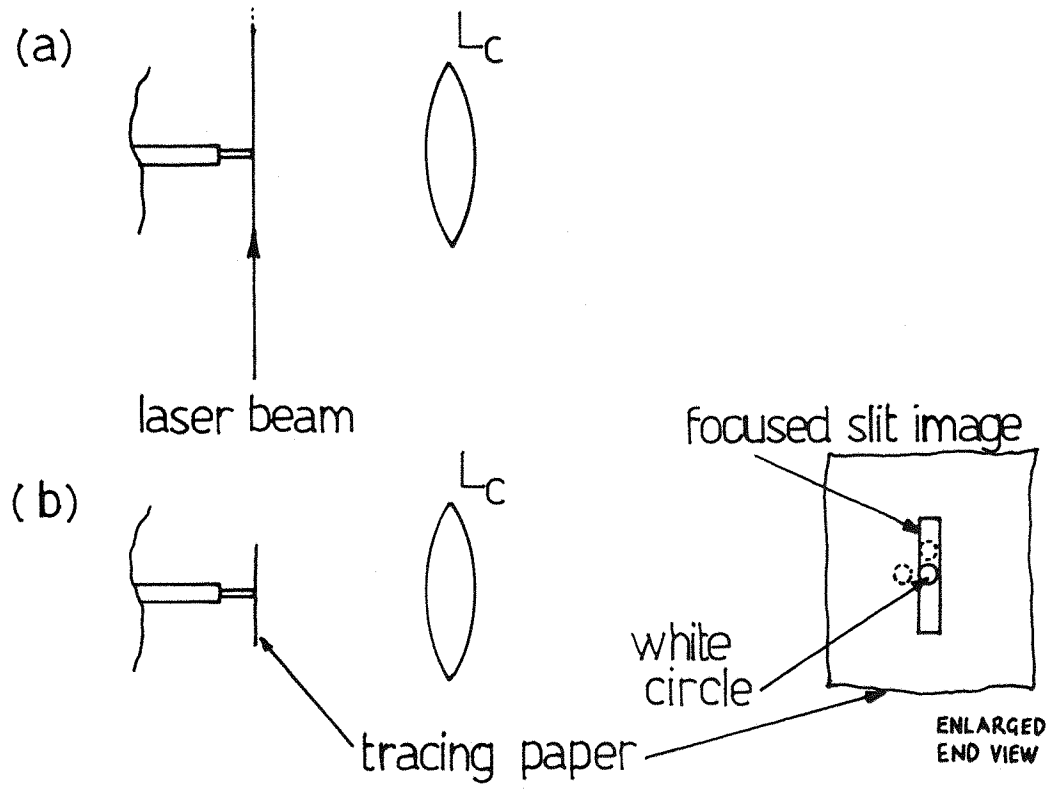

Figure 2.5

Use of the back illumination system to align optical fibre collection unit; (a) laser beam method, (b) tracing paper method. L_C = collection lens.

If the back projection lamp is powerful enough, an image of the slit can be located in a dark sample cabinet using a piece of tracing paper. The fibre may then be moved up to the well focused image and lined up almost exactly with the slit (see figure 2.5(b)), using the small white circle of light transmitted by the fibre from the outside of the cabinet.

2.2.1 Preparation of the Fibre

The protective coating and cladding material is stripped back for about 20mm, using a fibre stripping tool (or by using thin fishing

wire if there is no protective overcoating). A fine scratch is then scored on the fibre perpendicular to its axis, a few millimetres from the end of the cladding, using a keen glass cutting blade* (e.g. Jencons "King Cut"). The fibre is then wetted and will break at the score using a small amount of pressure (see figure 2.6). The cleaved fibre is then placed in the fibre illuminator and inspected by eye through the microscope objective. The end should appear perfect and show no chipping, distortion or asymmetry. (Poor end quality can be avoided if the glass cutting blade is well protected and only used for cleaving fibres. The score must be a single stroke and if the score is good, hardly any pressure is required to produce a clean break).

To further test the quality of both input and output faces of the laser transmitting fibre, the fibre should be illuminated with laser light in the usual way and the output projected onto a screen placed about 30cm away from the end of the fibre. A finely speckled, round, evenly illuminated patch of light should appear. A damaged fibre end will result in failure of this test.

Asymmetry or skew in the projected pattern indicates poor end quality, and misalignment or poor end quality at the illuminator is manifested by a relatively low intensity pattern on the screen. A ring output (see figure 2.7) indicates focus error in the illuminator, transporting light through the cladding material rather than the core.

Thinner fibres can be prepared with greater ease than thicker fibres. Experiments with core sizes of 600μ showed a rejection rate of approximately 90% using the above method of preparation, with 200μ core approximately 25% were rejected, and with 50μ core less than 10% proved unsatisfactory. Polishing fibre ends in an attempt to improve end quality was difficult, time consuming and with the 200μ fibre the performance was poorer than that obtained using the cleaving method.

*Note:- This blade should be exclusively used for the preparation of optical fibres.

1. Stripping.

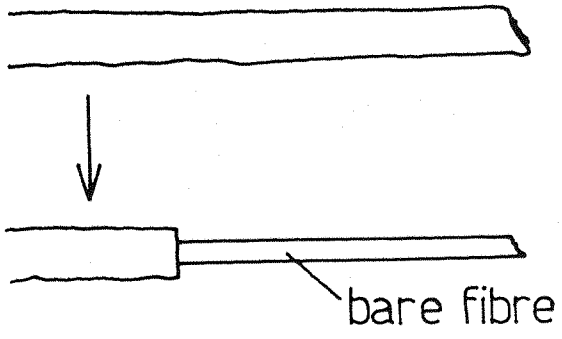

2. Scoring.

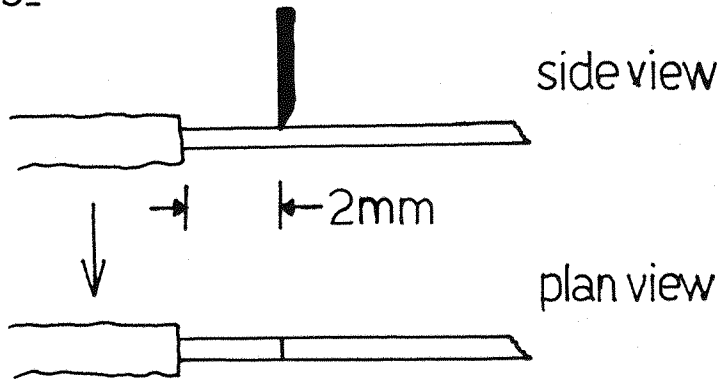

3. Wetting and breaking.

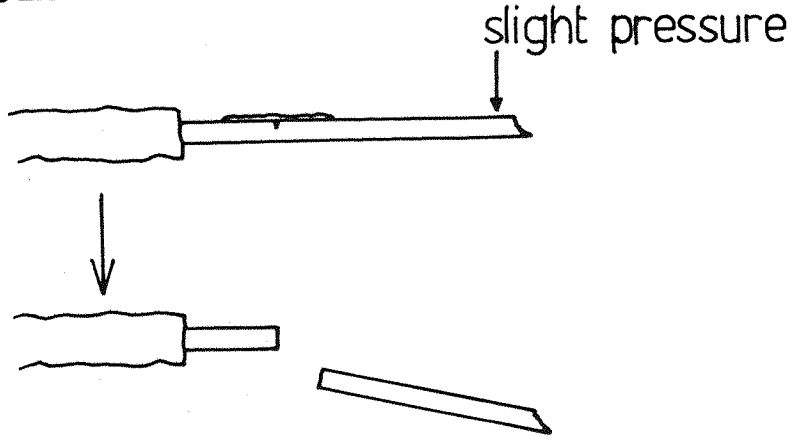

Figure 2.6

End preparation of an optical fibre

Common image phenotypes	Description	Remedy
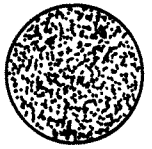	Perfect image	-
	Chipped* or distorted image	Repeat end face preparation
	'ring' image	Check injection system alignment
	Low power	Check laser power, check injection end face quality and alignment

Figure 2.7

Image projected onto screen from the output of a laser stimulated optical fibre: Diagnosis chart

* Some chipped fibres give an acceptable Raman performance.

2.2.2 Illumination of the Fibre

If the laser beam is focused onto the fibre using a x10 objective lens (f = 16.9mm) a beam waist diameter (Wo) of 22μ is achieved at the focus, if an Ar^+ laser beam with a diameter (d) of 1mm is used (see figure 2.8). However, this relationship applies

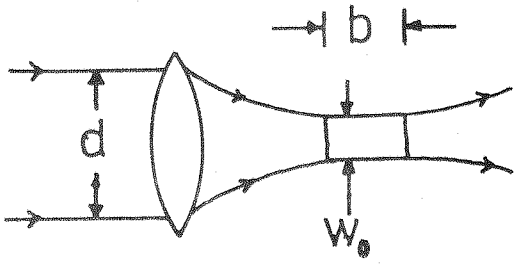

$\lambda = 514.5nm$
$d = 1.0mm$

$$w_o = 8\lambda f / \pi d$$
$$b = 8\lambda f^2 / \pi d^2$$

Figure 2.8

Diffraction limited spot size of a focused laser beam.

only for a perfectly collimated, coherent, Gaussian beam. None of these characteristics apply in the case of the source radiation typically available from a commercial laser as fitted to a Raman spectrometer i.e. the value of 'd' and the subsequent waist diameter are larger than those expected. The focal length of the objective (i.e. its power) should be such that the focused beam arriving at the fibre end has a cone angle of 2θ or a little less to efficiently illuminate the fibre end (see figure 1.20). Further, the focused spot must be significantly smaller than the end face of the fibre.

Since many of the parameters are unknown on a commercial spectrometer, several microscope objectives were considered and their efficiency of illumination recorded (see table 2.1). Although the x40 (f = 4.38mm) objective lens provides the closest aperture match to the optical fibre, the depth of focus for this lens is very small and difficult to locate on the fibre end. However, the x20 (f = 8.13mm) objective lens has a depth focus $3\frac{1}{2}$ times greater than that of the x40 lens, and consequently gave marginally better performance in this study.

Objective lens	Focal length f*(mm)	Lens half angle, θ_L, + assuming a collimated laser beam 1.0mm diameter λ = 514.5nm (degrees)	Calculated waist diameter ω_o (μ)	b_o (μ)	Overall illumination efficiency (arbitrary units)
x 10	16.90	3.5	22	374	11
x 20	8.13	7.1	11	87	41
x 40	4.38	13.2	6	25	36
x 60	2.85	20.5	4	11	11

* supplied by Gallenkamp UK Ltd.

+ The fibre used had the following characteristics 200μ core
NA = 0.26
θ = 15°

NB If the laser beam had satisfied the characteristics in column 3 an objective of approximately 50x would have been ideal. Column 6 demonstrates that the beam characteristics used were poor.

TABLE 2.1

Overall illumination efficiency and lens characteristics of injection objective lenses

2.2.3 Throughput

Once an evenly illuminated circle of light is achieved, a power meter can be set up to record the laser intensity at the exit face of the fibre. If allignment is adequate at injection and an appropriate objective lens has been selected, a good quality multimode plastic-coated silica (PCS) fibre 200μ in diameter should transmit 70% or more of the radiation, defined as

$$\text{Efficiency} = \frac{\text{Total power from end face of fibre}}{\text{Energy entering spatial filter}} \times 100\%$$

over a 3 meter length of fibre. In our experience thinner fibres transmit significantly less than the above. The vast majority of losses are experienced in coupling. The losses in transmission down the fibre due to inhomogeneties were estimated at 1.5% per metre for a 3 metre length of fibre using laser light of wavelength 514.5nm.

2.2.4 Collection

The optimum method for illuminating the sample and collecting the radiation was investigated. A series of Raman experiments were carried out using the intensity of selected Raman lines and comparing them with one another in different experimental arrangements. Where appropriate, the efficiency of the fibre-optic experiment was compared against conventional excitation (figure 1.17(d) and (e)).

In all cases constant laser power and spectral slit width were used.

A. Angular Dependence

The input fibre was positioned vertically in a sample of nitro-benzene and the collection fibre was placed adjacent to the input end face on an angularly adjustable mount. The angle subtended between the input and output fibres was varied and spectra collected at a number of positions. The fibre ends remained in contact throughout their rotation at a point adjacent to the end face (see figure 2.9(b)). For each angular displacement the signal at the spectrometer was optimised

using lateral adjustment of the input fibre, to ensure that the fibres remained in the same plane.

Measurements of the Raman intensity of the $\Delta\nu$ = 1346cm^{-1} band (aromatic ring breathing mode) were made at each angle and plotted against the subtended angle in figure 2.9(b).

The Raman intensity of the peak was taken as the peak height (maximum) minus a background value at around $\Delta\nu$ = 1320cm^{-1}. There were no variations in the peak intensity of this band relative to the other bands in the spectrum, nor in the background profile, with variation of angle.

The parallel orientation appears to be the most efficient.

B. Vertical and Axial Spacing Dependence

Two fibres were held parallel to one another and lowered vertically into a sample of nitrobenzene. The input fibre was secured and the collection fibre was moved relative to it. The displacements were monitored using a travelling microscope. Ten values of Raman intensity were recorded for each incremental change and a graph of displacement versus the Raman intensity of the $\Delta\nu$ = 1346cm^{-1} band in nitrobenzene was plotted in figure 2.9(a).

From vertical adjustment of the fibres the maximum intensity was obtained when the end face of the collection fibre was placed about 2mm above that of the injection fibre. This can be explained in terms of simple geometry by considering the overlap of the two 'cones' defined by the numerical aperture of the fibres.

The exit numerical aperture in nitrobenzene is different from that in air;

$$NA_{\text{nitrobenzene}} = \frac{NA_{\text{air}}}{(\text{nitrobenzene})}$$

$$= \frac{0.26}{1.553} = 0.7, \quad \underline{\theta \simeq 9.6^{o}}$$

where = refractive index of nitrobenzene.

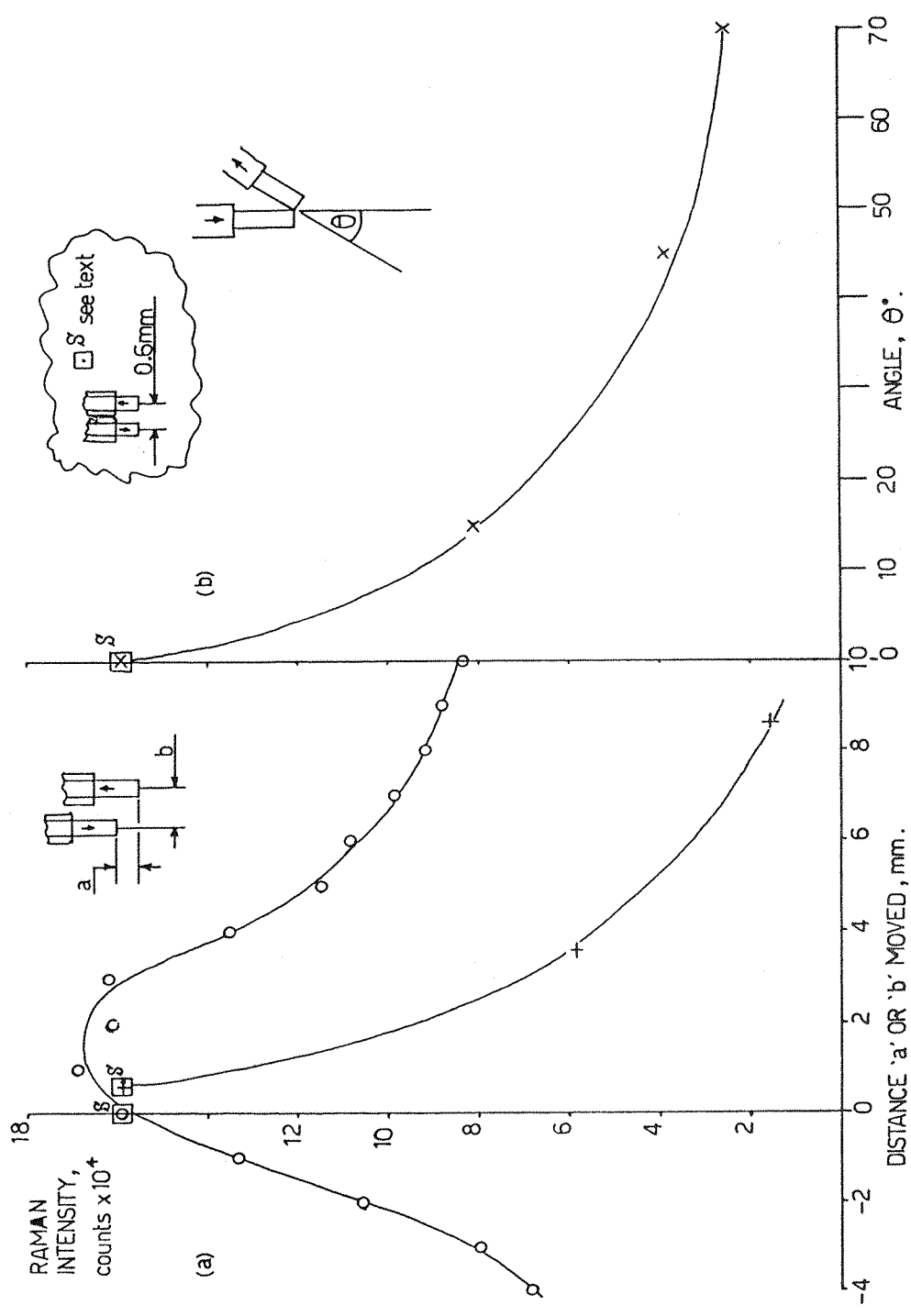

Figure 2.9

Variation in Raman intensity of the $\Delta\nu$ = 1346cm^{-1} band in nitrobenzene recorded using optical fibres, versus; (a) vertical and axial spacing of fibres, where o = variation of 'a' (b=0.6mm) and + = variation of 'b' (a=o); (b) angle of fibres, with respect to one another.

The intensity of light emitted from the input fibre falls off with distance, x, travelled into the sample. Thus, the contribution to the Raman intensity I_R from a point scatterer will be reduced the further into the sample that it lies (see figure 2.10(a); $I_R(X_1) > I_R(X_2)$.

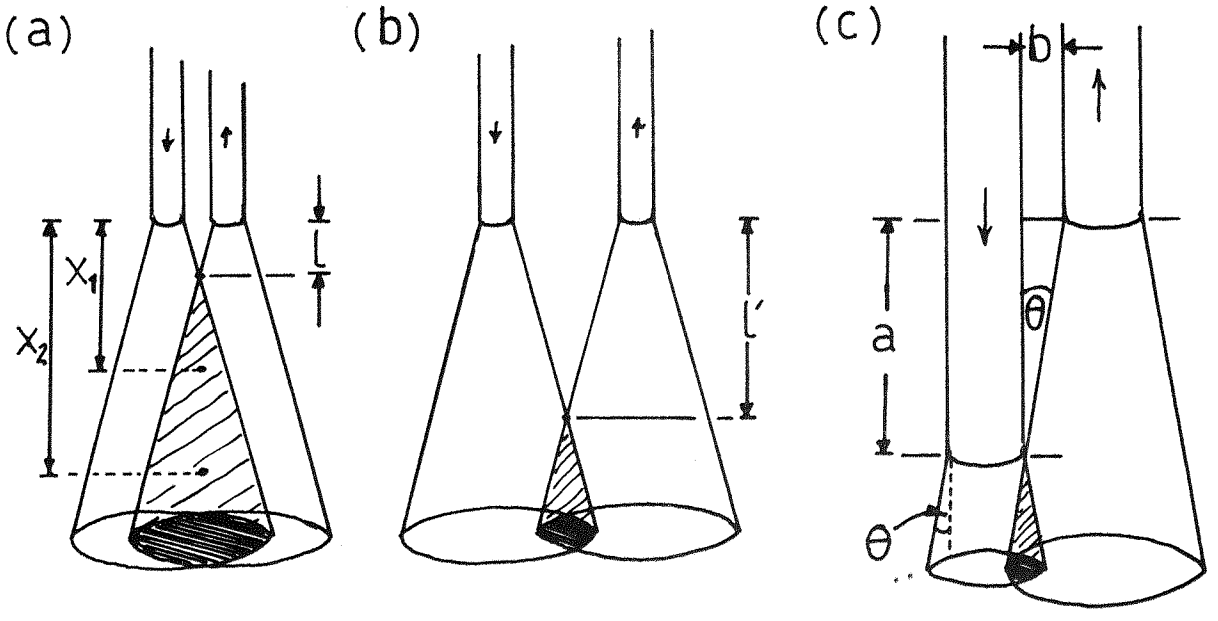

Figure 2.10

Projected cone overlap for two optical fibres in a liquid sample.
NB changes with the index of refraction of the sample

The incremental distance of the input, a, for maximum overlap can be calculated from $a = b/\tan\theta$. (2.10(b). A value of 2.35mm verifies the maximum in the curve in figure 2.10. An increase in 'b' by separation of the fibres axially will alter the depth into the sample, l, at which the 'cones' overlap. From figure 2.10(c) we can see that this is the case and consequently the intensity of the Raman signal is lowered; as 'b' increases, 'l' increases and $I_R(L)$ is reduced.

C. 90° Collection

Preliminary observations with a 90° collection system given a variety of relative input and output fibre positions, show very poor Raman signals when compared with the above.

D. Capillary Experiments

Using an internally reflecting tube all optical arrangements outperform the bare fibres, particularly if the tube diameter is small. Using small bore thick walled glass tubing the improvement is quite dramatic, giving approximately 25% of the signal intensity of that available using conventional (lens) excitation, using only a single collection fibre. The experimental arrangements are shown in figure 2.11. Further, the intensity of the signal increases with 'x' in figure 2.11 up to a value of 60mm (see figure 2.11(b)).

2.2.5 Refractive Index of Liquids

In order to vary the refractive index a range of liquids were selected. All of the liquids except nitrobenzene were colourless. In this case a comparison of fibre-optic experiments were made with conventionally excited spectra.*

The experimental arrangements are as in figure 1.17e and the point 's' in figure 2.9. It will be noted from table 2.2 that there is no correlation between index of refraction and Raman efficiency.

An interesting result was obtained when monitoring the -OH stretch at $\Delta\nu \sim 3400 cm^{-1}$ in water and milk. A significant improvement in the signal intensity was observed. This must be related to the turbidity of the sample.

2.2.6 Solids

(A) Powdered Samples

A variety of solid samples were considered in powdered or granular form. The fibre probe was embedded several millimetres into the samples. This resulted in much stronger signals being detected than when the fibres were suspended just above the powder surface.

* The absolute Raman intensity, however, excited, depends upon the index of refraction. No special allowance is made for this effect. It is assumed to apply equally regardless of the method of illumination.

Sample	Refractive Index	% relative intensity	$\Delta\nu$,cm^{-1}
LIQUIDS:			
Water	1.3330	3.5	3400
Diethyl ether	1.3538	1.0+	1458
Acetone	1.3620	1.1+	805
Carbon tetrachloride	1.4607	4.2	471
Glycerol	1.4730	1.3+	1469
Decalin	1.4758	2.6	1448
Turpentine	1.4800	0.6+	1457
Xylene	1.4933	1.4+	1009
Toluene	1.4969	1.7	1010
Benzene	1.5011	2.0	1000
Nitrobenzene	1.5530	2.4	1346
Milk	-	37.0	3400
POWDERS:			
Potassium oxalate		46	1452
Potassium carbonate		340	1061
Polyethylene: rigidex 50		118	1295
rigidex 006-60		152	1295
Polytetrafluroethylene		246	725
BULK:			
Polyethylene 006-60 ++		26	1295
Polyethylene 006-60, ++ wrapped in foil		49	1295
Potassium chromate +++		82	1562

\+ weak signals; recorded on different settings and ratioed.

++ extruded onto fibre probe.

+++ crystallised onto end of fibre probe.

TABLE 2.2

Relative Raman intensities (expressed as a % of the signal intensity using conventional methods) obtained from a number of samples with the fibre-optic sampling system.

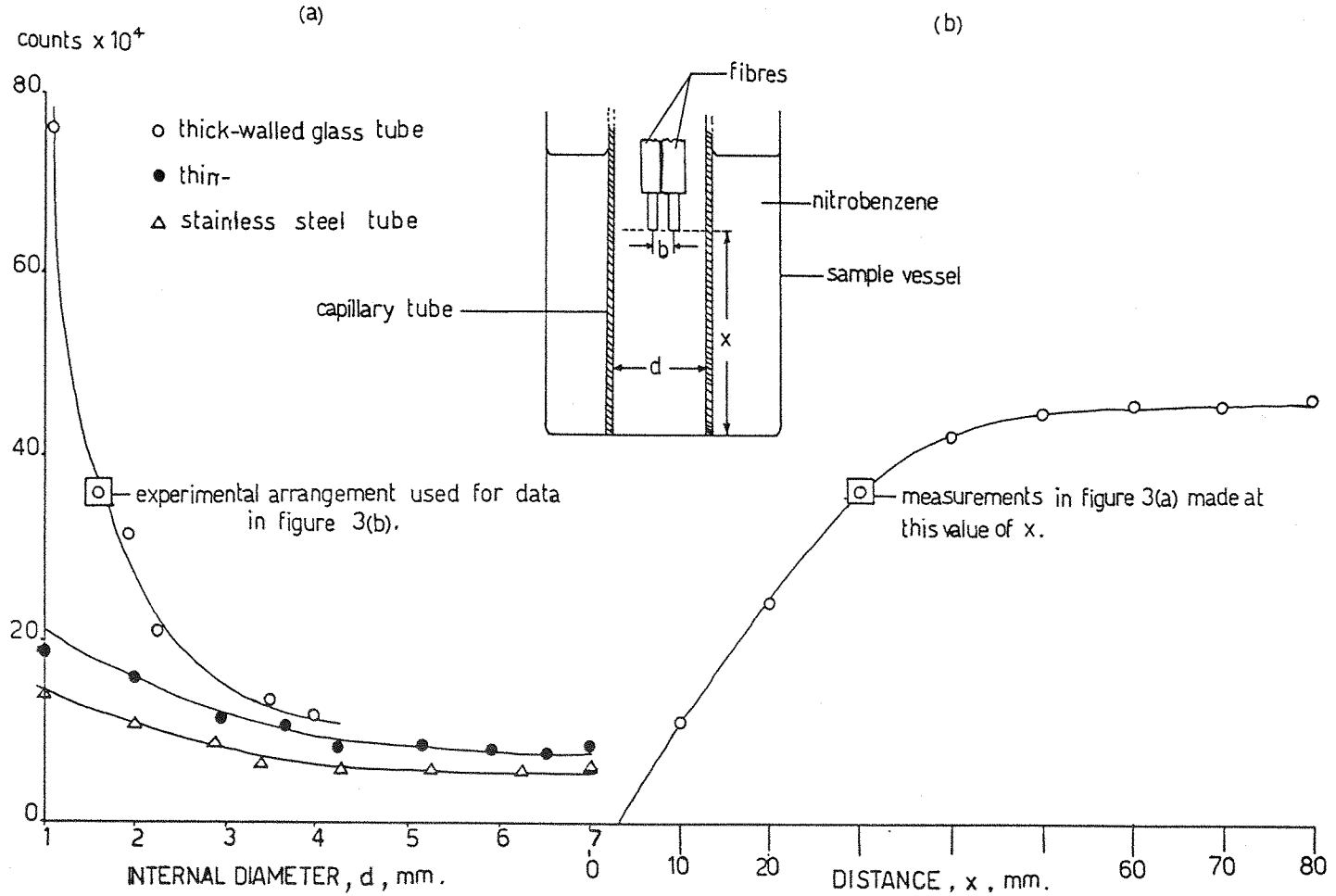

Figure 2.11

Raman intensity of the $\Delta\nu = 1346 cm^{-1}$ band in nitrobenzene, recorded inside capillary tubing with parallel input and output fibres (b = 0.6mm). II(a) variation of internal diameter, d, of capillaries (x = 30mm); II(b) variation of sample depth, x, inside a capillary of internal diameter, d = 1.7mm

It is clear that conventional and fibre-optic illumination are of similar efficacy. There is some indication that fine powders perform better than coarse ones.

When studying powders, one input and one collection fibre appears to be a favourable method when compared with conventional (lens) excitation (see table 2.2). An indication of the quality of the spectra obtained is given in figures 2.12 and 2.13.

For many experiments it would be advantageous to study the sample with fibre ends suspended rather than embedded. It appears that the Raman signal falls in intensity when the fibres are removed from the powder. The fall being greater when the powder is coarse.

If the powder is introduced into an internally reflecting capillary tube then an improvement in signal intensity can be observed similar to that in liquids, and this may be a useful method when only relatively small amounts of the sample are available.

Raman spectra of polytetrafluroethylene (PTFE) powder recorded using both fibre-optic and conventional lens excitation are shown in figure 2.14. PTFE is notably a difficult sample to record due to very high background levels.

(B) Bulk Samples

Having studied liquids in contact with the fibres, and powders touching the fibres it was decided to investigate solids in mutual contact with the fibre surfaces.

Polyethylene. The fibre-optic probe was embedded into freshly extruded molten polyethylene (BP Rigidex 006-60) which was then compressed so that there was close contact between the fibre ends and the polymer. The extrudate, once allowed to cool, was then cut into a manageable block (see figure 2.15). The fibres were introduced into the injection

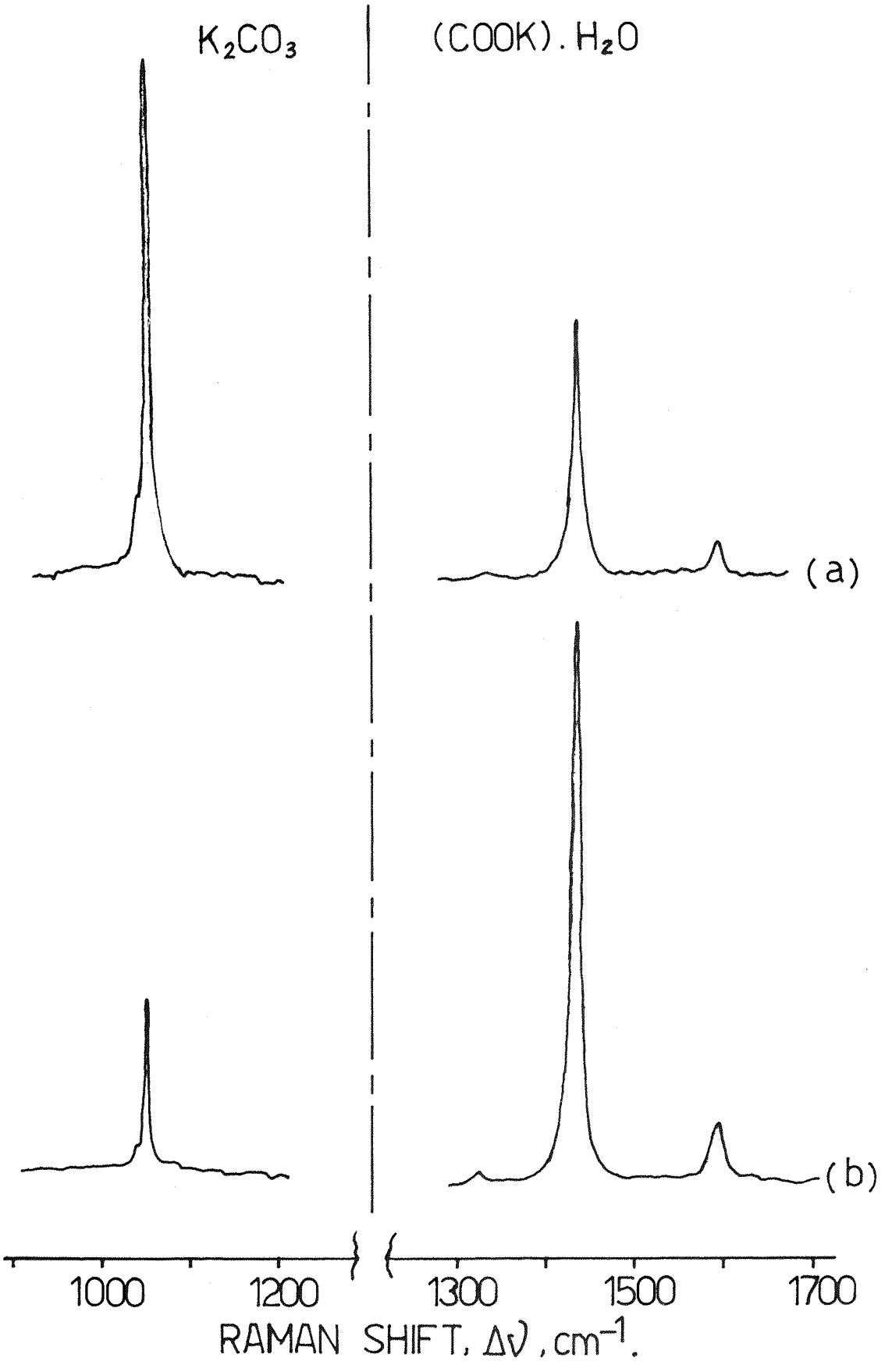

Figure 2.12

Raman spectra of potassium carbonate and potassium oxalate recorded, (a) with fibre-optics, and (b) conventionally

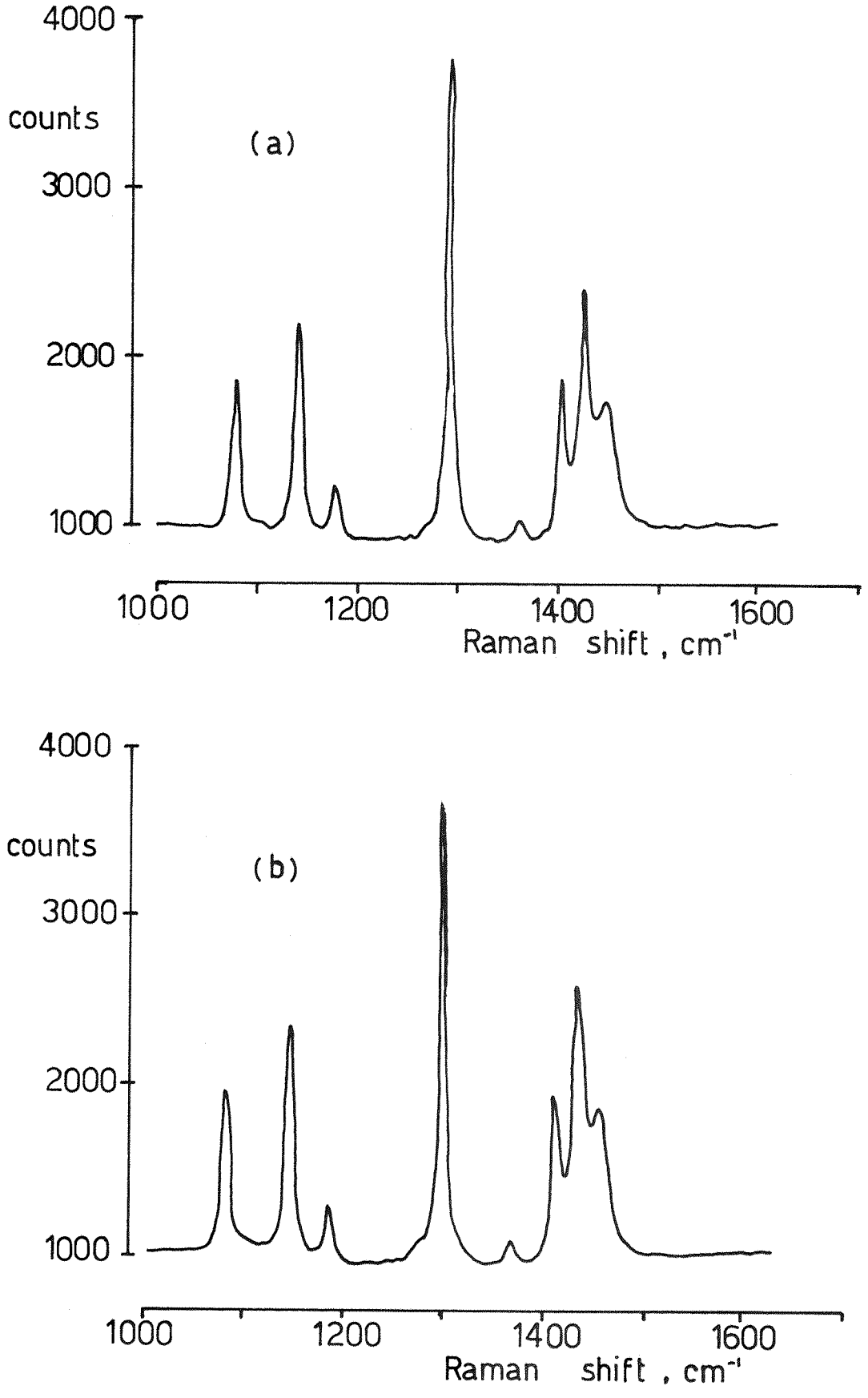

Figure 2.13

Raman spectra of polyethylene (Rigidex 50 powder) recorded, (a) with fibre-optics, and (b) conventionally

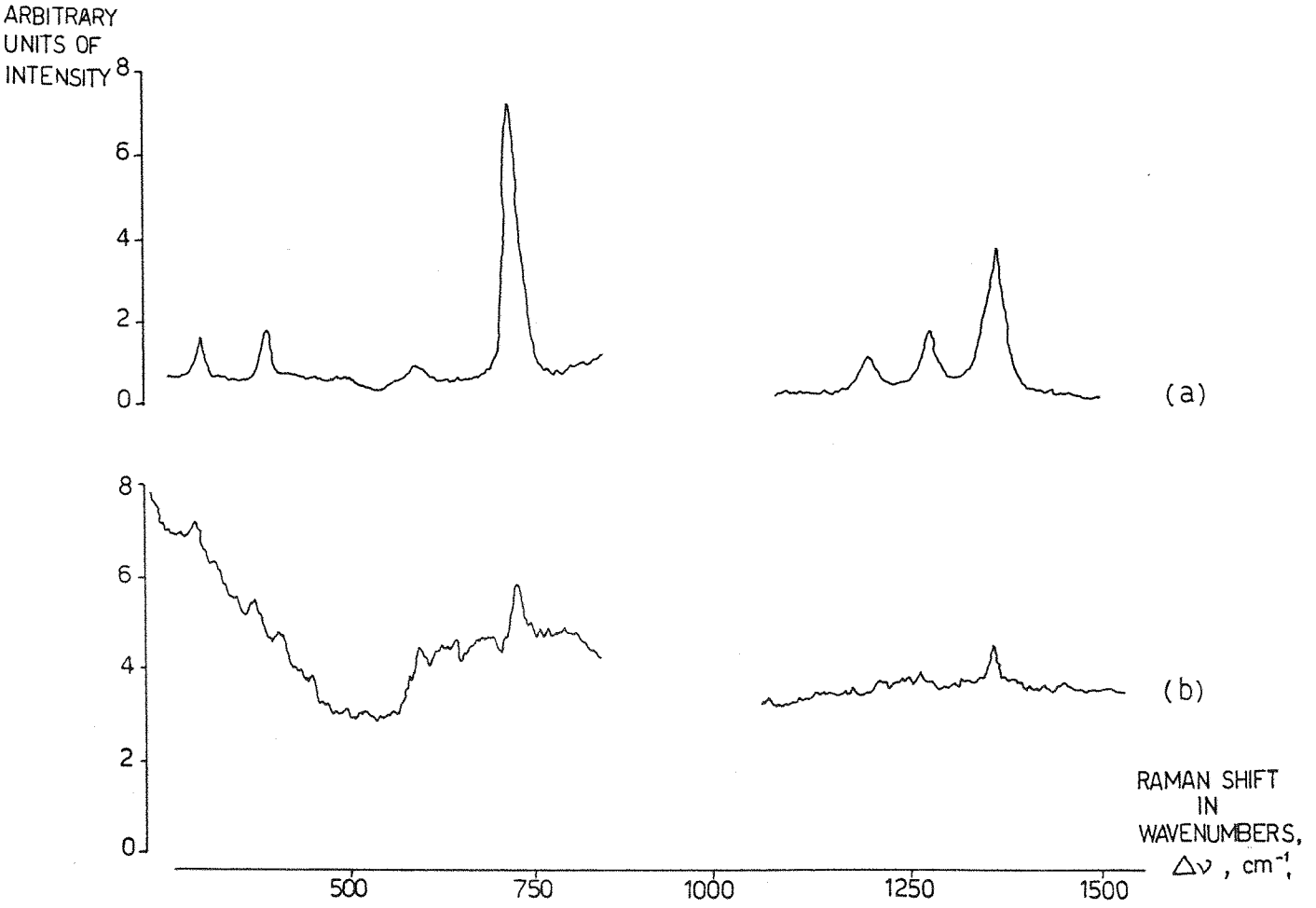

Figure 2.14

Raman spectra of PTFE powder recorded, (a) with fibre-optics and, (b) conventionally

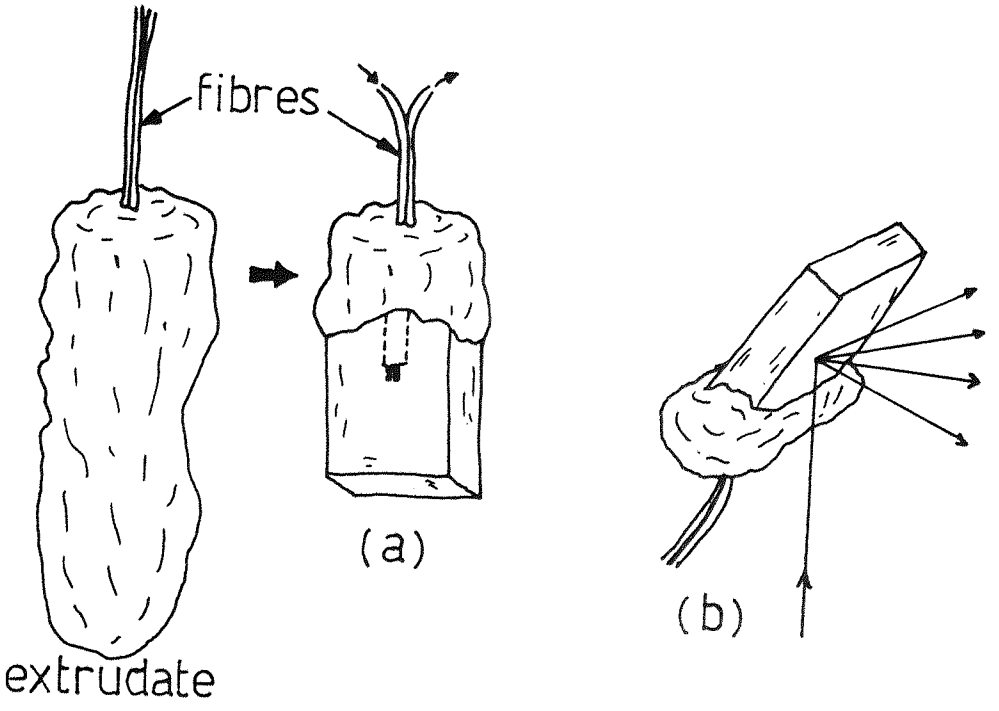

Figure 2.15

Sample preparation for Raman spectroscopy of bulk polyethylene, (a) fibre-optics, (b) conventional excitation

and collection mounts, and with a pre-set laser power (measured at the end face of the input fibre before it was embedded in polymer) the peak at $\Delta\nu$ = 1296cm^{-1} was optimised at the detector. A spectrum was recorded and compared in table 2.2 with that obtained conventionally. See figure 2.15 for sampling orientations.

It would appear that the signal obtained from the bulk polymer is not as relatively intense as that from the powder. Wrapping the specimen in aluminium foil however, has a desirable effect (see table 2.2).

Potassium chromate, K_2CrO_4. Large crystals of potassium chromate were grown slowly from a saturated solution over a period of one week, onto the end of a fibre-optic probe. A spectrum was recorded and is shown in figure 2.16.

(C) Surfaces

A sheet of high density polyethylene (BP Rigidex 006-60) 5mm thick with a relatively flat and homogeneous surface was used to assess the performance of the fibre-optic method under various orientational parameters. All measurements were taken over the same region of the sheet.

Initial measurements showed the signal intensity obtained to be poor. However, significant improvements were observed when reflective surfaces were placed around the fibres. The aluminium alloy blocks covered with aluminium foil were carefully pushed up against the fibres, and showed a $3\frac{1}{2}$ times improvement in the recorded signal intensity. These were used in all subsequent experiments (see figure 2.17).

(i) Variation of Collection Angle

The injection fibre was placed perpendicular to the surface of the sheet and the collection fibre was placed adjacent to it, and the subtended angle varied using an angularly adjustable mount. The intensity of the Raman signal at $\Delta\nu$ = 1296cm^{-1} was measured at each angular increment. The procedure was repeated, this time with the collection fibre perpendicular and the angle of the injection fibre varied.

(ii) Variation of Fibre Heights from the Surface

a) With both injection and collection fibres arranged at an angle of 17^{o} to the perpendicular. The Raman intensity of the $\Delta\nu$ = 1296cm^{-1} band was recorded as the height of the fibres above the surface was altered.

b) With the injection fibre perpendicular and in contact with the surface and the collection fibre at 17^{o} to the perpendicular the Raman intensity was measured as the collection fibre was raised to a height of 10mm above the surface. See figure 2.17(b).

The best results obtained from the surface were with angled fibres, providing an intensity 37% of that obtained conventionally (11% without reflective blocks). Also, the closer the blocks to the fibres, the better the enhancement of the spectra.

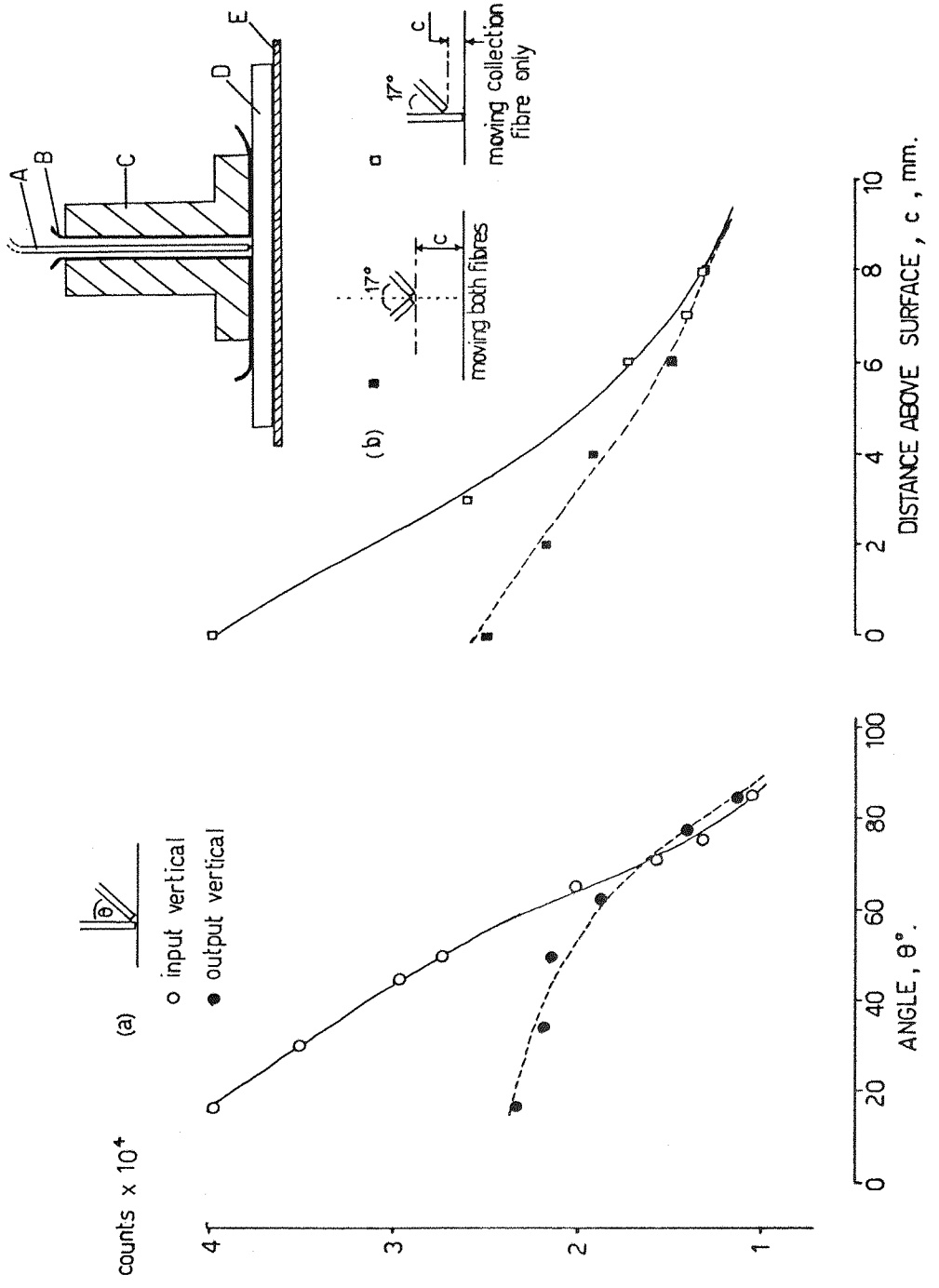

Figure 2.17

Raman intensity of $\Delta\nu$ = 1296cm^{-1} band in polyethylene, recorded at the surface of the polymer using the arrangement shown in inset, (End view: A = fibre, B = aluminium foil, C = aluminium alloy blocks, D = polyethylene sheet of thickness 5mm, E = block surface) with, (a) variation of angle between input and output fibres, and (b) variation of height above the surface of the fibres.

2.27 Probe Design

Since it was found that removal of the fibres from the surfaces of both powders and liquids was deleterious in terms of the intensity of the Raman signal collected, and by placing windows between the fibres and the sample resulted in further losses, a new probe was constructed. This incorporated a fluid filled cavity containing a colourless viscous liquid with the same refractive index as the silica core of the fibre* (see figure 2.8). The index matching fluid removes the need to produce a perfect end face, and it couples the fibre to the quartz window without flow.

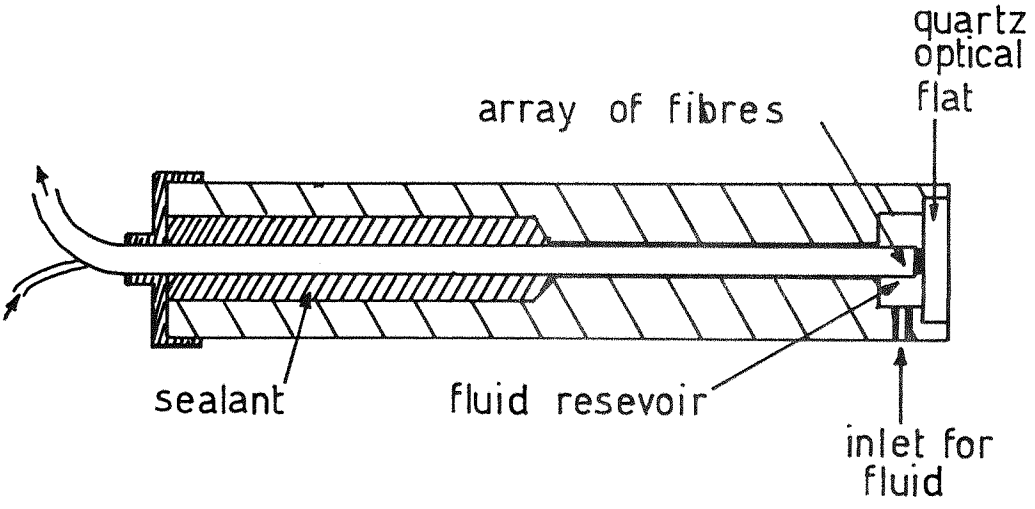

Figure 2.18

Index matched probe.

In the probe, two parallel fibres were pushed close to the quartz window, minimising the distance between the fibres and the sample. The index matching fluid was forced into the cavity using a syringe. The Raman intensity obtained using the index matching system showed a $3\frac{1}{2}$ times

* η = 1.4538

improvement compared with the original dry parallel-fibre probe using the $\Delta\nu$ = 1346cm^{-1} band in nitrobenzene for comparison. There was no evidence in the scattering spectrum of the Raman characteristics of the window material, or that of the index matching fluid.

CHAPTER 3

RAMAN SPECTROSCOPY OF FLOWING MOLTEN POLYETHYLENE

3.1 Introduction

The design and fabrication of polymer products relies heavily on the properties of the material flowing under strictly controlled conditions. Consequently much interest exists regarding the precise nature of the flowing polymer melt. Explanations of macroscopic flow phenomena such as die-swell, sharkskin and melt-fracture have been tendered by rheologists. In many cases these properties have been related to molecular behaviour through the concepts of entanglement and orientation, even though no direct evidence is available for these at the molecular level.

The polymer properties group at Southampton has been engaged in a direct in situ approach. Studying molten polyethylene terephthalate (PET) flowing down simple circular glass tubes using Raman spectroscopy they concluded that no well developed order was apparent (1). However, some form of pseudo-crystalline molecular species involving the rotation of the carbonyl group relative to the benzene ring was proposed to explain frequency shifts in the vibrational spectra of the polymer under shear.

An extension of the work was initiated (2) involving a re-design of the sampling system in an attempt to improve the sensitivity of the experiment. Rectangular slot-shaped metal/glass channels were used, improving the optical efficiency markedly. A variety of polymers were studied including polyethylene, polypropylene and nylon-6 as well as PET. No shear induced effects were found, hence it was concluded that no order was induced by shear.

Problems were encountered with signal intensity, whilst both studies observed the polymers well downstream of the die inlet region. This could be very important because orientation induced at the die-entrance could be removed from the flowing polymer downstream, by relaxation, and thus its observation would become difficult, or impossible.

Recent advances in fibre-optic technology in this labaratory has permitted us to design a new sampling technique which overcomes the

problems of alignment and vibration that lead to poor signal intensities and high background in conventional Raman sampling. In this study a fibre-optic probe has been successfully incorporated into the inside of a pressure flow system specifically designed to directly observe flowing molten polyethylene in the die entry region.

3.2 Extrusion and Polymer Flow

The screw extruder is, with few exceptions, the basic tool of all polymer processes. It consists simply of a long Archimedian screw operating in a heated barrel, fed by a hopper containing the raw material (Fig 3.1). This device melts the polymer by contact with the barrel and, combined with the action of the screw, homogenises and compresses the material. Polymer, uniform in composition, temperature and deformation history is thus transported past the tip of the screw. The design of the screw, temperature gradients along the barrel, the form and supply of the raw polymer and the construction of the nose of the extruder are all very sophisticated. Modern machines are capable of providing a steady stream of molten polymer at high constant reproducible pressure and temperature with a considerable degree of homogeneity.

Downstream of the extruder the type of flow induced is a function of the viscosity of the polymer, the profile of the tube down which it is forced, and the applied pressure; the extruder provides the necessary force to maintain constant output regardless of the temperature (viscosity) of the polymer, and hopefully the bore of the tube.

In a cylindrical tube, the melt tends to adhere to the boundary wall and flow rapidly along the central channel (see figure 3.2(a)). When such a flow occurs the layers near to the walls are sheared. Shear is then the dominant factor. However, in convergence from the barrel of an extruder to a die the flow may be considered as having two components; shear and extension (see figure 3.2(b)). If the angle of taper is very slight then there will be very little stretch, but the shearing component is high, i.e., the sharper the angle of taper, then the greater the elongational flow component.

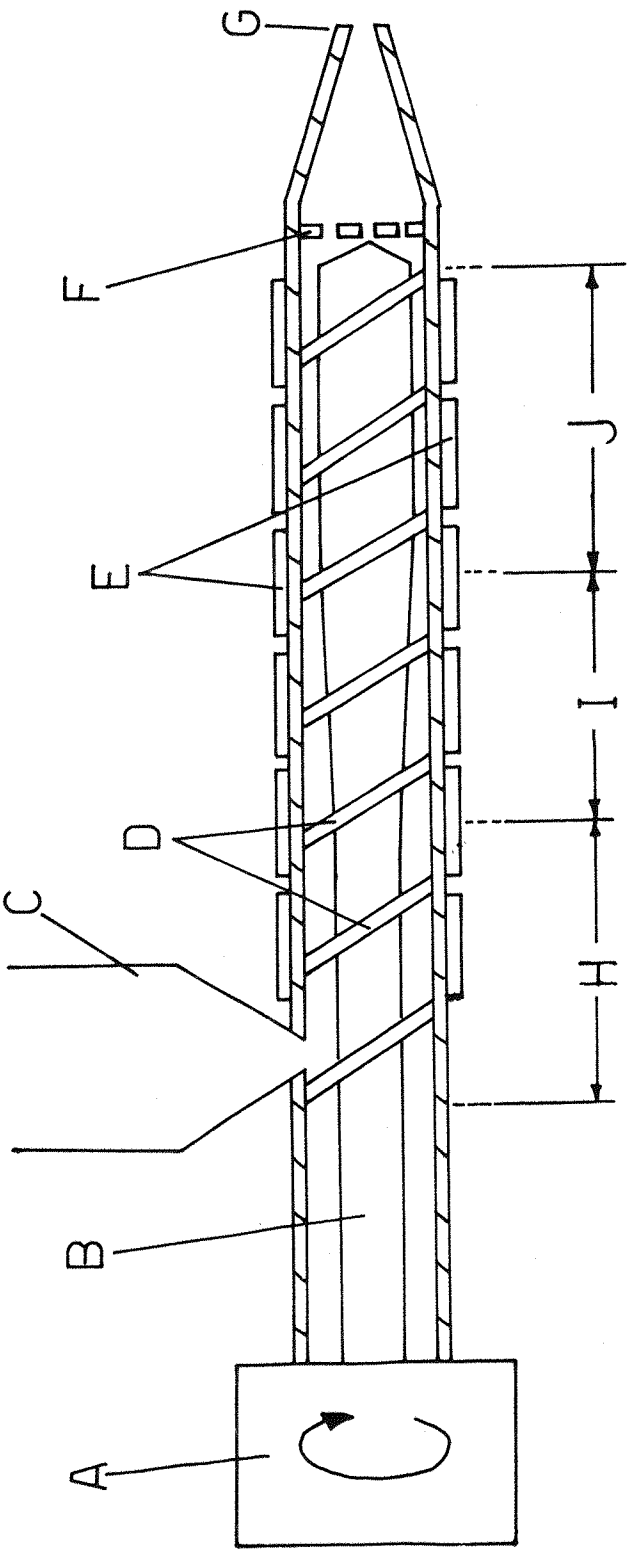

Figure 3.1

Extruder (single screw) schematic.
A. Motor, B. Screw, C. Hopper, D. Flights, E. Heaters, F. Breaker Plate, G. Die, H. Feed Zone, I. Compression Zone, J. Meter Zone

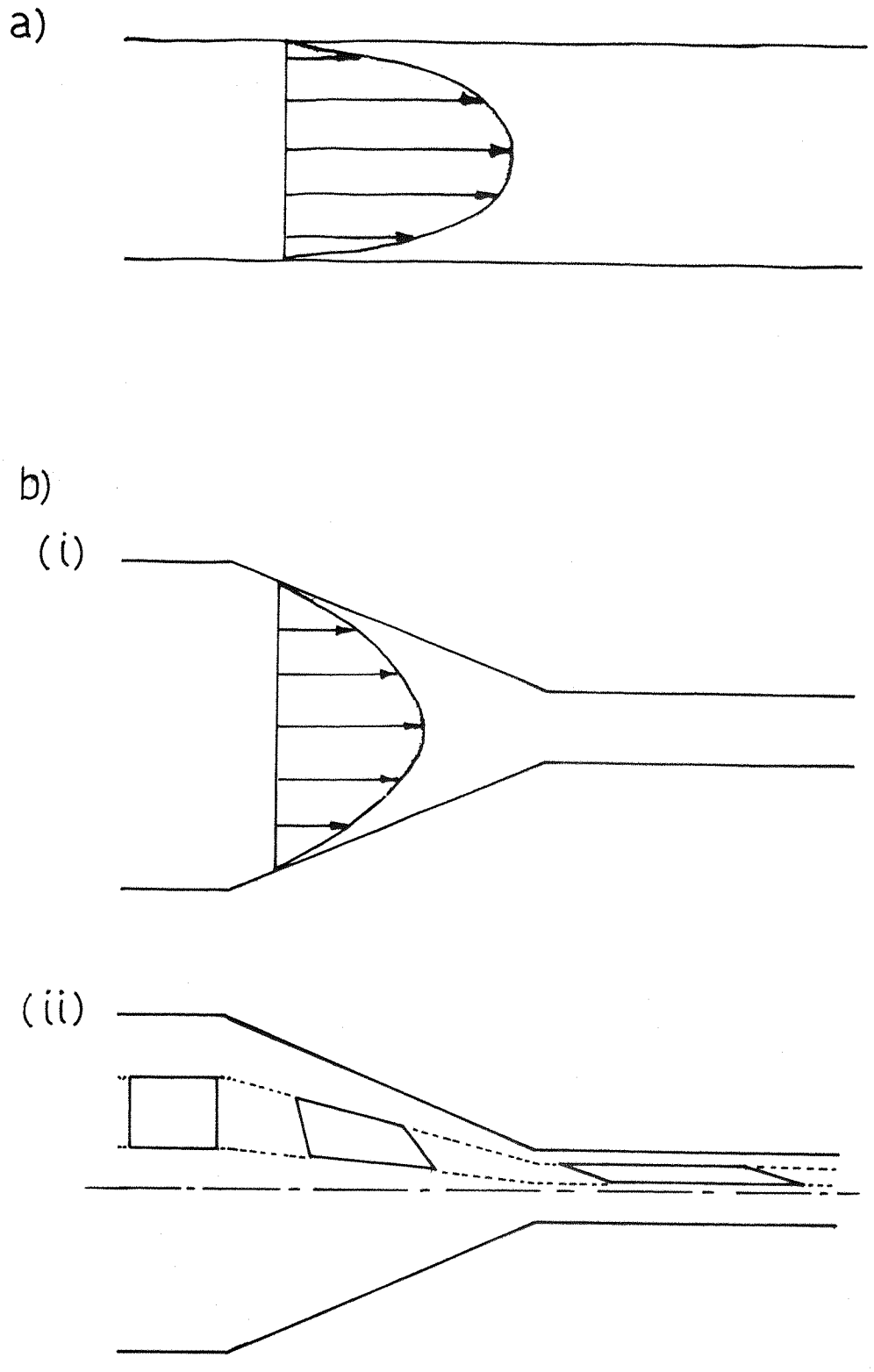

Figure 3.2

Velocity profiles of polymer melt flow a) in a cylindrical channel; b) in a convergent channel (i) shear flow, (ii) elongational flow

The appearance of the extrudate can be explained by the behaviour of the polymer melt in the die entry region, where a change occurs in the profile of the tube down which the melt is forced. This results in a disturbance of the laminar flow. At higher pressures, this disturbance can severely alter the behaviour of the polymer, generating effects such as lack of adhesion of the polymer melt to the die walls (plug flow) as well as knobbliness, coiling, melt fracture and other defects in the extrudate. These effects can sometimes be removed by using long die channels, allowing the polymer melt enough time to relax and re-establish laminar flow. However, the onset of turbulence in the flowing melt is directly related to the viscosity (ν) of the material, its flow velocity (u) and the diameter of the die (d). If the Reynolds number (R_e) for the system, calculated from,

$$R_e = \frac{\nu u}{d}$$

is greater than an optimum value, then laminar flow will not be established, and the resulting turbulent flow will be manifested in the extrudate.

3.3 Experimental

3.3.1 The Extruder

The extruder used was a Baugn 1:¼" machine fitted with a general purpose screw having a length : diameter ratio of 20:1. The screw was hydraulically driven and its speed monitored by an electronic tachometer. The variation in screw speed throughout a particular run was negligible. A specifically designed die was attached to the extruder by an extension piece containing a melt thermocouple, two melt-mixer units, a breaker plate and a melt pressure transducer. Melt temperature was controlled by the use of two-term temperature controllers along the barrel, as far as the extension piece (figure 3.3).

Temperature was maintained in the die using a cartridge heater controlled by a CAL-7000 variable temperature controller. Melt temperatures over the whole apparatus were monitored using a system of chromel-alumel thermocouples which were switched into a digital voltmeter.

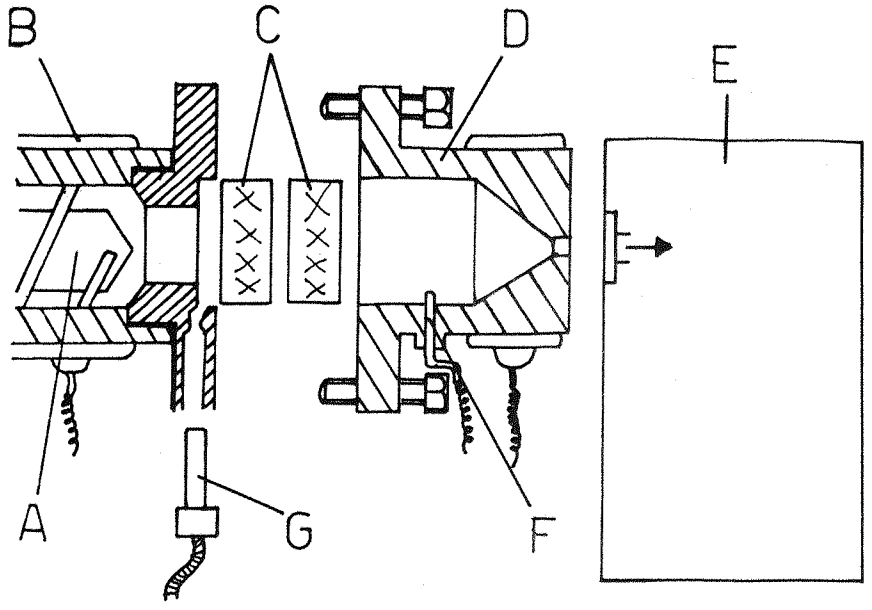

Figure 3.3

Arrangement at Extruder tip. A. Screw tip, B. Band heater, C. Mixers, D. Extension piece, E. Die, F. Thermocouple, G. Pressure transducer

3.3.2 System Design

Two important considerations were embodied in the design of the apparatus. Firstly, that the die had to possess the capability of generating high shear rates with relative ease, and secondly, that a fibre optic probe could be successfully incorporated without difficulty.

3.3.3 The Die

The die is illustrated in figure 3.4 with its related accessories in figure 3.5. The fully assembled apparatus is represented in figure 3.6, showing the internal detail by section. The system is comprised of three major components; the block, the nozzle and the sampling unit. The block is constructed from aluminium alloy and has an internal bore diameter of 12mm. This acts as a reservoir. The output nozzle, also of aluminium alloy, is interchangeable with other nozzle designs

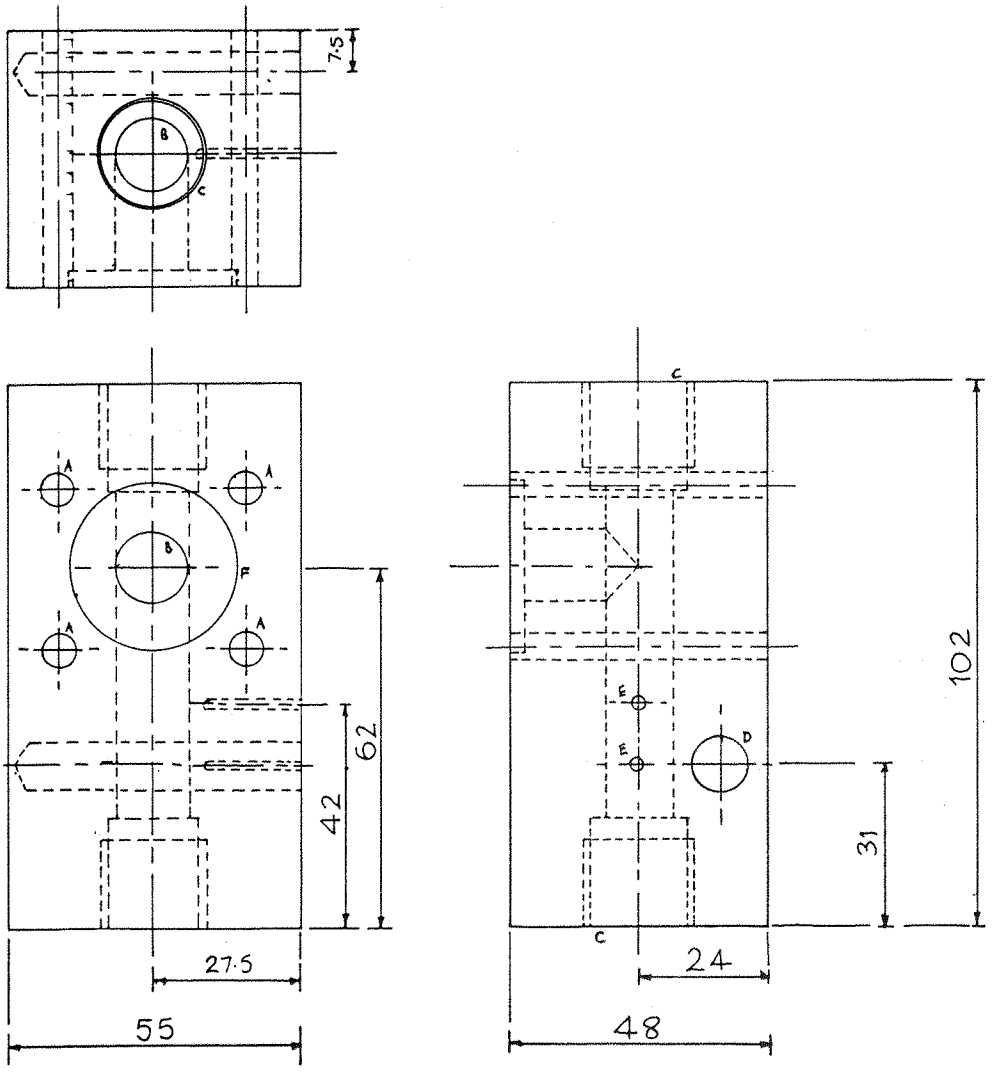

A. FOUR HOLES M6 CLEARANCE
[ON A 45MM PITCH - EQUIDISTANT]

B. TWO HOLES Ø 12 MM

C. TWO HOLES DRILLED 18MM Ø TO 20MM, TAPPED 3/4 WHITWORTH TO 16MM DEPTH

D. ONE HOLE Ø10MM, DEPTH 53 MM

E. TWO HOLES Ø 2MM, DEPTH 18 MM

F. MILLED HOLE, 3MM DEEP, Ø31

Figure 3.4

Three projections of the aluminium alloy block die used in the experiment

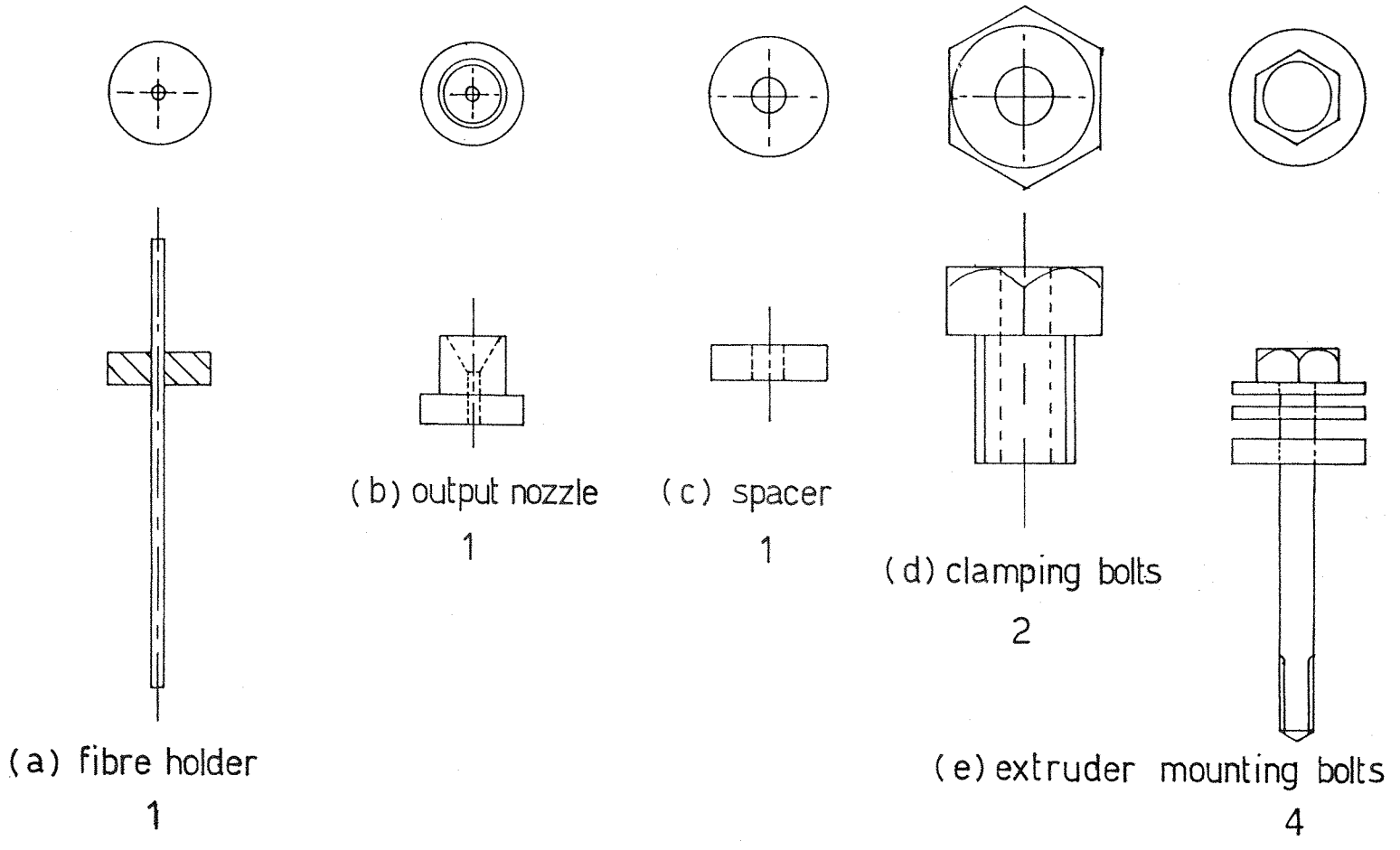

Figure 3.5

Accessories for the die shown in figure 3.4

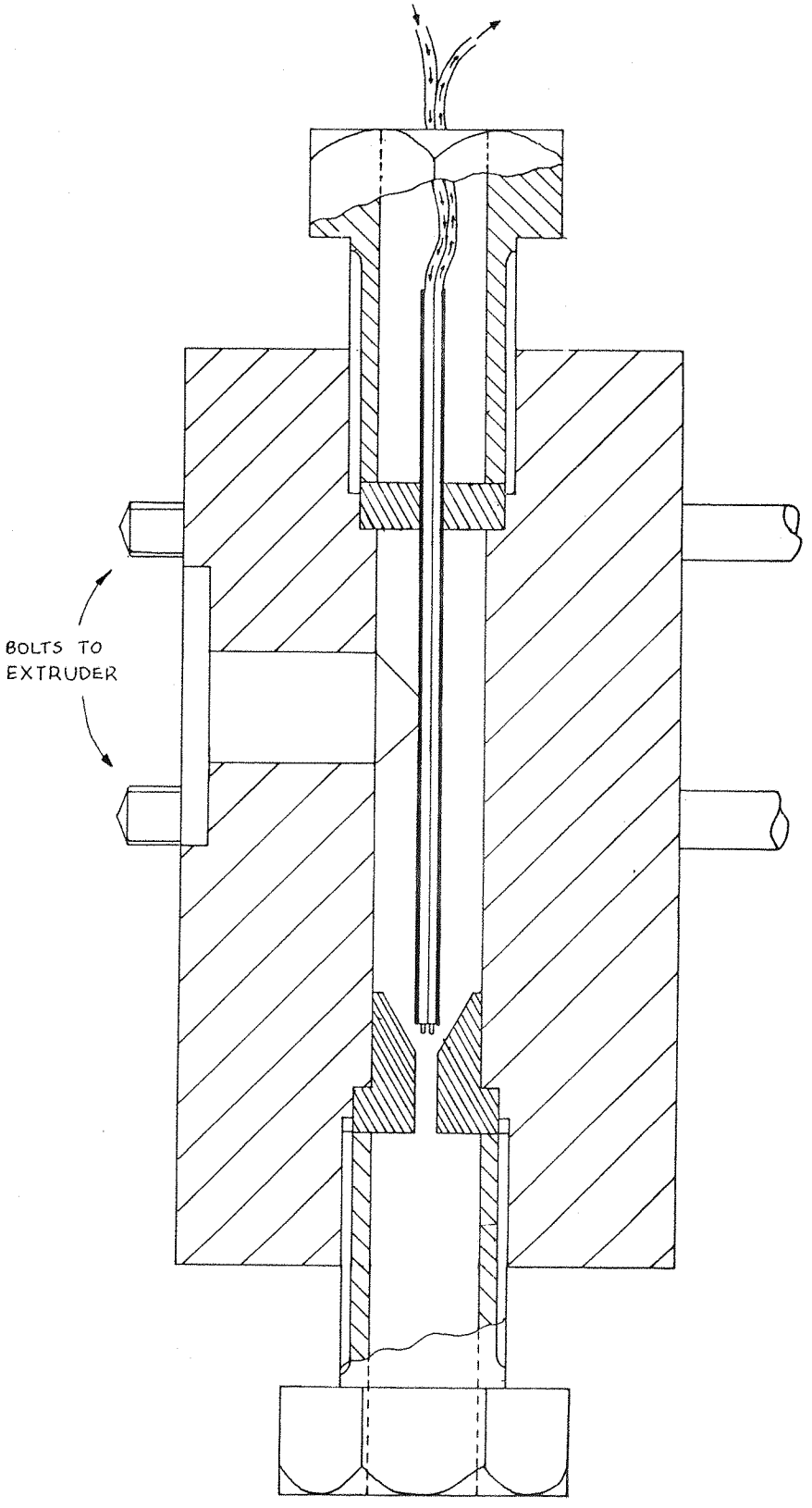

Figure 3.6

Die system, assembled (shown in section)

to the whim of the experimentor. The sampling unit and the nozzle are tightly clamped into the ends of the block by $\frac{3}{4}$" Whitworth bolts with 10mm holds drilled through their centres.

3.3.4 The Fibres

The sampling unit comprises of a length of thin stainless steel hyperdermic tubing (internal diameter = 1.0mm, external diameter = 1.6mm) silver soldered into a stainless steel disc. The tubing was centred in the hob using a lathe, so that when it was firmly clamped into the die it ran concentrically down the barrel of the die. Inside the tubing, two optical fibres were sealed.

The fibres were carefully pushed down into the tubing (which was a very tight fit) until they emerged from the sample end. They were then pulled clear. The fibres were prepared using the method described in chapter two such that their freshly cleaved end faces were parallel, with 1mm of bare silica core exposed. Silicone rubber was smeared onto the fibres 1cm behind the prepared ends to a distance of 6cm along the length. The fibres were then drawn back into the tube, leaving only the 1mm bare core exposed. Extreme care was taken not to allow any sealant to spoil the prepared ends. The unit was allowed to stand for 24 hours to ensure a strong seal, and then tested by tugging the long ends of the fibres whilst holding the unit fixed. The sampling geometry in the die is shown in figure 3.7.

Two three metre lengths of 200μ PCS fibre were used. The injection system consisted of an optical bench layout based upon the experience detailed in chapter two (figure 3.8(a)). Fine adjustments of the beam entering the fibre were crude; however the throughput was acceptable; approximately 60% of the light available at injection was transmitted to the sample.

At the spectrometer, the collection fibre was held securely in a pin-chuck at the approximate imaginary image of the first slit (figure 3.8(b)). Unfortunately the intensity of the back-projected image of the slit in the Coderg T800 is very weak and cannot be

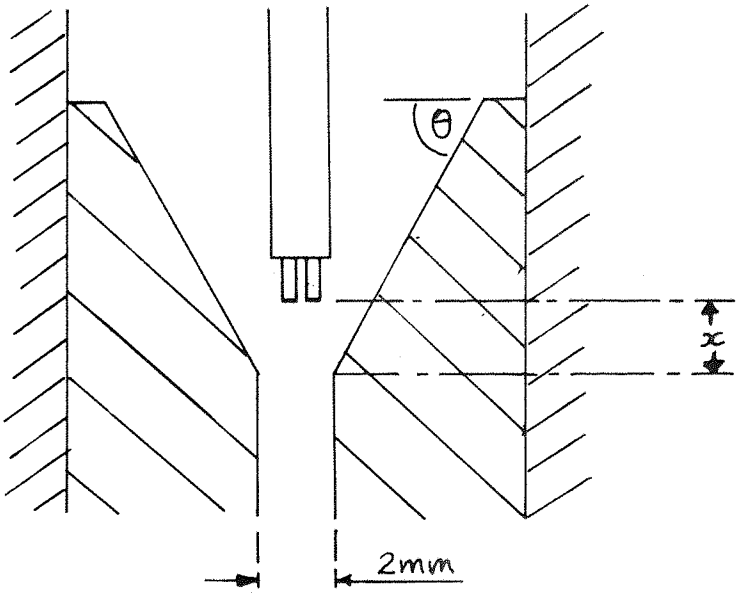

Figure 3.7

Fibre sampling geometry - x = 2mm, θ = 60°, scale 5:1 (mm)

located easily. However, lining up the laser beam with the slit using the conventional no-parallax adjustment and then moving the fibre until the laser beam just clips the end face is a sufficiently adequate first approximation, given that the collection mount is positioned such that the fibre axis in the vice and the lens axis are the same (see chapter two).

A known Raman peak was used to optimise the signal at the spectrometer (by triaxial adjustment of the sample plate to which the collection unit was clamped) before the sampling unit was installed in the die. The laser power was adjusted to give approximately 150 mW of laser radiation at the end face of the illumination fibre (measured using a Spectra Physics Model 210 Power Meter).

3.4 Method

3.4.1 System Testing

The polymer used was Rigidex 006-60. This is an extrusion grade

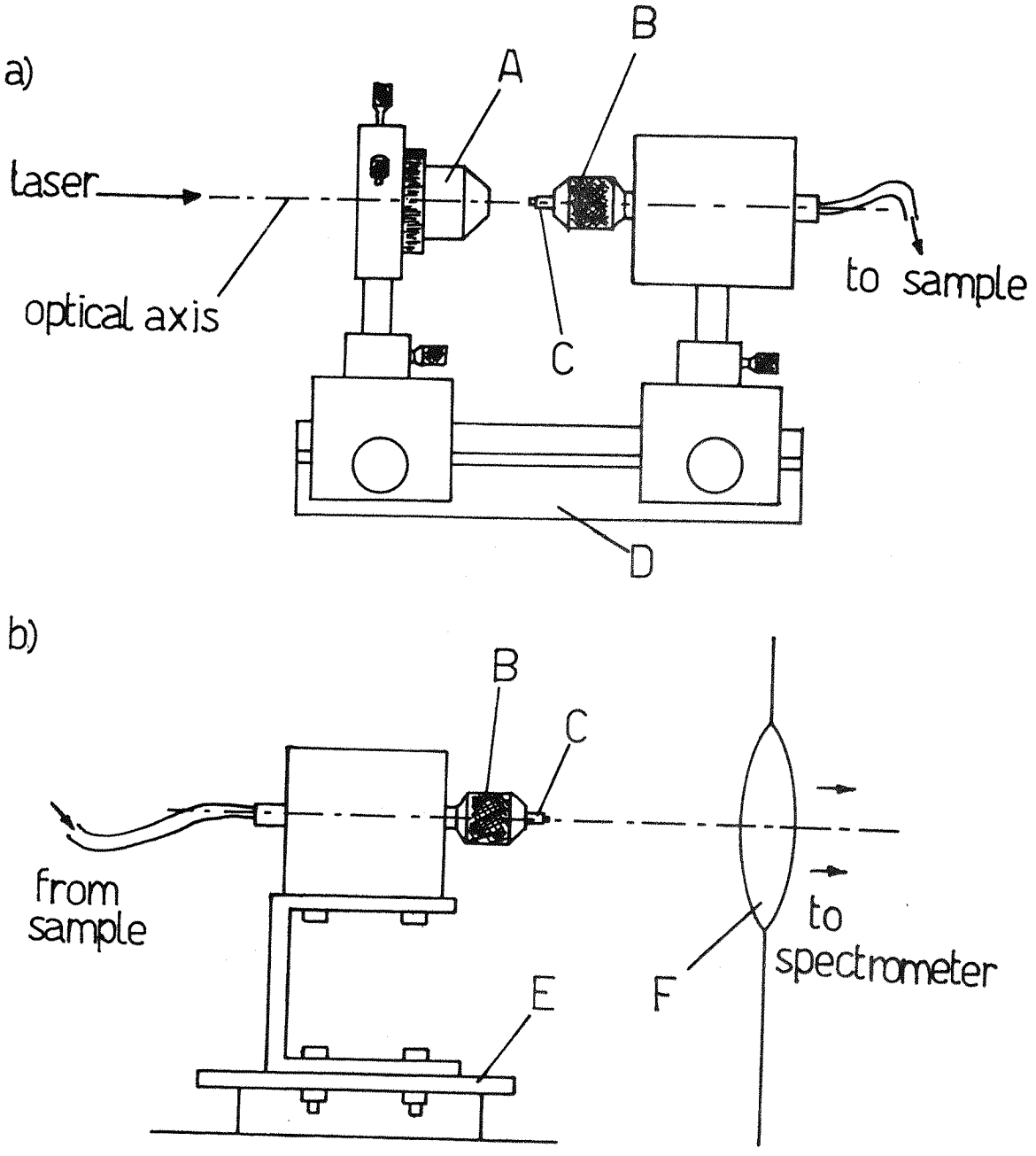

Figure 3.8

(a) Optical bench injection system and (b) arrangement at spectrometer
A. microscope objective lens, B. pin-chuck, C. fibre, D. triangular optical bench, E. spectrometer sample table (xyz adjustable), F. spectrometer collection lens

high-density polyethylene and was supplied by British Petroleum. This particular grade is of high molecular weight, M_W = 130,000, Mn = 19,500, and has a melt flow index (3) of 0.6. This was introduced into the pre-heated extruder, and after stabilisation of the output at low screw speed (i.e. exclusion of all entrapped air bubbles and foreign particles) the output was gradually increased and the fibre unit was carefully monitored.

At a screw speed of 15rpm and a pressure of 1900psi (at 170°C) the fibres were forced from their holder.

The unit was rebuilt. This time the fibres were sealed using a pressure and temperature resistant potting compound intended for high vacuum applications ('Chromix' by Fortafix Ltd.). This was applied using a slight modification of the method used for the silicone rubber, and allowed a setting time of 48 hours. The above test was repeated and it was found that this new arrangement could withstand maximum screw speed (100rpm) at the same temperature. The pressure was measured as approximately 3600psi.

3.4.2 Recording Raman Spectra

The Coderg T800 was used in preference to the Anaspec LR-36 because of its higher resolution and excellent stray light characteristics. The bandpass, $10cm^{-1}$, and scan time, $10cm^{-1}$ per minute were kept constant for all spectra. Signal to noise ratios were good, and thus a direct comparison of spectra at various shear rates was possible. The fibre-optic system, pre-aligned before installation, was capable of detecting Raman signals immediately, however as a final check the band at $\Delta\nu$ = $1305cm^{-1}$ was used to optimise the system. The instrument was then scanned across the range 1000 - $1550cm^{-1}$.

3.5 Results

Samples of molten polyethylene were collected over 10 second intervals for screw speeds of 2.5, 5, 10, 20, 40, 50, 60, 70 and 75rpm and die head temperatures of 150 and 170°C. The polymer samples

were allowed to cool to room temperature, and weighed. The results are given in table 3.1 for the average weight from five samples at each screw speed for both temperatures.

SCREW SPEED (±0.5rpm)	TEMPERATURE AT DIE HEAD °C	
	150(±2)°c	170(±2)°C
2.5	0.55	0.50
5.0	1.20	1.20
10	2.00	2.20
20	4.80	4.95
40	9.65	9.70
50	10.30	10.30
60	12.85	12.85
70	14.40	14.45
75	--	16.10

TABLE 3.1

Weight of cooled high-density polyethylene collected during a 10s extrusion (±0.05g)

The shear rate at the nozzle entrance was assumed to be the same as that in a tube of 0.2cm diameter, and was calculated using the following expression,

$$\gamma = \frac{4Q}{\pi r^3} \qquad (4)$$

where γ = apparent shear rate (s^{-1}),
Q = output ($cm^3 s^{-1}$),
r = radius of nozzle (cm).

The values for calculated shear rate and observed pressure of polymer entering the die are shown in table 3.2, for different temperatures and flow rates. The results show that the temperature of the die does not significantly alter the shear rate. Increasing the flow rate (by turning up the screw speed) causes a proportional increase in shear rate, assuming that there is no leakage past the screw, and an increase in the pressure of the polymer. Figure 3.9 shows that by increasing

the temperature of the die, the pressure on the polymer is reduced for a given rate of flow. It is presumed that this is due to a fall in the viscosity of the polymer at the elevated temperatures (5).

3.5.1 Die Swell

The die swell and the appearance of the extrudate were recorded. Measurement of the diameter of the molten polymer at a distance of 3cm from the exit hole gave results shown in table 3.3. A graph was plotted of swelling ratio against shear rate. It was found that at 170°C there appeared to be no correlation between the shear rate and the swelling ratio. However at 150°C it was found that the swelling ratio decreased with increasing shear rate (figure 3.10). This suggested the onset of melt fracture (5). However the appearance of the extrudate did not confirm this. Sharkskin was observed at 150°C for higher shear rates. No sharkskin was observed at 170°C. This was to be expected, since it is considerably delayed by increase in temperature (6).

3.5.2 Raman

Figures 3.11 and 3.12 show a series of spectra recorded at 170°C. Figure 3.11 is recorded with the molten polymer stationary in the system, with the extruder running. Figure 3.12 shows spectra recorded at shear rates of $155s^{-1}$, $635s^{-1}$, $1310s^{-1}$ and $1845s^{-1}$ respectively at 170°C.

Figures 3.13 and 3.14 show spectra of static (shear rate = 0) and flowing (shear rate = $75s^{-1}$) molten polyethylene at 150°C.

Three broad bands were found in the spectra recorded. The band at around $1440cm^{-1}$ is due to C-H bending vibrations (7), and those due to methylene twisting at $1303cm^{-1}$ (8) and C-C stretch in the $1080cm^{-1}$ region (7) are clearly present.

As far as could be seen there were no changes in band position, band profile or relative band intensities when the polymer was

TEMPERATURE ±2°C	SCREW SPEED ±0.5rpm	FLOW RATE ±0.01cm³s⁻¹	APPARENT WALL SHEAR RATE ±10s⁻¹	PRESSURE ±10 psi
150	2.5	0.06	75	1300
	5.0	0.12	155	1500
	10	0.20	255	1900
	20	0.48	610	2300
	40	0.97	1235	2550
	50	1.03	1310	2600
	60	1.29	1640	—
	70	1.44	1835	2750
170	2.5	0.05	65	500
	5.0	0.12	155	1300
	10	0.22	280	1650
	20	0.50	635	2000
	40	0.97	1235	2400
	50	1.03	1310	2500
	60	1.29	1640	—
	70	1.45	1845	2800
	75	1.61	2050	2900

TABLE 3.2

Calculated values of apparent shear at the nozzle entrance and pressure of molten polyethylene as flow rate increases, for two temperatures

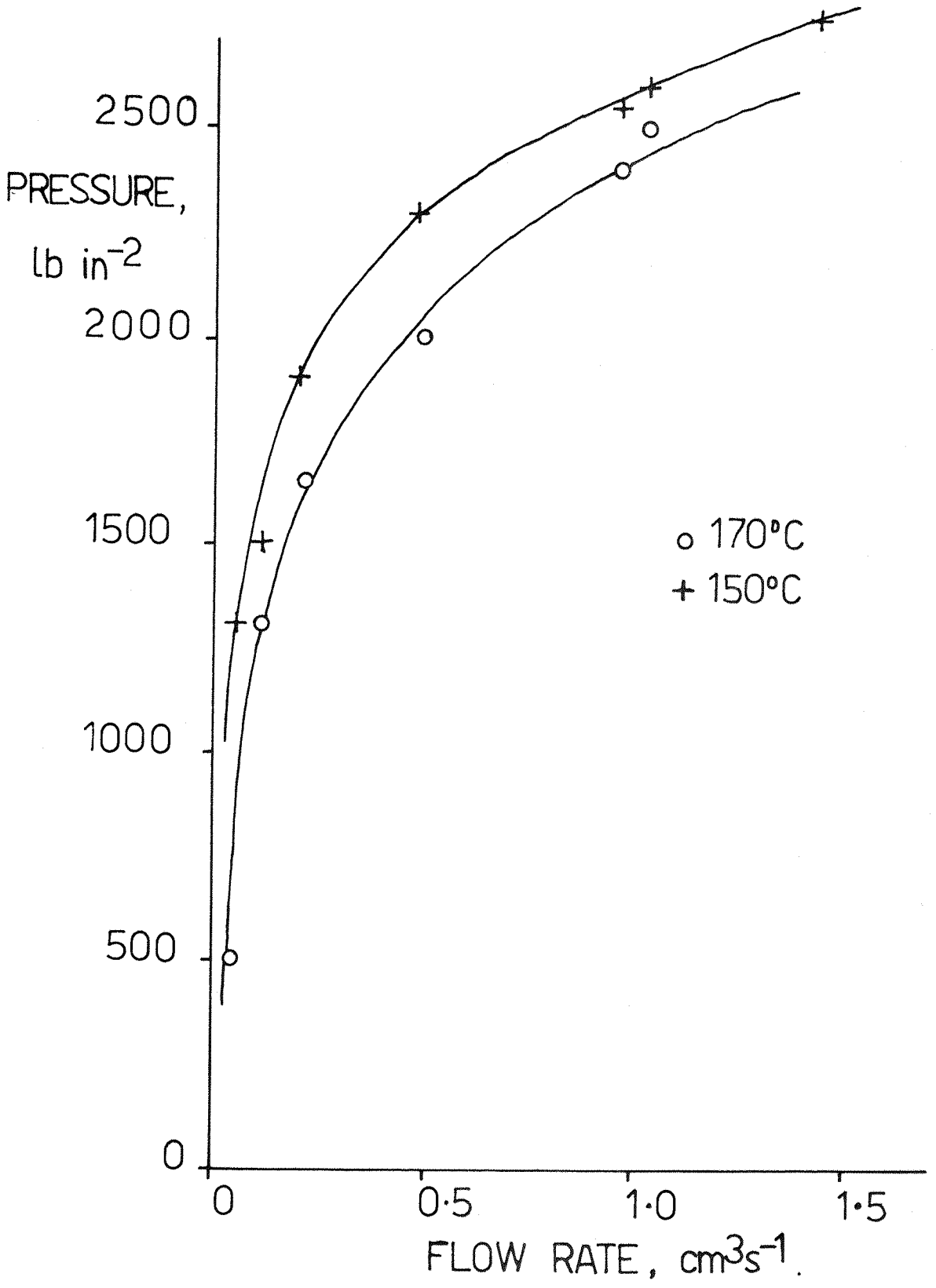

Figure 3.9

Graph to show the effect of increasing flow rate and die head temperature on the pressure of the molten polymer entering the die

TEMPERATURE °C	APPARENT SHEAR RATE ±10s^{-1}	DIAMETER OF POLYMER f(dieswell) mm die diameter = 2mm	SHARKSKIN? Y/N
150	610	15.0	No
	1235	10.9	Yes
	1310	10.2	Yes
	1845	10.0	Yes
170	65	12.0	No
	155	12.0	No
	280	13.0	No
	635	10.5	No
	1235	9.0	No
	1310	13.0	No
	1845	10.5	No

TABLE 3.3

Measured extrudate diameter at different shear rates for both temperatures

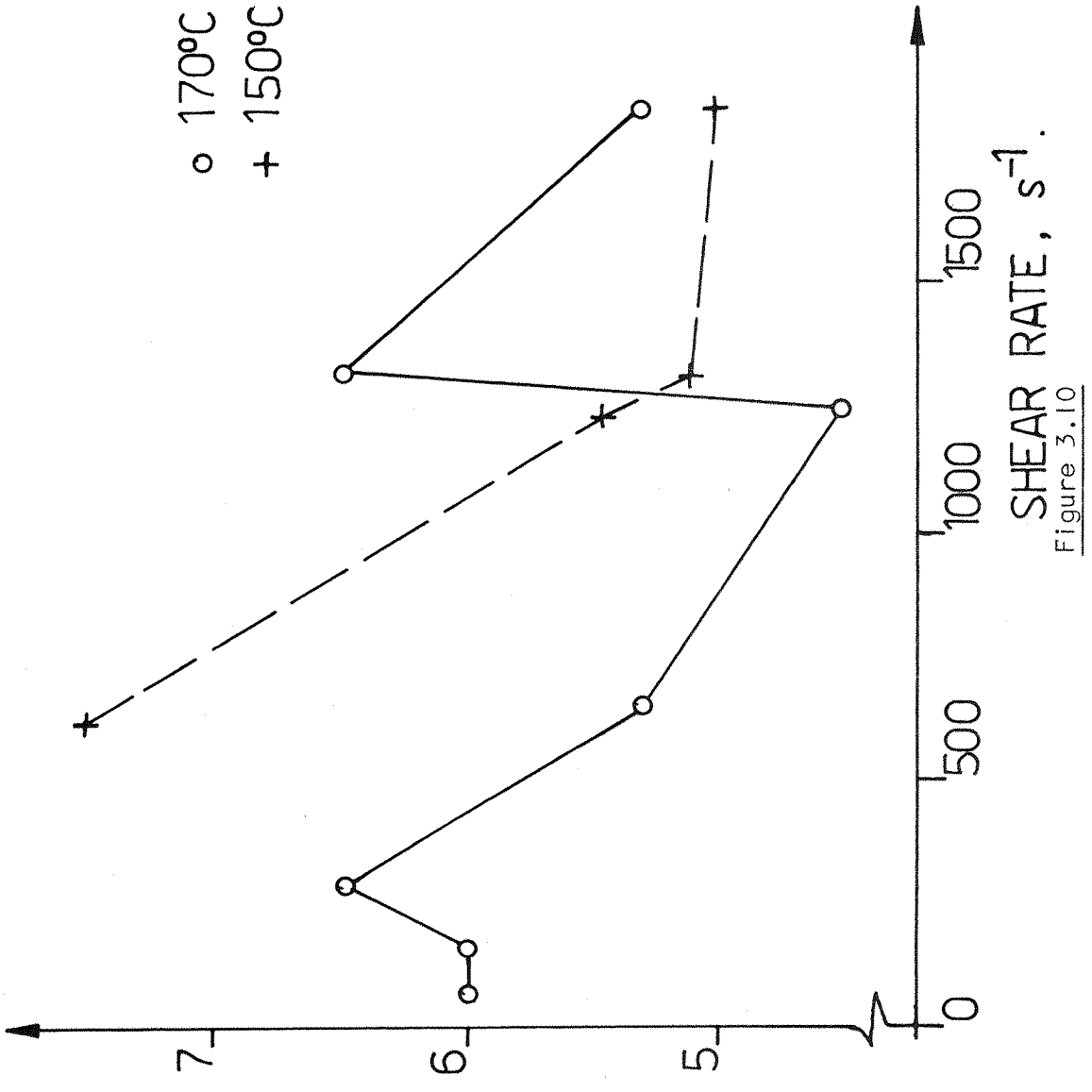

Figure 3.10

Graph of apparent wall shear rate versus swelling ratio, which is measured as the diameter of the extrudate divided by the diameter of the die exit

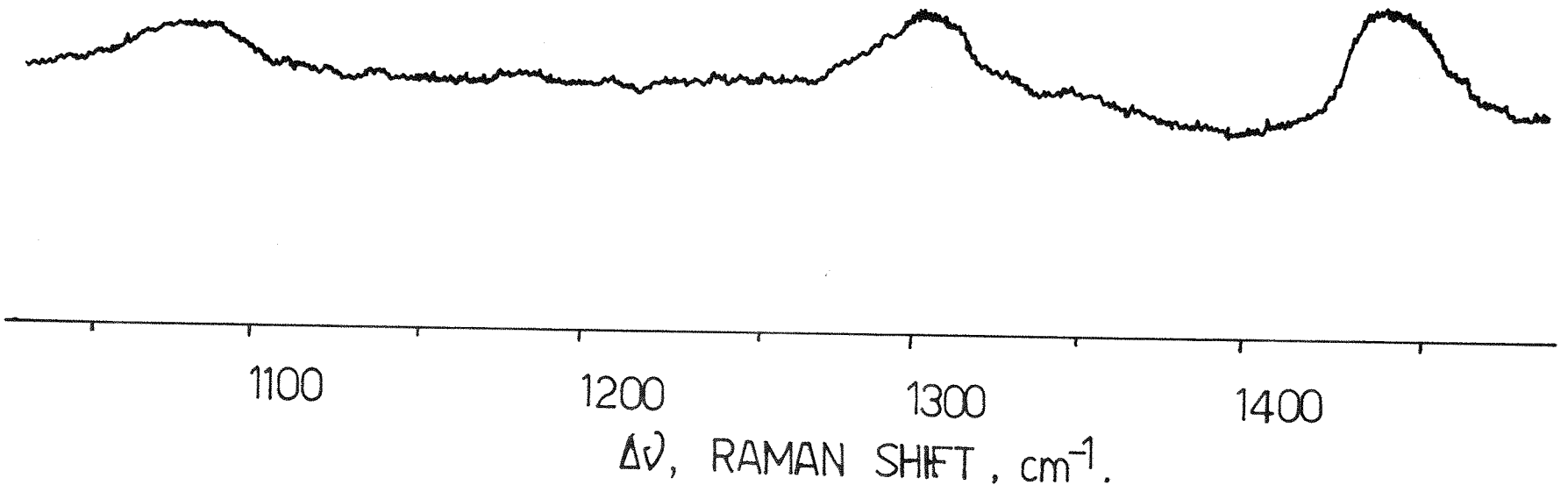

Figure 3.11

Raman spectrum of static molten polyethylene in extruder die at 170°C

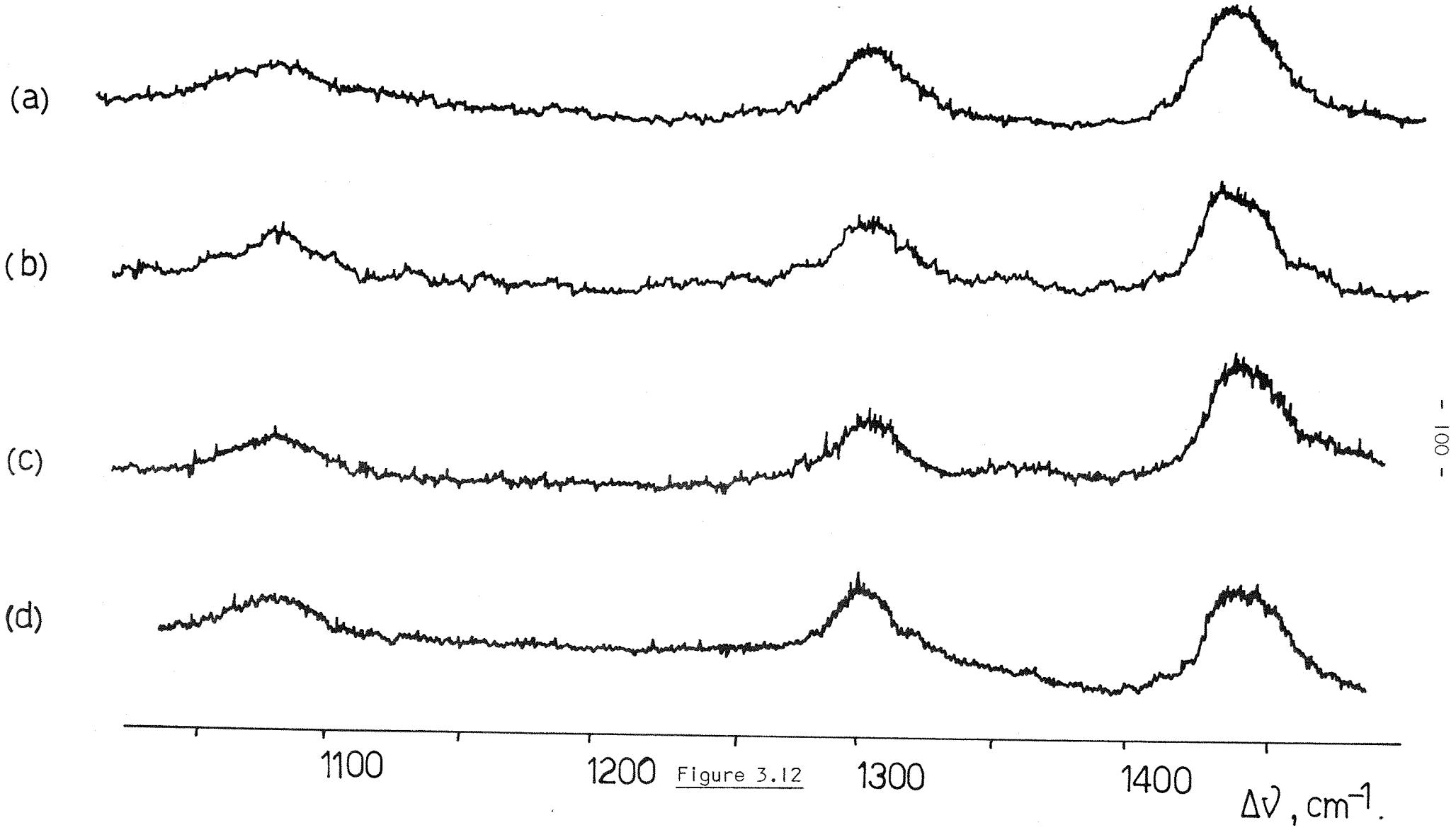

Figure 3.12

Raman spectra of molten flowing polyethylene at shear rates (a) $155s^{-1}$, (b) $635s^{-1}$, (c) $1310s^{-1}$, (d) $1845s^{-1}$, Temperature = 170°C

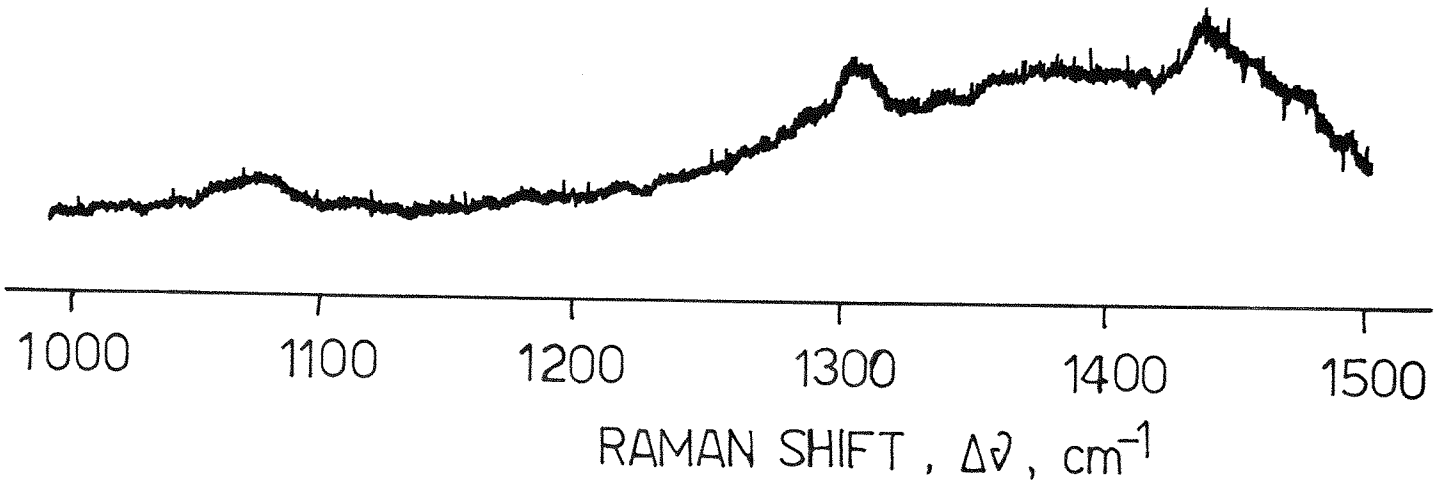

Figure 3.13

Raman spectrum of static molten polyethylene at 150°C

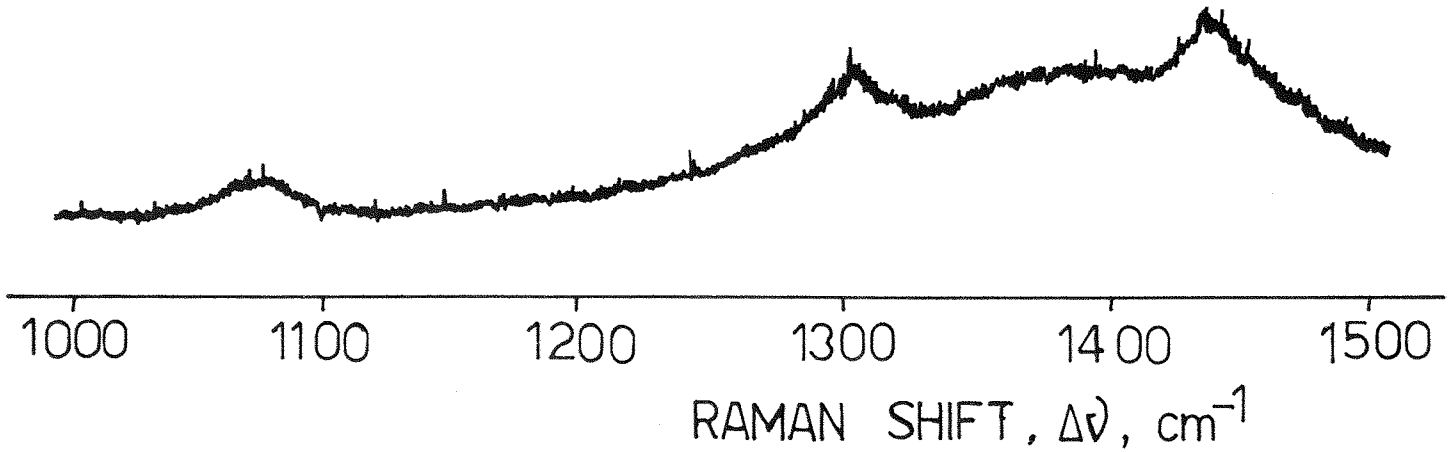

Figure 3.14

Raman spectrum of flowing molten polyethylene, 150°C, shear rate = $75s^{-1}$

subjected to a range of shear rates at 150 and 170°C. Only two spectra are reported for the experiments at 150°C because at a shear rate of 155s^{-1} (1500psi) the signal was suddenly lost. After exhaustive attempts to recover the signal had failed the apparatus was dismantled and it was discovered that the collection fibre had snapped at the end, and no scattered light was being transferred to the instrument.

3.6 Discussion of Results

The use of optical fibres has allowed the first *in situ* molecular level study of the behaviour of molten polyethylene at the entrance to a capillary die.

Since the fibre-optic probe is situated within the flow stream the requirement for windows is completely removed, and the high reflectivity of the internal surfaces of the die improves the collection efficiency. This results in excellent quality spectra from only a single collection fibre. This has the added advantage of minimising the probe diameter.

The length of the fibre-optic cable can be considerable. Thus the extruder can be far removed from the spectrometer. This prevents the possibility of damage to the spectrometer optics by fumes, and removes the inevitably high levels of background in the spectra caused by vibration of the apparatus originating in the processing machinery.

Unlike previous Raman studies of flowing polymer melts (1,2) the design of the equipment optimises the efficient collection of Raman data, rather than being a modification of existing or conventional designs to incorporate a sampling system. As a consequence, alignment is trivial, repeatable and constant, allowing accurate selection of the region of the die to be studied.

From the results it has been clearly shown that, although the polyethylene has been subjected to violent shear, no significant molecular level changes are resolvable.

These observations are in full agreement with X-ray diffraction studies (9) and infrared data (10) derived by other members of the polymer properties group. However, the lack of shear-dependant spectral changes disagrees with accepted molecular level explanations of rheological phenomena.

The mechanism of die-swell, for example, is explained as the relaxation of shear oriented chains once they emerge from the die, causing lateral expansion and longitudinal contraction of the extrudate. The shear induced orientation proposed at the die entry region (11,12) is not detectable by Raman spectroscopy, even though very considerable die-swell was apparent at both temperatures.

Work on dilute polymer solutions using optical birefringence methods have shown uniform and aligned fringe patterns. It has been suggested that these indicate orientation of the polymer chains. This work has been extended to polymer melts and successful observations of stress-induced birefringence patterns have been made and interpreted to indicate molecular orientation. A wealth of data is available relating the patterns to factors such as shear rate and die profile (13,14). The fringe patterns can only be a function of the orientation, and their extrapolation to molecular level behaviour is not as simple as one might prefer.

Processes such as flow induced crystallisation (15) and frozen-in orientation in solids produced by cooling flowing melts (16) have been reasoned in terms of alignment of the polymer chains by the flow field. These explanations of orientation in extrudates and quenched melts in terms of shear induced structure must, however, be dismissed. The oriented crystalline regions observed must be solely a consequence of the crystallisation process. However, it is not unreasonable to suggest that the effects of shear will profoundly influence a small number of nuclei (17).

It is obvious that the flow patterns involved in this system are complex (see figure 3.15). The factors affecting the flow profile of the molten polymer in the extrusion apparatus described were:

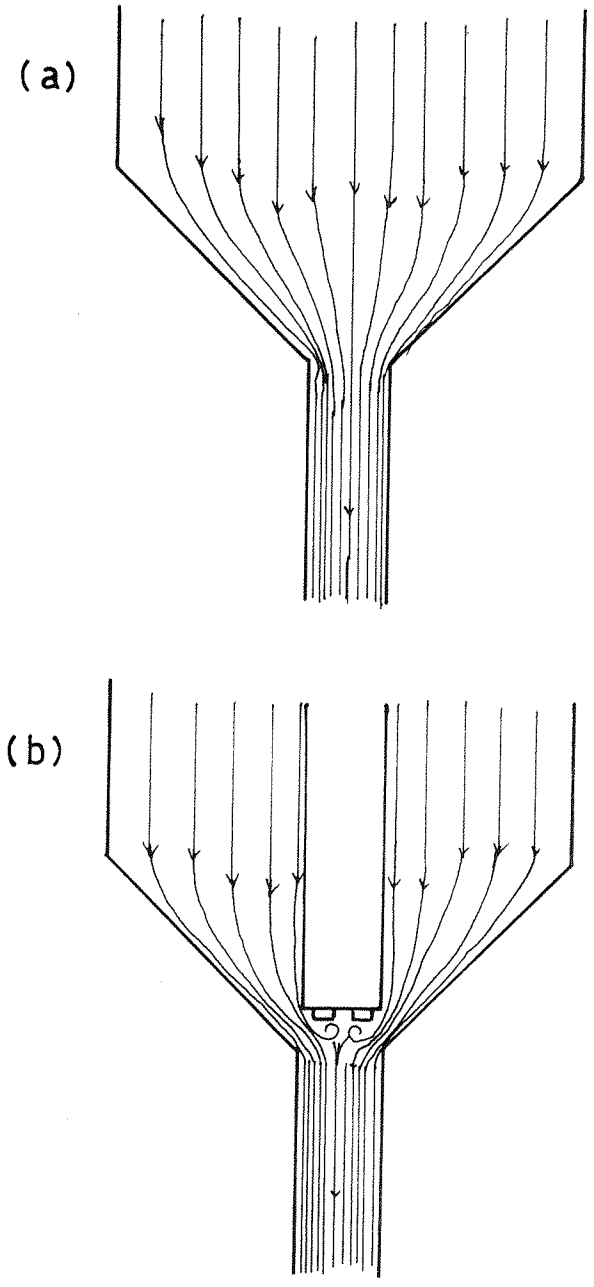

Figure 3.15

(a) Schematic representation of flow behaviour at the die entrance (18).

(b) As above, modified for the fibre-optic system used in this study.

i) the alteration of the flow direction by 90°;

ii) the positioning of the fibre probe, in the centre of the flow field;

iii) the proximity of the fibre ends to the die entrance.

However, the extrudate only showed slight defects in surface texture. Since the length of the die is small, this suggests that either:

a) effects generated by the above factors are relatively small at the shear rates and temperatures involved, or

b) the viscosity of the polymer is significantly low that relaxation can occur before the extrudate emerges from the die.

3.7 Conclusions

1. The Raman spectra of flowing molten polyethylene have been successfully recorded from the entrance to a capillary die for the first time. Using an optical fibre system specially designed for this purpose, laser radiation was transmitted to the die, and scattered radiation collected and transferred to a Raman spectrometer.

2. The use of optical fibres in hostile conditions of high temperature and pressure has been successfully demonstrated. The apparatus was shown to have some limitations. However, further improvement of the probe's resilience and flexibility will allow a large number of possibilities to be explored with regard to understanding the nature of this system.

3. This study has led to the conclusion that over the range of shear rates and temperatures considered there is no resolvable molecular level structure in the molten polyethylene.

References

1. P.J. Hendra, D.B. Morris, R.D. Sang, H.A. Willis, Polymer 23 9 (1982)

2. A.J. Peacock, PhD Thesis, Univ. of Southampton (1984)

3. R.P. Brown (ed), "Handbook of Plastics Test Methods", Goodwin (1981)

4. I.M. Ward, "Structure & Properties of Oriented Polymers" Appl. Sci. Pub (Lond) (1975)

5. J.A. Brydson, "Flow Properties of Polymer Melts" Illife (1970)

6. E.R. Howells, J.J. Benbow, Trans. Plast Inst 30 240 (1962)

7. S.L. Wunder, Macromol 14 1024 (1981)

8. R.G. Brown, J. Chem. Phys. 38 221 (1963)

9. M.A. Taylor, PhD Thesis, University of Southampton (1985)

10. L.A. Hunsden, (unpublished data)

11. J.H. Southern, R.S. Porter, H.E. Bair, J. Macromol. Sci. Phys. B, 4 541 (1970)

12. J.H. Southern, G.L. Wilkes, J. Polym. Sci. Polym. Lett. 11 555 (1973)

13. C.D. Han, L.H. Drexler, J. Appl. Polym. Sci. 17 2329 2355 2369 (1973)

14. C.D. Han, L.H. Drexler, J. Appl. Polym. Sci. 19 2403 (1975)

15. M.R. Mackley, F.C. Frank, A. Keller J. Mat. Sci. 10 501 (1975)

16. J. Vile, PhD Thesis, Southampton (1983)

17. T.W. Haas, B. Maxwell Polym. Eng. Sci. 2 225 (1969)

18. P. Clegg, "The Rheology of Elastomers" Pergamon Press (1958)

CHAPTER 4

EFFECTS OF A SWELLING AGENT ON THE LOW FREQUENCY RAMAN SPECTRUM OF POLYETHYLENE

4.1 Introduction

Melt crystallised polyethylene contains regions of well ordered crystalline material called lamellae, together with a substantial amount of amorphous material. The nature of the relationship between these two components is the subject of much debate. However, it is widely accepted that there is a regular alternation between crystalline and amorphous material (1), see figure 4.1.

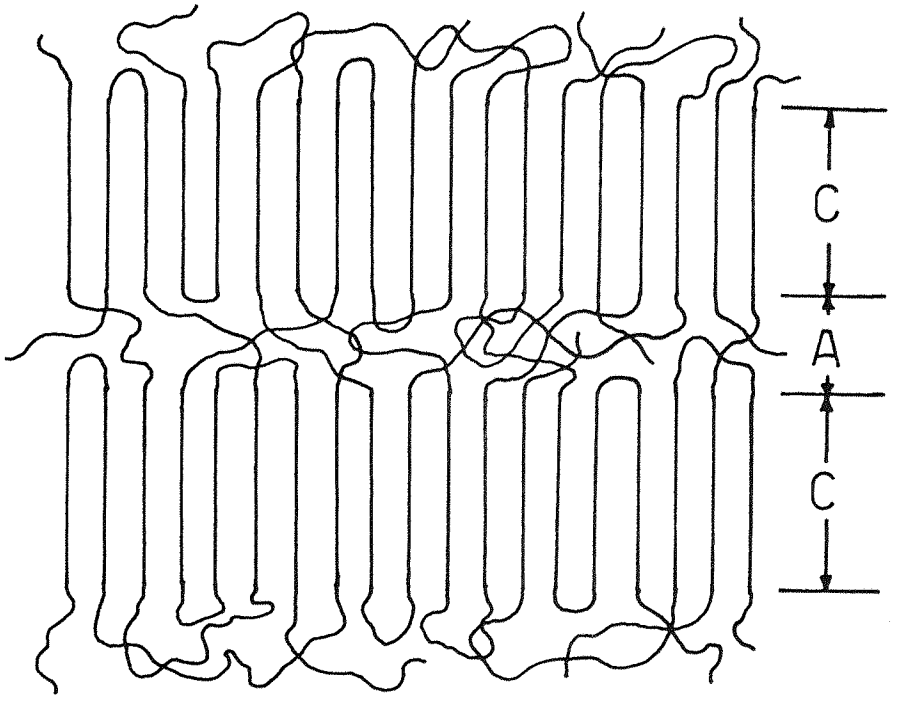

Figure 4.1

Lamellar structure of a polymer. C = crystalline, A = amorphous region

4.1.1 Lamellar Structure

Several methods have been used to study the lamellar structure of polymers. Small angle X-ray scattering (SAXS), electron microscopy, chemical methods of oxidation with G.L.C. analyses are well established techniques, and their contributions to the understanding

of polymer morphology are widespread. However, their reliability depends upon tedious and precise sample preparation. Subsequently much excitement was generated with the observation of a low frequency vibration in the Raman spectrum of polyethylene (2,3), which could be related to lamellar thickness. The Raman method was relatively simple, and offered the possibilities of routine characterisation of polymer structure and morphology. However, the derivation of the exact relationship between the Raman data and the thickness of the lamellae is highly controversial.

4.1.2 The Longitudinal Acoustic Mode (LAM)

Low frequency Raman active vibrations of this type were first observed in a series of short chain solid n-paraffins (4). These were assigned to the vibration of the carbon atoms in the direction of the chain axis (see figure 4.2), and using simple acoustical theory,

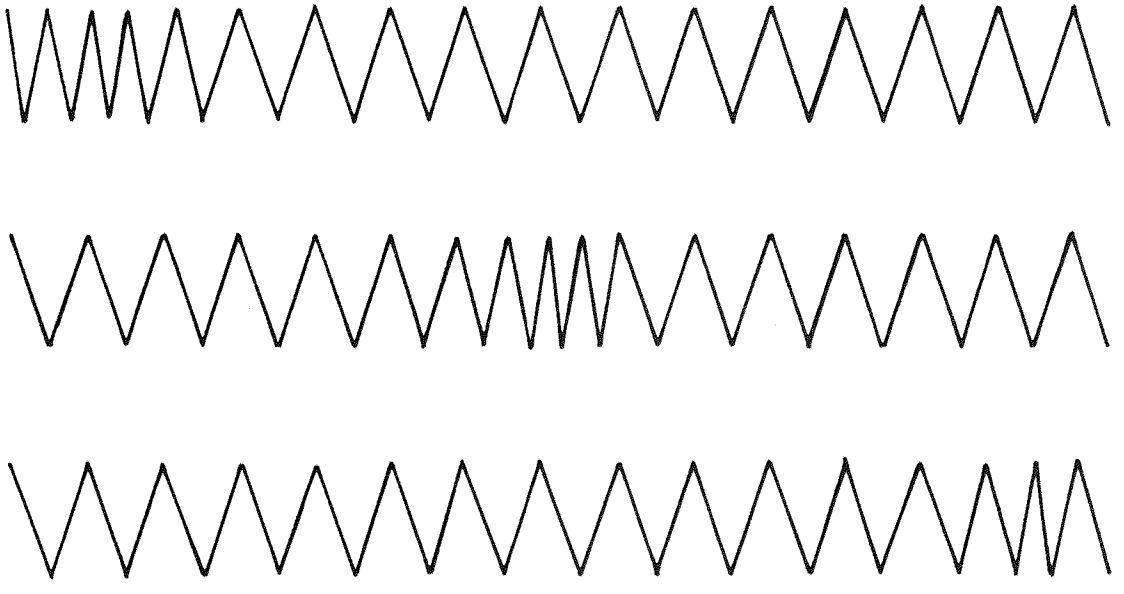

Figure 4.2

Progression of accordian longitudinal acoustic mode (LAM-1) along the chain axis.

based on the vibration of a rigid rod, the length of the chain, L, was related to the frequency of the vibration, ν by the expression (4)

$$\nu\ (cm^{-1}) = \frac{M}{2cL} \left(\frac{E}{\rho}\right)^{\frac{1}{2}} \qquad \text{e.q. 4.1}$$

where c = velocity of light, E = modulus, ρ = density and M = an integer corresponding to the number of nodes in atomic displacement (see figure 4.3). A plot of the frequency of vibration versus the

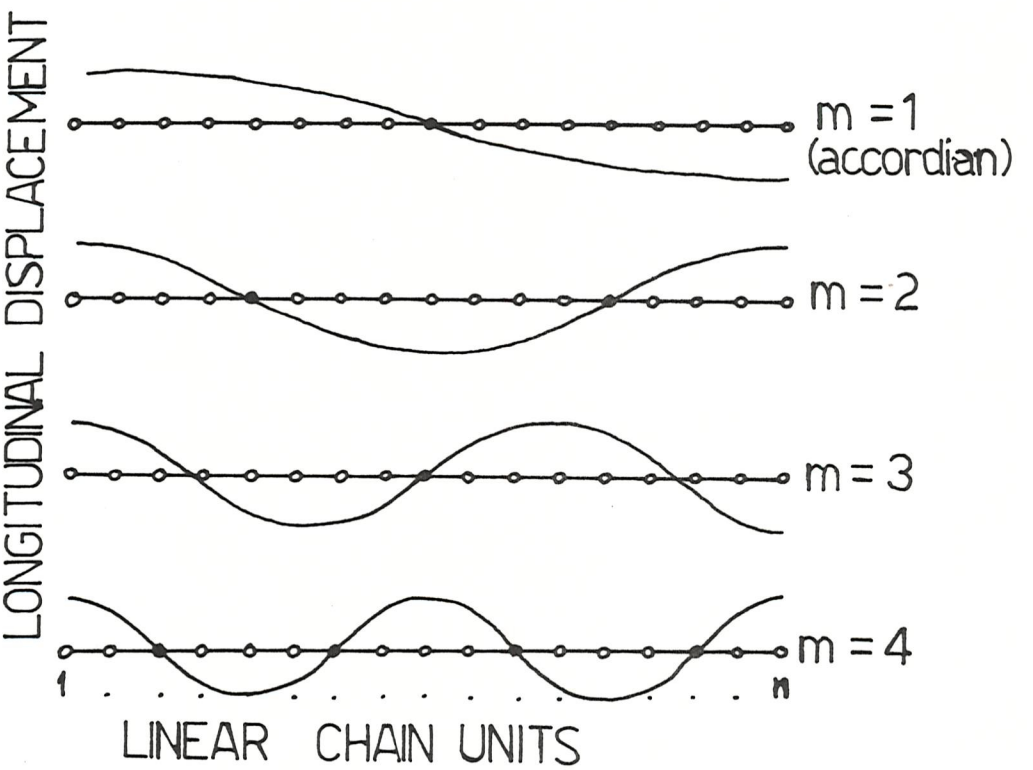

Figure 4.3

Vertical plot of the longitudinal displacements of a linear chain, showing nodes

inverse of the number of carbon backbone atoms for these alkanes give a linear result (5). Consequently the above expression has been used to calculate the value for the length of the vibrating section of a polymer chain within a lamella.

The simplest interpretation of the spectroscopically derived lamellar thickness is that in which the all-trans chain is terminated by a gauche unit at the surface of the lamella, at each end. The correlation between the Raman derived chain length and the X-ray long spacing (see figure 4.4) was such that the Raman measurement

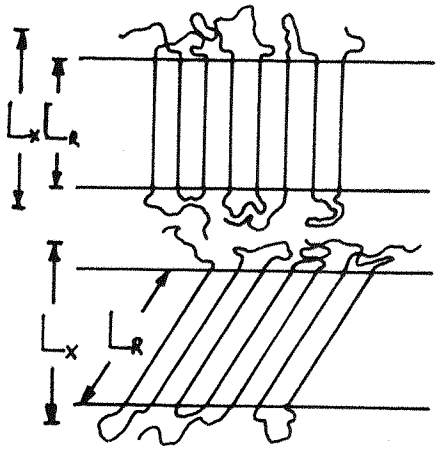

Figure 4.4

Measurement of lamellar thickness, L_X, small angle X-ray scattering long period; L_R, Raman stem length, and effect of chain tilt

could be assumed representative of the crystalline core alone, whereas the X-ray data measures the overall layer thickness (i.e. core + intercore zone). Hence, the Raman derived chain length is usually smaller than the X-ray spacing, but instances have been reported where, as a result of chain tilting (figure 4.4), the Raman length is found to be the greater (3,6).

There is conflicting evidence as to the interpretation that the LAM is completely representative of the crystalline core.

Olf et al(3) undertook a detailed study in which they found that on annealing polyethylene no significant changes in the LAM frequency

were observed, whereas Koenig (7) has shown annealing to increase the apparent lamellar thickness.

Removal of the amorphous material by etching (8,9,10) have shown identical values of the LAM before and after treatment, in both quenched and annealed samples.

Mandelkern (11) has also supported the rigid rod model, since participation in the vibration by amorphous material would result in a crystallinity dependence, which is not observed.

However, it has been suggested that the folds at the surface of the lamellae influence the frequency of the vibration by coupling with the vibration of the all-trans sequence (12). It appears that the frequency of the LAM is most sensitive to the structure of the first few groups beyond the all-trans sequence, but is very insensitive to those beyond six CH_2 units (13).

Perturbations due to material external to the crystalline core have been theoretically considered by a number of authors (14-18) and several models have been proposed. However, application to polymer systems have proved difficult.

4.1.3 Swelling of Polymers

A number of studies (19-22) have involved the addition of a non-solvating liquid to polymer samples, in order to determine the effect of interlamellar forces on the LAM frequency.

Ugadawa and Keller (19) found an increase in the SAXS long spacing on the addition of swelling agents to single crystal mats of polyethylene. These were found to return to their original periodicity on removal of the swelling agents. Raman measurements (20) revealed that the LAM frequency underwent reversible shifts upon swelling. This and other studies (21,22) suggested that the lowering of the LAM frequency was a result of the coupling of amorphous material with

the vibration of the crystalline core, rather than any change in the lamellar thickness. One study (22) does, however, leave interpretation open.

It is apparent that the current understanding is unsatisfactory, and that more evidence is required.

The swelling of bulk crystallised polyethylene has not previously been studied using Raman spectroscopy. With the newly developed fibre-optic sampling technique, the effect of the swelling agent on the LAM frequency is to be approached, with a view to understanding more fully the nature of the LAM, and its value as a spectroscopic determinant of the crystalline core thickness.

4.2 Experimental

4.2.1 Sample Preparation

The polymer chosen was Rigidex 006-60 high density linear polyethylene, available as pellets.

Three different sample types were considered:

(a) Extruded at 190°C (as in Chapter 3). Length of 10cm was cut from die during extrusion and allowed to cool to room temperature.

(b) Pellets heated to 190°C in hot press, 50psi. Allowed to cool slowly ($\sim\frac{1}{4}$°C/minute) in press. Thickness 0.5mm.

(c) Pellets heated to 190°C in hot press, 50psi. Removed from press and rapidly cooled by quenching in ice-water.

Samples for Raman spectroscopy were prepared as in figure 2.15 (Chapter 2) for the fibre-optic method. For conventionally recorded spectra small samples 0.5 x 10 x 10mm were prepared for 'b' and 'c', and chips of similar dimensions were taken from the centre of the extrudate for 'a' (a 90° collection orientation was used).

4.2.2 Raman Spectroscopy

Raman data was recorded using the Coderg T800, using ~100mW of Ar^+ laser radiation at 5145Å. Low frequency spectra were recorded using a spectral bandpass of $1cm^{-1}$, and internal mode spectra were recorded with a spectral bandpass of $6cm^{-1}$.

Raman Crystallinity Measurements

All crystallinity measurements were made according to the method of Strobl and Hagedorn (23) using the relationship

$$c = \frac{I(1416)}{I(1296+1303) \times 0.46} \times 100\ \% \qquad \text{e.q. 4.2}$$

where c is the percentage crystallinity, 0.46 is the normalisation factor and I(1416), I(1296) and I(1303) are the integral intensities of the orthorhombic methylene bending vibration, the crystalline methylene twisting vibration and the amorphous methylene twisting vibration respectively. The areas under the peaks were measured using a Du Pont 310 curve resolver.

Sources of error in the Raman measurements arise from deconvolution. The $\Delta\nu = 1416cm^{-1}$ band is difficult to separate from its neighbours, but fortunately the area under the low frequency half of the band has a negligible contribution from the other bands. Thus by curve fitting to match this half of the band consistant results with errors in crystallinity of ±3% are possible.

4.2.3 Differential Scanning Calorimetry. (DSC)

DSC provides information on the thermal properties of materials. Basically, the instrument heats a sample and a reference (usually just a sample container) at a programmed rate. When a transition takes place in the sample an exothermic or endothermic reaction takes place. The difference between the power supplied to the sample and the reference holders to keep them at the programmed temperature is output as a peak or a trough on a chart recorder. The operation of the instrument is shown diagrammatically in figure 4.5.

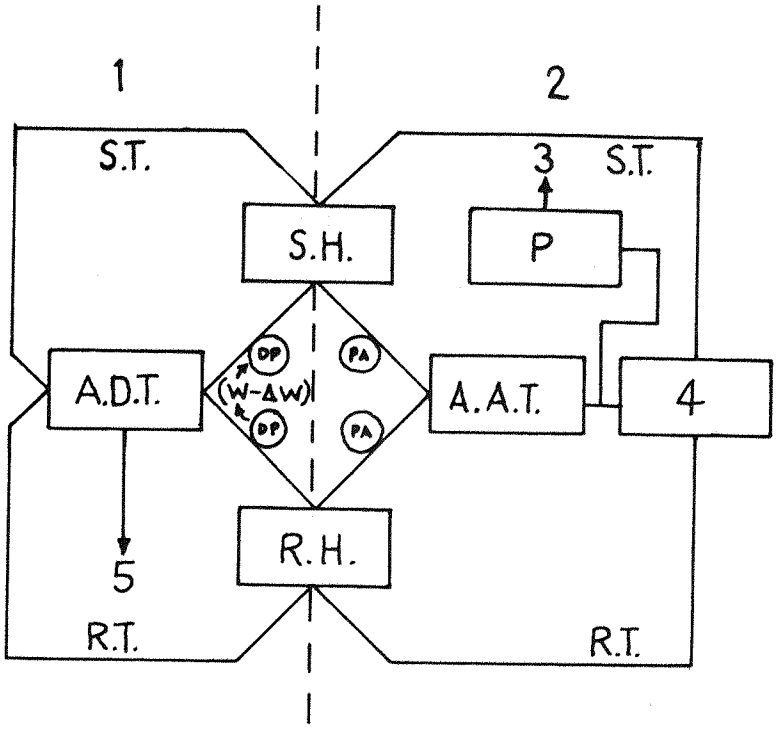

Figure 4.5

Block diagram of DSC-2 scanning calorimeter. ST = sample temperature, RT = reference temperature, SH = sample holder, RH = reference holder, PA = power (average), DP = differential power, AAT = amplifier (average temperature), W = power, P = programmer, 1 = differential temperature control loop, 3 = recorder (temperature marking, 4 = temperature averaging network, 5 = recorder (differential power)

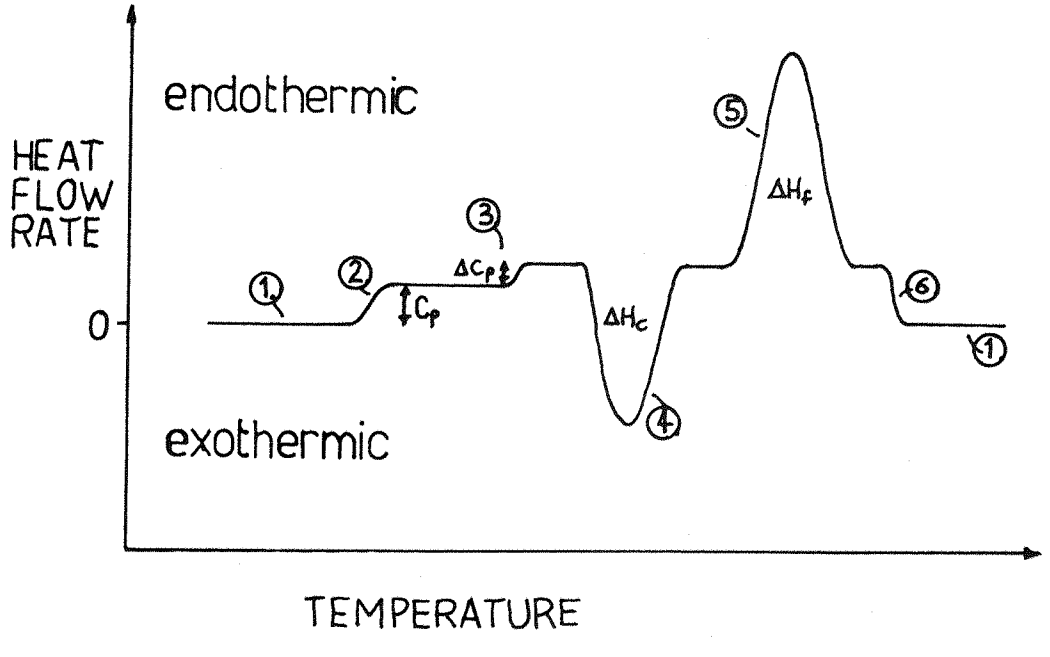

Figure 4.6

Conventions for representing thermal analysis data. 1, thermal equilibrium; 2, starting transient; 3, glass transition; 4, crystallisation; 5, fusion; 6 ending transient.

The instrument used was the Perkin-Elmer DSC 2. The samples were encapsulated in aluminium sample pans. These, and empty pans, were placed in platinum/iridium alloy 'cups' contained in a massive aluminium block. When a melting transition occurs in the sample material, an endothermic reaction takes place. Figure 4.6 shows the conventions used in thermal analysis. The area under the peak indicates the total energy transfer to or from the sample compared with the reference specimen.

The melting temperature, Tm, for a pure crystalline material producing a pure amorphous melt is given by the expression

$$Tm = \frac{\Delta Hf}{\Delta Sc} \qquad \text{e.q. 4.3}$$

where ΔHf and ΔSc are the enthalpy and entropy of fusion respectively. Polymer systems, however, are never 100% crystalline and consequently the melting temperature is given by a more complicated relationship (24)

$$\frac{1}{T} - \frac{1}{Tm} = \frac{R}{\Delta Hf} \left(\frac{1}{xWa} + \frac{1}{x-L+1} \right) \qquad \text{e.q. 4.4}$$

where Wa = weight fraction of the amorphous material at temperature T, R = gas constant, x = degree of polymerisation (related to the molecular weight) and L is a parameter related to the size of the crystallites.

This relationship indicates that T will increase as x, and hence molecular weight, becomes larger. Similarly as L increases, so does the melting temperature due to the increased surface energy of the larger crystallites. In any real polymeric system, these parameters will have a distribution of values and polymers will have a melting range rather than a well defined melting point.

It is possible to measure melting points and heats of fusion directly by using a differential scanning calorimeter. The heat of fusion data can be converted into crystallinity, c, using equation 4.5

$$c = \frac{\Delta Hfs}{\Delta Hfc} \times 100\% \qquad \text{e.q. 4.5}$$

where the subscripts s and c refer to the sample and 100% crystalline material respectively.

The enthalpy of fusion for each sample was determined by measurement of areas beneath dsc traces and calibrating with an indium standard. ΔHf_s was given by

$$\Delta Hf_s = \Delta Hf_i \frac{WiAsRsSi}{WsAiRiSs} \qquad \text{e.q. 4.6}$$

where subscript i refers to indium, s refers to sample. W = weight, A = area under curve, R = instrument range and s = the plotter chart speed.

A heating rate of 10°C per minute was used, and experimental errors in determination of crystallinity were estimated at ±4% between samples from the same specimen.

4.2.4 Density Column Measurements

Density measurements were made on a standard density gradient column with an ethanol/water mixture. The degree of crystallinity was calculated from the following relationship,

$$c(\%) = \frac{\rho s - \rho a}{\rho c - \rho a} \times 100$$

where ρs = density of sample

ρc = density of 100% crystalline polyethylene = $1.013 gcm^{-3}$ (25)

ρa = density of 100% amorphous polyethylene = $0.855 gcm^{-3}$ (26)

4.2.5 Swelling

The samples were swollen in xylene at 60°C for up to one week. The Raman spectra were recorded using optical fibres on the same samples after repeated removal from and replacement in the xylene. In all other measurements, excess xylene was removed using a tissue.

In one of the samples in which fibre-optics were used, the xylene was removed using a vacuum oven at 40°C.

4.3 Results

4.3.1 Raman Method

Conventional and optical fibre Raman spectra were recorded from a bulk sample of polyethylene. Comparisons showed no discrepancy in relative band position and intensity.

Low frequency L.A. mode spectra are shown in figure 4.7. For spectra such as these, the instrument is scanned over a frequency range very close to that of the exciting radiation. The intensity of the exciting line is $\sim 10^6$ times the intensity of a strong Raman signal, and consequently the L.A. mode is superimposed on a steeply sloping background.

It was noticed that the optical fibre method allows the spectroscopist to scan closer to the exiting line - to within $5cm^{-1}$ - and achieves a more acceptable band definition with the same instrumental settings.

4.3.2 Raman Longitudinal Acoustic Modes: Effects of Swelling

Raman spectra recorded using the fibre-optic method showed significant changes in the L.A. mode when the sample was exposed to xylene at 60°C. These changes were reversible; on evacuation of the xylene the L.A. mode returned to its original position (see figure 4.8).

The L.A. mode frequency appears to decrease and the distribution of the band broadens with length of time in xylene.

An analysis of the L.A. mode was made, and a conversion into lamellar thickness based on the rigid rod model is included in table 4.1.

The conventional spectra obtained from quenched, slow cooled and extruded chip samples did not show these effects upon swelling in xylene.

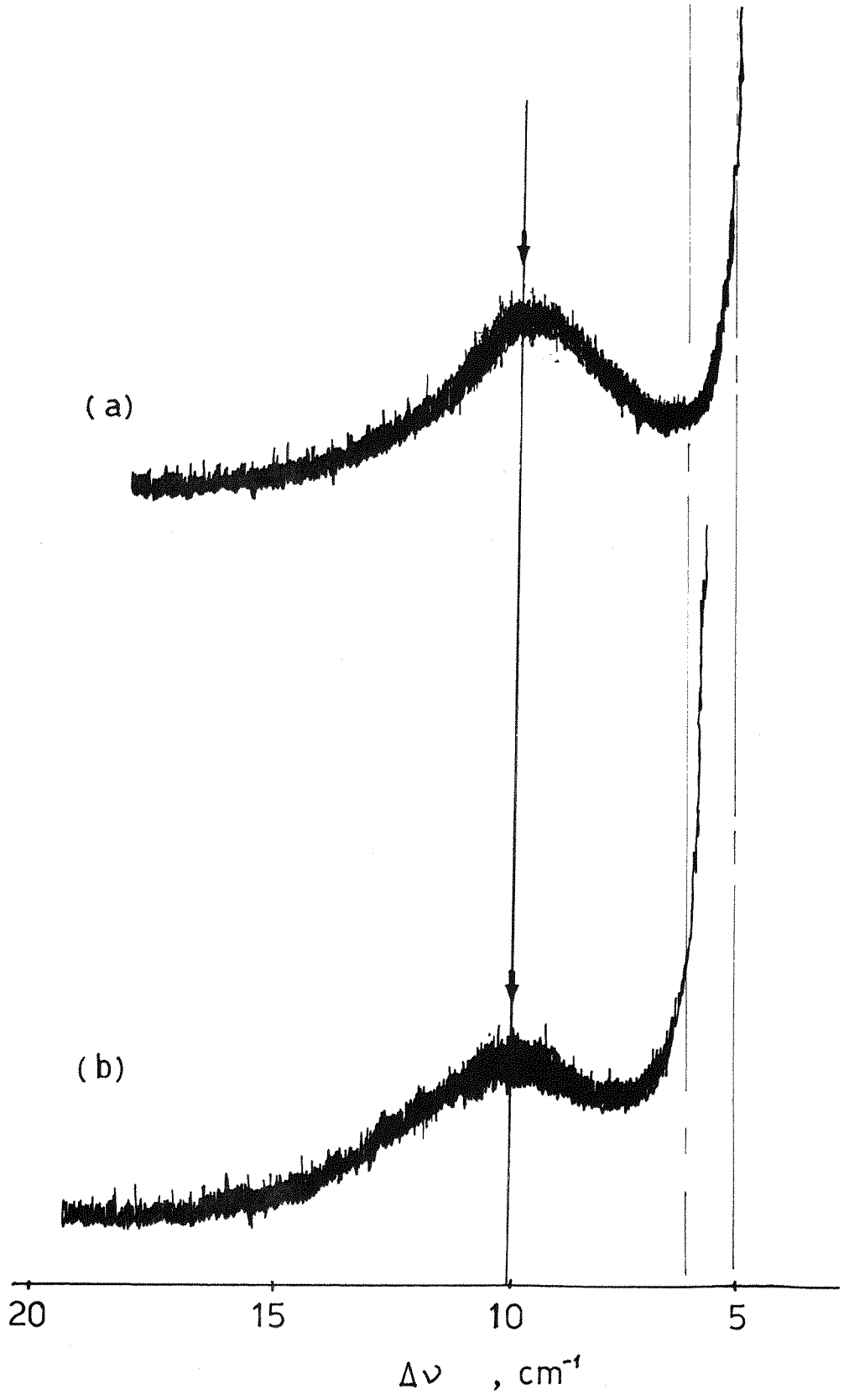

Figure 4.7

LA modes in polyethylene recorded using (a) fibre-optics, and (b) conventional Raman techniques.

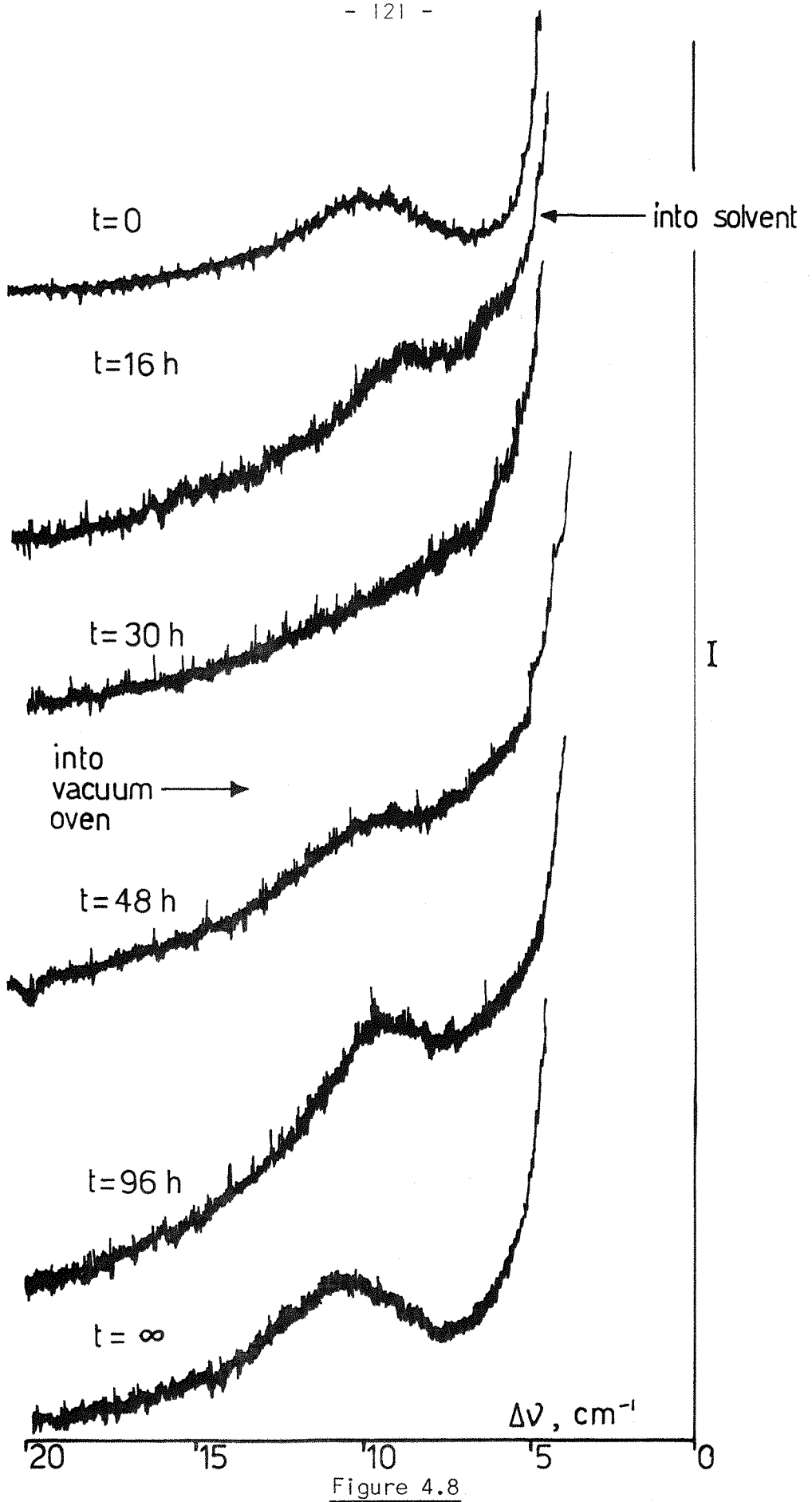

Figure 4.8

Changes in low frequency Raman spectra of polyethylene on swelling with xylene.

4.3.3 Raman Internal Modes

The relative intensity of the L.A. mode and the methylene twisting vibrations at $\Delta\nu$ = 1296 and 1303cm^{-1} (internal standard) was calculated for one of the samples. The intensity of the LAM appeared to decrease relative to the internal standard with the addition of xylene.

The Raman derived crystallinity was shown to increase with time in xylene, and the effect was reversible, shown by a decrease in the crystallinity on removal of xylene (table 4.1).

Time (h)	Raman crystallinity (%)	$\Delta\nu$, LAM (cm^{-1})	L (Å)	$\Delta\nu_{\frac{1}{2}}$	$\frac{I(LAM)}{I(1296)}$
0	88	9.5	355	6	1.3
24	91	7	455	8	1.1
35	97	6	535	-	0.9
0	82	11	290	5.5	-
16	-	9	355	6.5	-
* 30	96	8	400	-	-
78	87	9	355	6	-
126	-	10	320	5.5	-
168	78	10.5	305	5	-

* Placed in vacuum oven at 40°C after measurement

TABLE 4.1

Raman crystallinity and L.A. mode results for swelling of polyethylene in xylene

4.3.4 DSC/Density Crystallinity

These were measured for samples 'a', 'b' and 'c'. A trend of increase in crystallinity with increasing xylene content was observed+ (table 4.2).

+ The xylene was not removed from the samples before dsc and density measurements were taken. This may have an effect on the results.

Sample	Time (h)	Crystallinity %		$\Delta\nu$, LAM (cm^{-1})
		dsc	density	
a	0	66	66	11
	25	67	69	-
	48.5	74	75	-
	96	-	79	-
	173	74	78	-
b	0	67	66	17
	25	66	66	-
	48.5	68	67	-
	96	69	68	-
	173	68	70	-
c	0	73	78	8.5
	25	71	77	-
	48.5	76	78	-
	96	78	90	-
	173	78	85	-

TABLE 4.2

DSC, density crystallinities and $\Delta\nu$(LAM) for quenched, slow cooled and extruded samples of polyethylene swollen in xylene

4.4 Discussion

The determination of the lamellar thickness in polymers using the low frequency Raman-active LAM vibrations has been the subject of much controversy.

The newly developed fibre-optic sampling technique was used to investigate this very important issue further, and it is clear from the preliminary results that the experimental technique is favourable.

Comparisons between fibre-optic and conventional data show that the spectra obtained are identical, as are the results of Raman crystallinity measurements within expected margins of error.

The fibre-optic method can observe the same region of the sample each time, thus increasing the repeatability of experiments and reducing overall errors.

The fibre-optic method allows one to scan closer to the exciting line. This may suggest that the Raman scattered radiation is transmitted by the fibres more efficiently than scattered radiation at the exciting frequency. This is unlikely. The Raman spectrophotometer, however, is sensitive to the polarization of the radiation which it collects. Since multimode optical fibres produce circularly polarised light (polarised in all directions, i.e. scrambled), the improvement in the L.A. mode spectra may simply be due to the alteration in the polarization characteristics of the system.

Considerable changes in the LAM's obtained from a sample of extruded polyethylene were observed when the sample was placed in xylene over a period of one week. The frequency of the LAM bandhead decreased with length of time in the xylene, and the distribution of LAM frequencies broadened. This effect was reversible, and has been previously observed in single crystal mats and similar polymer systems (19-22).

The difference in the relative positions of the LAM in the untreated sample (figure 4.9a), and that after the sample had been treated and fully evacuated (figure 4.9f) suggests that some annealing has occurred. This is surprising at such a low temperature. However, similar results have been previously reported (27).

A decrease in the frequency of the LAM indicates an increase in the lamellar thickness given that the rigid rod model applies. This increase in lamellar size is supported by the crystallinity data. The Raman crystallinity was also shown to decrease on removal of the xylene.

However, penetration of xylene into the crystalline regions is negligible (13), and no swelling of the core is expected. The changes in the LAM observed indicate massive structural chantes in the polymer. A reversible rearrangement which results in an increase in the lamellar thickness of 200Å seems unlikely, especially given the crystallisation conditions, and polyethylene with a lamellar thickness of 535Å is unusual. No changes in the physical dimensions of any of the samples were observed.

Although the trends in the low frequency spectroscopic data are consistent, the magnitude of the changes they suggest is unusual. The reason for this effect is unknown at present, but may arise from:

(a) a breakdown in the acoustic theory which defines the relationship between the LAM and the lamellar thickness, for this particular system of bulk polyethylene; or

(b) an optical effect at low frequency due to the presence of xylene within the polymer sample.

It is clear that optical fibres, when used in the Raman spectroscopy of polymer samples, can produce interesting data, and allow another approach to this very important field of polymer science.

A more detailed study, and further development of this technique in the investigation of the LAM is needed before more clear structural evidence can be provided.

4.5 Conclusions

1. The Raman spectrum of polyethylene was recorded using fibre-optics. When compared to the conventional method, the information obtained was identical. The fibre-optic data, however, had the advantage of greater repeatability.

2. The LAM in polyethylene was recorded using fibre-optics for the first time. The method appears to exclude a proportion of the Rayleigh scattered radiation allowing

the user to scan closer to the exciting line. Only a single injection and a single collection fibre was used.

3. The fibre-optic system was used to study the effects of swelling of polyethylene with xylene. It was found that:

   (a) The LAM moved to lower frequency and broadened on addition of xylene.

   (b) The Raman crystallinity increased on addition of xylene.

   (c) On removal of the xylene both the LAM frequency and the Raman crystallinity returned to their original values.

   (d) The magnitude of the effect is unusual. This suggests either:

      (i) the acoustic theory cannot be satisfactorily applied to this system; or

      (ii) a low frequency optical effect due to the xylene.

4. Fibre-optic methods have the potential of revolutionising the way in which the Raman spectra of polymers are obtained, and may be particularly valuable where low frequency work is involved.

References

1. P.J. Flory, J.Am. Chem. Soc. 84 2857 (1962)

2. W.L. Peticolas, G.W. Hibler, J.L. Lippert, A. Peterlin, H.G. Olf, Appl. Phys. Lett.18 87 (1971)

3. H.G. Olf, A. Peterlin, W.L. Peticolas, J. Polym. Sci. 12 D359 (1974)

4. S. Mizushima, T. Simanouchi, J. Chem. Phys. 47 3605 (1967)

5. J.F. Rabolt, CRC Critical Rev. Solid State Mater. Sci. 12 165 (1984)

6. M.J. Folkes, A. Keller, J. Steiny, G.V. Fraser, P.J. Hendra, Kolloid Z, uZ Polym. 253 354 (1975)

7. J.L. Koenig, D.L. Tabb, J. Macromol Sci. Phys. B9, 141 (1974)

8. A. Peterlin, G. Meinl, J. Polym. Sci. 83 1059 (1970)

9. D.J. Priest, J. Polym. Sci. Polym. Phys. Ed. 9 1777 (1971)

10. P.J. Hendra, E.P. Marsden, M.E.A. Cudby, H.A. Willis, Die Makromol Chem 176 2443 (1975)

11. M. Glotin, L. Mandelkern, J. Polym. Sci. Polym. Phys. Ed. 21 29 (1983)

12. D.J. Cutler, P.J. Hendra, G.V. Fraser, Dev. in Polym. Char. 2. ed Dawkins (1978)

13. C. Chang, S. Krimm, J. Appl. Phys. 54 5526 (1983)

14. S.L. Hsu, S. Krimm, J. Appl. Phys. 48 4013 (1977)

15. S. Krimm, S.L. Hsu, J. Polym. Sci. Polym. Phys. Ed. 17 2163 (1979)

16. G.R. Strobl, J. Polym. Sci. Polym. Phys. Ed. 21 1357 (1983)

17. G.R. Strobl, R. Eckel, J. Polym. Sci. Polym. Phys. Ed. 14 913 (1976)

18. G. Minoni, G. Zerbi, J. Phys, Chem. 86 4791 (1984)

19. A. Keller, Y. Ugadawa, J. Polym. Sci. A2 437 (1971)

20. G.V. Fraser, A. Keller, E.J. George, D. Dreyfuss, J. Macromol Sci. Phys B9 141 (1974)

21. C. Chang, S. Krimm, J. Polym. Sci. Polym. Phys. Ed 22 1871 (1984)

22. J. Runt, B.D. Hanrahan, I.R. Harrison, J. Polym. Sci. Polym. Phys. Ed. 20 1687 (1982)

23. G.R. Strobl, W. Hagedorn, J. Polym. Sci. Polym. Phys. Ed. 16 1181 (1978)

24. P.J. Flory, J. Chem. Phys. 7 223 (1945)

25. R.B. Beavers, J. Polym. Sci. A2 5257 (1964)

26. W.D. Niegisch, K.D. Swan, J. Appl. Phys. 31 1906 (1960)

27. P.J. Hendra, H.A. Willis, M.A. Taylor, Polymer 26 1501 (1985)

CHAPTER 5

CONCLUSION

5. Conclusion

The Southampton group is well known for its pioneering activities in the exploitation of Raman spectroscopy, and its application to novel areas of chemistry and physics. Thus, applications of the method to combustion systems, catalysts, *in situ* analysis of electrochemical processes, and polymer structural problems were all pioneered at Southampton.

One major problem still restricting the exploitation of Raman spectroscopy as a more effective technique is that of sample alignment within the spectrometer. In infrared spectroscopy, and u.v./visible spectrophotometry, the sample is simply placed in a beam of radiation, saturated with light, and the absorption/transmission characteristics are measured. Obtaining a Raman signal is in principle more versatile, and yet in practice more difficult. The difficulty arises with samples that generate weak Raman signals - these are usually the most interesting since all of the 'easy' samples have already been studied! In these cases it is frequently impossible to optimise the sample alignment since the Raman signal is invariably swamped by noise and background emissions. As a consequence, a potentially valuable experiment can be aborted simply because adequate alignment cannot be achieved. This is particularly frustrating when using modern instruments, which are capable of maximising sensitivity by accumulating spectra over long time periods.

In an attempt to overcome the alignment difficulties, two solutions have been proposed; the use of pre-aligned microscopes, and the use of fibre-optics.

Microscopic sampling techniques have been developed very rapidly of late, and successfully applied elsewhere. In fact, all manufacturers of Raman spectrometers now offer microscope illumination/viewing facilities. The applicant was asked to investigate fibre-optics following some preliminary studies made by a visitor to the department, Professor Richard McCreery of the University of Ohio.

Fibre-optics have been successfully developed as a Raman sampling system. It is now clear that:-

1. Fibre-optic illumination of the sample is efficient, and operable over relatively long distances. Losses in injection and along the fibre itself are acceptably small.

2. Fibre-optic collection of Raman scatter is highly efficient for some samples, and less so for others. No Raman characteristics of the optical fibres were produced in the spectral data recorded. Attempts were made to illucidate the exact form of the coupling between the Raman scatter and the collection fibre, but with little success.

3. Losses in optical fibres are low. Hence it is clear that, in favourable cases, illumination, collection, and consequently Raman measurements, are feasible far remote from the spectrometer.

4. No polarised data is available. This is due to the fact that multimode optical fibres produce circularly polarised light irrespective of the polarisation of the input laser beam, or that of the scattered radiation.

5. In at least one case, it appears that the spectra obtained are remarkably free from stray light. Attempts were made to explain this observation, since it is very unexpected, but with little success. Its exploitation was demonstrated.

6. No alignment at the sample is necessary once the fibre-optic system has been installed in the spectrometer. In certain applications (for example, surfaces), the orientation of the fibres with respect to the sample can improve the Raman data.

Hence, the outcome of this study has been highly satisfactory. The use of fibre-optics as an alternative sampling technique seems capable of exploitation, and this prediction has been demonstrated since the completion of the research reported here. A fibre-optic probe system is now available commercially, a development with which the candidate is involved. Further, scientists at B.P.'s research centre * are now exploiting the method in their work.

* Raman Laboratories, B.P. Research Centre, Sunbury-on-Thames

Future Developments

(a) In this work a system based upon two lengths of optical fibre - one to stimulate the sample, the other to collect the scattered light - has been developed. The obvious next step is to use a number of fibres to collect the scattered light, and thus increase the amount of scattered radiation entering the spectrometer. This work has already been initiated, and workers at B.P. have developed a multi-element probe. It is clear, from their results, that the expected gains are realised.

(b) The use of microlenses, to focus the output of the laser-light-carrying fibre may prove advantageous in certain specific sampling arrangements. SELFOC* microlenses are currently under consideration.

(c) With the increasing utilisation of microcomputer technology in spectroscopy, the future development of a standard fibre-optic system for remote sampling needs serious consideration. With the high capital investment, servicing and running costs inevitably associated with Raman spectrometers, a more efficient use of instrument time would prove invaluable to many existing and potential users. The development of a central spectrometer (or series of) with a fibre-optic and microcomputer network linked to a number of isolated experimental locations has obvious appeal. However, a project on this scale will require the financial and developmental resources of a large commercial organisation.

(d) Specific applications of Raman spectroscopy tend to involve the use of additional apparatus in order to access the sample to the spectrometer. Many Raman 'cells' have been developed over the years to cope with these tasks. Since fibre-optics allows a much greater flexibility in experimental geometry, a whole new generation of sampling cells can be developed. Fibre-optics should reduce the need to modify experimental environments to suit the spectroscopist, and problems previously neglected because of sample alignment difficulties can be reconsidered.

*Nippon Sheet & Glass Company

(e) The recent developments in Fourier Transform Raman spectroscopy (F.T.R.) make the use of fibre-optic sampling even more exciting. The entrance pupil of the F.T. system, the Jacquinot stop, is a circular aperture. This can be ideally matched to a fibre collection system. Further, near-infrared excitation is typically used - the 1.65μ Nd-YAG laser is popular. The red-shifted Raman scatter should be very effectively carried by modern telecommunication-grade optical fibres.

Application of Fibre-Optic Technology to the Raman Spectroscopy of Polymers

To demonstrate the value of the techniques developed in their work (chapter 2), a brief excursion into the realms of polymer science was undertaken, and two projects were perused.

It was shown that:-

(a) No orientation effects are observable in the Raman spectrum of a flowing polyethylene melt.

An optical fibre probe was placed in the centre of an extruder die, parallel with the flow direction, and adjacent to the entrance of a cylindrical die 1mm in diameter. The probe withstood conditions of high temperature and pressure, to successfully record Raman spectra of high quality.

The alignment of polymer chains along the direction of flow in highly sheared melts has been used to explain such phenomena as stress induced birefringence patterns, die-swell and frozen-in orientation. The coaxial flow experiment undertaken in this study can be sensitive to molecular alignment during flow only in terms of changes in the rotameric structure of the polymer chains. The CH_2-CH_2 gauche/trans ratio is defined solely by temperature; alignment will be expected to affect the distribution of rotamers, favouring those of form $(trans)_n$ and $(gauche)_n$ rather than the (trans-gauche). As a result the internal mode structure ought to be shear rate dependant. This *in situ* study of molten polyethylene under conditions of high shear has shown that the rotameric structural sensitivity to shear is slight.

Although the rheological/optical effects produced in the processing of polymers may be a function of molecular alignment and/or orientation induced while the polymer is in the molten phase, their extrapolation to the molecular level behaviour of the polymer chains is far more complicated than their tidiness suggests.

In the polymer processing industry, complete control of the degree and direction of orientation is much sought after. A full understanding of the mechanisms of orientation would revolutionise the design and fabrication of synthetic polymer products. It has yet to be successfully shown that the behaviour of the molecules melt decides the final properties of the polymer product. The secret must lie in the exact crystallisation conditions of the polymer, and the key to this must be the effect of shear on the nuclei present at the onset of crystallisation.

(b) The longitudinal acoustic mode (LAM) in solid linear polyethylene was shown to move to lower frequency, and broaden on swelling the polymer in xylene.

Fibre-optics were used to record the Raman data. The effect was reversible, and its magnitude and occurrence, combined with crystallinity data, suggests either:-

i) a deficiency in the acoustic theory with this system, or

ii) an optical effect originating from the xylene.

It is quite clear that close to the laser exciting line the background does change on the addition of xylene. However, if we were to assume that the xylene had no detrimental spectroscopic effects (as the internal mode spectra might suggest), the behaviour of the LAM would tend to imply that the acoustic theory should not be religiously applied to real polymer systems.

Complete abandonment of the Raman approach to the determination of the lamellar thickness of polymers would be a pity, since the method allows a great deal of versatility when compared with its counterparts.

Recording Raman bands close in to the laser wavelength, and their subsequent deconvolution from a steeply sloping background, can be difficult. However, optical fibres do appear to remove a proportion of the stray light, making this task a little easier. Clearly the observations cannot easily be ignored. However, further work is necessary in order that the exact relationship between the xylene and the spectroscopic data might be determined, before the application of the acoustic theory can confidently be challenged, and this is now in hand at Southampton.

Much of the work in this thesis is intended for publication. The appendix contains a paper prepared for the Journal of Raman Spectroscopy (in press). A paper including the work on flowing melts is also in preparation, and includes data from infrared and x-ray diffraction studies by colleagues in the Southampton polymer research group.

Since it is in the tradition of the Southampton group to consolidate its existing lines of research, the reader is referred to the work of future members of the group for further developments. Much of the work suggested above as "to follow" is already under way, with every prospect of an exciting outcome.

G. Ellis

APPENDIX

The Use of Optical Fibres in Raman Spectroscopy

P. J. Hendra and G. Ellis

Department of Chemistry, The University, Highfield, Southampton, Hants, SO9 5NH, U.K.

D. J. Cutler *

Applied Photophysics Ltd, 20 Albemarle St., London, W1, U.K.

* Current address Perkin-Elmer Ltd., Post Office Lane, Beaconsfield, Herts, HP9 1QA, U.K.

Abstract

This paper describes a detailed study of the parameters governing the design of an optical fibre system for use in Raman spectroscopy. The results have led to the design and construction of a flexible fibre optic remote sampling system which is easily adaptable for use on most commercial instruments. A variety of samples were used to evaluate the performance of the system and have been classified in terms of the efficiency of the new technique relative to more conventional methods of excitation and collection.

Introduction

This paper describes an investigation into some of the design parameters governing the production of an efficient and versatile fibre optic coupled sampling system. It compares this method of sampling with more conventional systems and outlines a number of implications important to the future development of fibre optic Raman techniques.

Previous experiments (1,2,3) have demonstrated the use of fibre optics in Raman spectroscopy and work in this laboratory (4) has introduced the concept of remote sampling leading to the development of a viable multi-element probe (5).

System Description

A fully enclosed system has been developed and its general applicability tested on both a multichannel (Applied Photophysics model LR-36) and a scanning (Coderg model T800 triple monochromator) laser Raman spectrophotometer .

Based on previous experience, separate fibres were used to illuminate the sample and to collect the scattered light for return to the spectrometer collection optics.

A modified commercial spatial filter was placed inside the pre-sample optical compartment of the spectrometer to collect the laser beam (Argon ion, 514.5 nm line) and focus it down on to the end face of an optical fibre. The latter was securely held in the centre of a pin chuck and was always gripped by its cladding - never the bared fibre end. The laser radiation used was always filtered by the pre-monochromator fitted to the LR-36, rather than the "raw" laser output.

In the experiments described below a standard telecommunication plastic coated silica (PCS) type optical fibre was used. The fibre consisted of a 200 micron silica core surrounded by a 125 micron sheath of silicon rubber with a nylon protective layer on the outside.

The system was designed such that the existing conventional spectrometer pre-slit optics did not need to be modified. The

spatial filter assembly was mounted such that it could easily be slid out of the way of the laser beam for conventional scattering experiments, and reliably replaced to inject the laser beam into the optical fibre.

The laser light is transmitted to the sample, where a second fibre collect some of the scattered radiation. This is returned to the other end of the fibre which is clamped in an adjustable mount in the sample compartment of the spectrometer. Conventional reverse illumination and Raman peak maximisation techniques were used to align the fibre with respect to the spectrometer collection optics.

Preparation of the Fibres

The protective coating and cladding materials were stripped back to about 2Ø mm from the end of the fibre. A fine scratch was scored on the fibre, perpendicular to its axis and a few mm from the end of the cladding, using a keen glass cutting blade (e.g. Jencons "King Cut"). When wetted, the fibre broke easily at the score mark when using a small amount of pressure. The cleaved end of the fibre was mounted in the spatial filter and inspected using the microscope objective. The cleaved end should appear "perfect" i.e. show no signs of chipping, distortion or assymetry.

As a further test of the quality of the fibres, they were illuminated by the laser in the usual way and the output laser beam projected on to a screen some 3ØØ mm from the end of the fibre. A finely speckled, round, evenly illuminated patch of light should appear if the fibre end is perfect. In order to observe this pattern, care must be taken to ensure that the laser focus is centred precisely on the fibre end and that the illumination direction is coaxial with the fibre.

Finally, the fibre is reversed and the quality of the other end checked in the same way. If either end of the fibre is damaged, the fibre will fail to produce the required pattern.

Illumination of the Fibre

The light gathering power of an optical fibre is denoted by its numerical aperture (NA). This parameter is solely governed by the refractive indices of the system (n_0, n_1, and n_2, see Figure 1) and is completely independent of the fibre length or diameter. Given that n_0 is usually air (1.0) the fibre will accept (or propogate) a cone of light whose half angle θ_m, is given by

$$\sin\theta_m = (n_1^2 - n_2^2)^{1/2}$$

Where n_1 = core refractive index, n_2 = cladding refractive index and $n_2 > n_1$.

θ_m defines the numerical aperture

$$N.A. = \sin\theta_m$$

Using a x10 objective (f = 16.9 mm) to focus a perfect 1 mm laser beam we would expect a diffraction limited spot ω_0 of ca. 22 microns. In reality, we would expect a larger spot size than this, but even so it would still be considerably less than the 200 micron diameter core of the fibre. The next problem is to make sure that the convergence angle of the focused laser beam is within the collection angle of the fibre. In our case the NA of the fibre was 0.26 giving a collection half-angle of ca. 15 degrees.

From the above analysis we would expect a x5Ø objective to be best, however, the effectiveness of several objectives are listed in table I and it is clear the the x2Ø objective provides the best compromise. The x2Ø objective was used for the rest of this study.

Having properly aligned the fibre assembly, as outlined previously, with the correct value of objective, a good quality multimode PCS fibre, 3 m in length and 2ØØ microns in diameter, should transmit > 7Ø% of the incident power as defined below

$$\frac{\text{Total Power From End Face of Fibre}}{\text{Total Power entering Spatial Filter}}$$

Illumination and Collection Geometry for liquids

The following section describes the investigation into the optimum method of sample illumination and Raman light collection. Unless otherwise indicated, the laser power and spectrometer operating conditions were kept constant, and the intensity of selected Raman lines were used to monitor the performance of different experimental arrangements. Where appropriate, the efficiency of the fibre optic system was compared against conventional excitation/collection methods.

(i) Angular Dependance

In this series of measurements, the fibre carrying the laser beam was clamped vertically in a sample of nitrobenzene. The collection fibre was placed at various angles θ to the illumination fibre whilst keeping the two fibre ends in contact and in the same vertical plane. For each angular position, the Raman spectrum of nitrobenzene was recorded after optimisation of the 1346 cm-1 band by small lateral movements ofthe illumination fibre.

Measurements of the intensity of the 1346 cm-1 band at 4 included angles, between Ø and 7Ø degrees, are shown in Figure 2(b). Clearly the parallel combination is the most efficient.

(ii) Vertical and Axial spacing Dependence

The experimental setup used here is also illustrated in Figure 2. Again, the illumination fibre was clamped vertically in a sample of nitrobenzene and the position of the collection fibre varied. This time the two fibres were maintained parallel and the effect of varying the inter-fibre separation (with the fibres at the same height), and the effect of relative vertical displacement (at constant fibre separation) were monitored and plotted in Figure 2(a). It appears that a slight vertical stagger of ca. 2 mm, with the two fibres as close together as possible is the most favoured configuration.

Use of Capillary Tubes

It was felt that shrouding the fibre ends in a capillary tube would enhance the collection efficiency by confining the laser illumination to a small volume. Three types of capillary were studied, thick and thin walled glass tube and stainless steel tube, all with diameters in the range 1 - 7 mm.

The experimental arrangement and results are presented in Figure 3(a). The illumination and collection fibres were clamped vertically, maintained close together and parallel, approximately 300 mm from the bottom of the sample vessel. As expected, increasing the diameter of all the tubes resulted in a reduction in the intensity of the 1346 cm-1 band of nitrobenzene. The thick walled glass tube was found to be the most efficient and the stainless tube the least. It is worth noting that all the arrangements, including 7 mm stainless tube, gave some enhancement over the case of the bare fibre ends, with the narrow thick walled glass tube giving some 25% of the signal available using conventional (lens) excitation and a single collection fibre.

Also monitored, was the effect of the distance between the end of the fibers and the end of the capillary. The results, for a 2 mm diameter thick glass walled tube, are shown in Figure 3(b). The intensity of the 1346 cm-1 band of nitrobenzene steadily increases with the length of the capillary projection up to a value of ca. 60 mm when it becomes relatively constant.

Effect of Refractive Index

From the definition of the NA of a fibre, it is quite clear that the acceptance half angle θ_m depends on the refractive index of the liquid in which the fibre ends are immersed.

In this experiment, a range of samples were used to obtain values of refractive index between 1.333Ø and 1.552Ø (the refractive index of synthetic fused silica is 1.4616 at 514.5 nm).

In this case a comparison between the fibre optic experiments and conventional excited spectra were made. The experimental arrangement were as in Figure 1, for the conventional method, and point 'S' in Figure 2. The results are listed in Table II*, where it can be seen that there is no apparent correlation between the index of refraction of the sample and Raman efficiency.

It is also clear that conventional and fibre optic illumination are of comparable efficiency i.e. within a factor of 2 or so, for most of the samples examined.

---

* The absolute Raman intensity, however excited, depends on the index of refraction. No special allowance was made for this effect and it was assumed (without justification) that it applied equally to both methods of excitation.

The interesting value for milk almost certainly results from the colloidal nature of the sample.

Illumination and Collection Geometry for Powders

A variety of powdered and granular samples were examined. It was discovered that stronger Raman signals were obtained with the probe buried several mm into the sample than when the fibre ends were suspended just above the sample surface.

The results, also listed in Table II, show that the fibre optic probe appears to be a favourable method when compared with more conventional lens excitation, together with some indication that the system performs better with fine powders than coarse or granular ones.

In many cases it may be necessary to study samples with the fibre ends suspended above the sample surface rather than embeded in it. However, it was observed that the Raman signal falls as the probe is removed from the sample, the effect being greater when the powder is coarse.

As with the liquid experiments, an improvement in signal intensity was observed if the powder was introduced into an internally reflecting capillary tube. This may be a useful method of recording Raman spectra when only small amounts of sample are available.

Another result worthy of note is the spectrum of polytetrafluroethylene (PTFE). Some commercial samples of this material can be very difficult to study (particularly for

multichannel machines) due to high levels of background. As can be seen from the results, shown in Figure 4, the fibre optic probe used here appears to minimise this problem, giving a clean spectrum without the use of any special data processing techniques.

Illumination and Collection Geometry for Surfaces

A sheet of high density polyethylene (BP Rigidex ØØ6-5Ø) 5 mm thick with a relatively flat and homogeneous surface was used to assess the performance of the fibre method under various orientational parameters. All measurements were taken over the same region of the sheet.

Initial measurements showed the signal intensity obtained to be poor. However, significant improvements were observed when reflective surfaces were placed around the fibres. Two aluminium alloy blocks covered with aluminium foil were carefully pushed up against the fibres, resulting in a 3.5 times improvement in the recorded signal intensity. These were used in all subsequent experiments (see Figure 5).

i) Variation of collection angle

The injection fibre was placed perpendicular to the surface of the sheet and the collection fibre was placed adjacent and the subtended angle varied using an angularly adjustable mount. The intensity of the Raman signal at 1296 cm-1 was measured at each angular increment. The procedure was repeated, this time with the collection fibre perpendicular and the angle of the injection fibre varied, see Figure 5(a).

ii) Variation with fibre height from the surface

With both injection and collection fibres arranged at an angle of 17 degrees to the perpendicular the Raman intensity of the 1296 cm-1 band was recorded as the height of the fibre above the surface was altered.

Then, with the injection fibre perpendicular and in contact with the surface, and the collection fibre at 17 degrees to the perpendicular, the Raman intensity was measured as the collection fibre was raised to a height of 10 mm above the surface, see Figure 5(b).

The best results were obtained from the surface were with the angled fibres, providing an intensity of ca. 37% of that obtained conventionally (ca. 11% without the internally reflecting blocks). Also the closer the blocks were to the fibres the greater the enhancement of the spectra.

Conclusions

It is clear that optical fibres provide a versatile method of linking experiments to Raman spectrometers. The method is particularly attractive where the experiment has to be distant from the spectrometer and/or hostile enviroments are involved. We have in fact demonstrated this in recording the spectra of flowing molten polyethylene in an extruder die (6).

Even when using only one collection fibre (and many can be used effectively) in some cases the method is superior to conventional lens excitation. If six collection fibres are use the method is competitive for a wide range of samples and for routine analytical work avoids the alignment problem.

Fluorescence and background impose severe difficulties in laser Raman spectroscopy both in sample alignment (if the Raman signal is swamped by a large background it may be difficult to locate a known line in order to optimise the peak intensity) and in the quality of the spectra produced. Optical fibres appear to remove much of the stray light which leads to high levels of background. The sample alignment is trivial and the spectra produced are of high quality.

There is some advantage in using an index matching fluid at the end of the fibres in this type of work. Further, use of internally reflecting cylinders around the fibre ends appears to be highly advantageous and leads to an obvious design developments

in the production of probes.

Although not specifically discussed in the body of this paper, fibres destroy the polarization of the laser and this means that polarised spectra are not available, but it does remove the need, in quantitative work, for polarization scramblers in the collection optical train.

References

1. G. R. Trott and T. E. Furtak, Rev. Sci. Instruments, 51 1493 (1980)

2. K. Newby, Appl. Opt., 23, 1812 (1984)

3. J. C. Schaefer and I. Chabay, Opt. Letts., 4, 227 (1979)

4. R. L. McCreery, M. Fleichmann and P. J. Hendra, Anal. Chem., 55, 146 (1983)

5. S. D. Schwab and R. L. McCreery, Anal. Chem., 56,2199 (1984)

6. In preparation

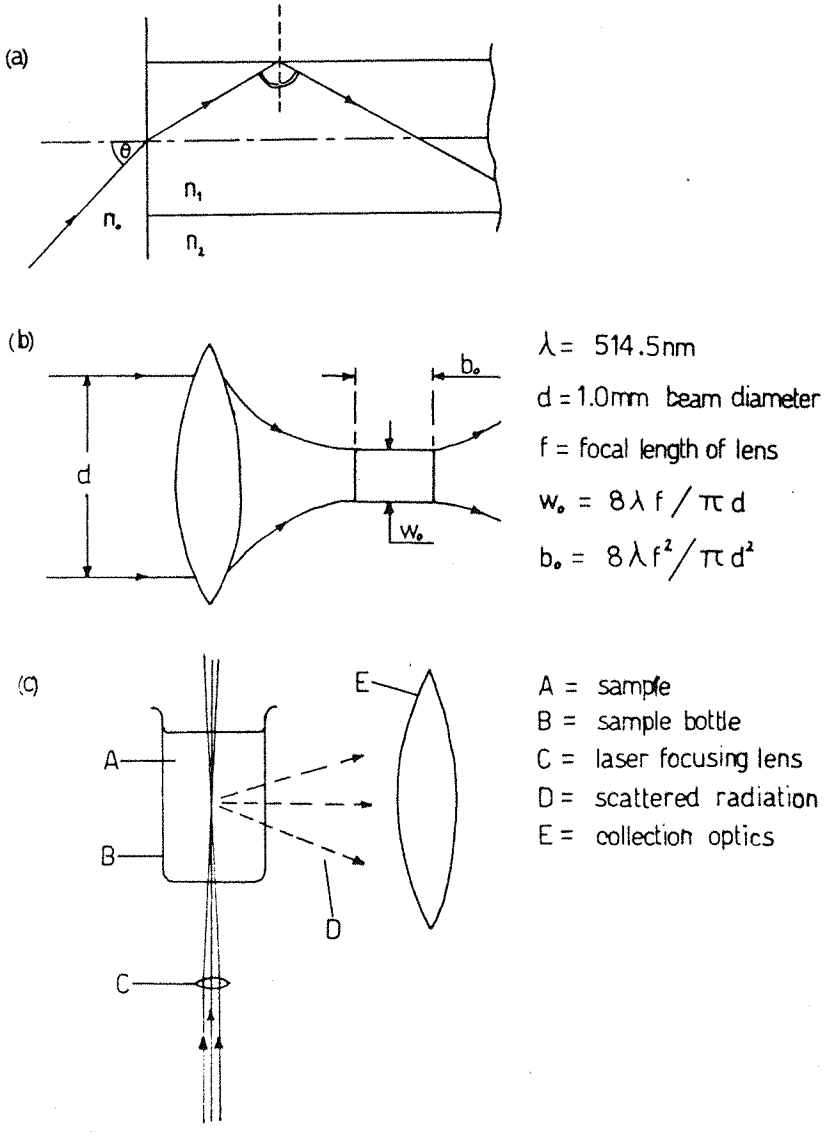

Figure 1 : (a) Transport of light within a single optical fibre; (b) diffraction limited spot size of a focused laser beam; (c) conventional lens excitation for Raman spectroscopy of liquid samples

Objective lens	Focal length f*(mm)	Lens half angle, θ_L, + assuming a collimated laser beam 1.0mm diameter = 514.5nm (degrees)	Calculated waist diameter W_o (μm)	b_o (μm)	Overall illumination efficiency (arbitrary units)
× 10	16.90	3.5	22	374	11
× 20	8.13	7.1	11	87	41
× 40	4.38	13.2	6	25	36
× 60	2.85	20.5	4	11	11

* supplied by Gallenkamp UK Ltd.

+ The fibre used had the following characteristics 200μ core
NA = 0.26
θ = 15°

NB If the laser beam had satisfied the characteristics in column 3 an objective of approximately 50x would have been ideal. Column 6 demonstrates that the beam characteristics used were poor.

TABLE 1

Overall illumination efficiency and lens characteristics of injection objective lenses

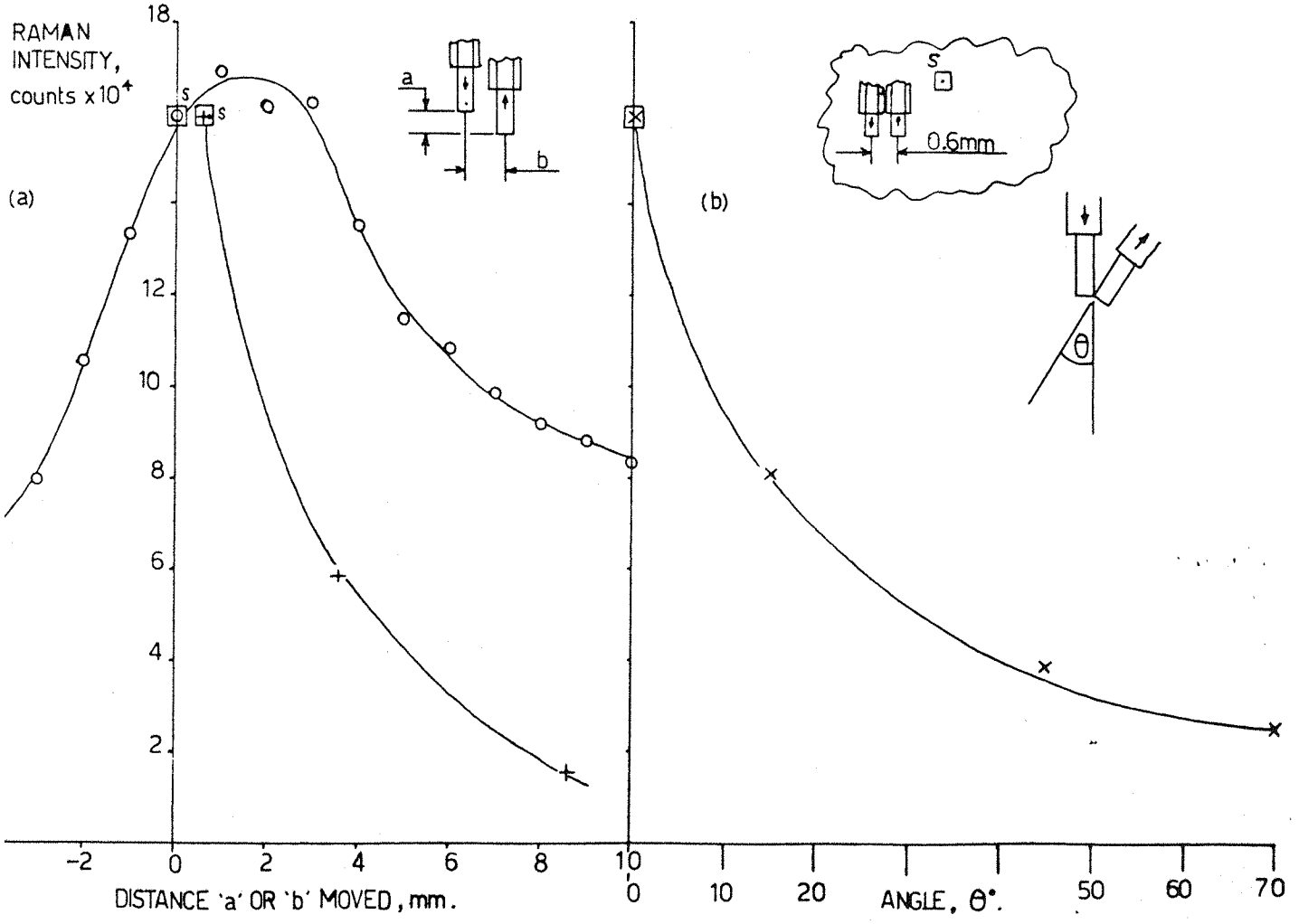

Figure 2 : Variation in Raman intensity of the $\Delta\nu = 1346 cm^{-1}$ band of nitrobenzene versus, (a) vertical and axial spacing of fibres; ○ = variation of 'a' (b = 0.6mm), + = variation of 'b' (a = 0) ; (b) angle of fibres; with respect to one another.

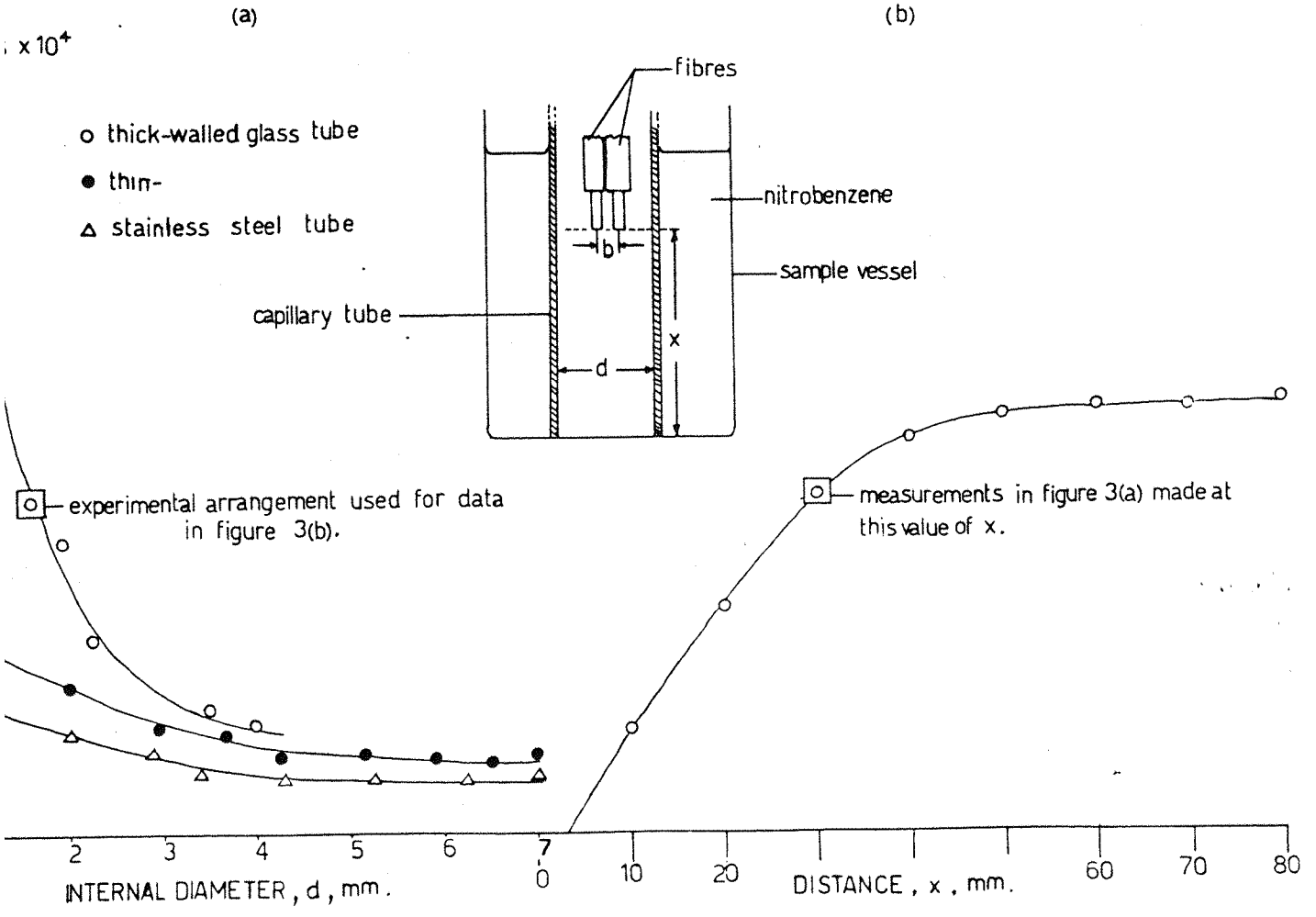

Figure 3 : Raman intensity of the $\Delta\nu = 1346 cm^{-1}$ band of nitrobenzene, recorded inside capillary tubing with parallel input and output fibres (b = 0.6mm).
(a) variation of internal diameter, d, of capillaries (x = 30mm),
(b) variation of sample depth, x, inside a capillary of internal diameter, d = 1.7mm.

Table II

Sample	Refractive Index	Relative Intensity	line/cm-1
Liquids			
Water	1.333Ø	3.5	34ØØ
Diethylether	1.3538	1.Ø*	1458
Acetone	1.362Ø	1.1*	8Ø4
Carbon tetrachloride	1.46Ø7	4.2	471
Glycerol	1.473Ø	1.3*	1469
Decalin	1.4758	2.6	1448
Turpentine	1.48ØØ	Ø.6*	1457
Xylene	1.4993	1.4*	1ØØ9
Toluene	1.4969	1.7	1Ø1Ø
Benzene	1.5Ø11	2.Ø	1ØØØ
Nitrobenzene	1.553Ø	2.4	1346
Milk		37.Ø**	34ØØ
Powders			
Potassium Oxalate		46	1452
Potassium Carbonate		34Ø	1Ø61
Polyethylene			
- Rigidex 5Ø		118	1296
- Rigidex ØØ6-6Ø		152	1296
Polytetrafluoroethylene		246	725
Bulk			
Polyethylene Rigidex ØØ6-6Ø			
- Extruded onto the probe		26**	1296
- Wrapped in foil		49**	1296
Potassium Chromate			
- crystals grown on fibres		82**	1562

* Weak signals; recorded on different settings and ratioed.
** Versus 45 degree measurement arrangement

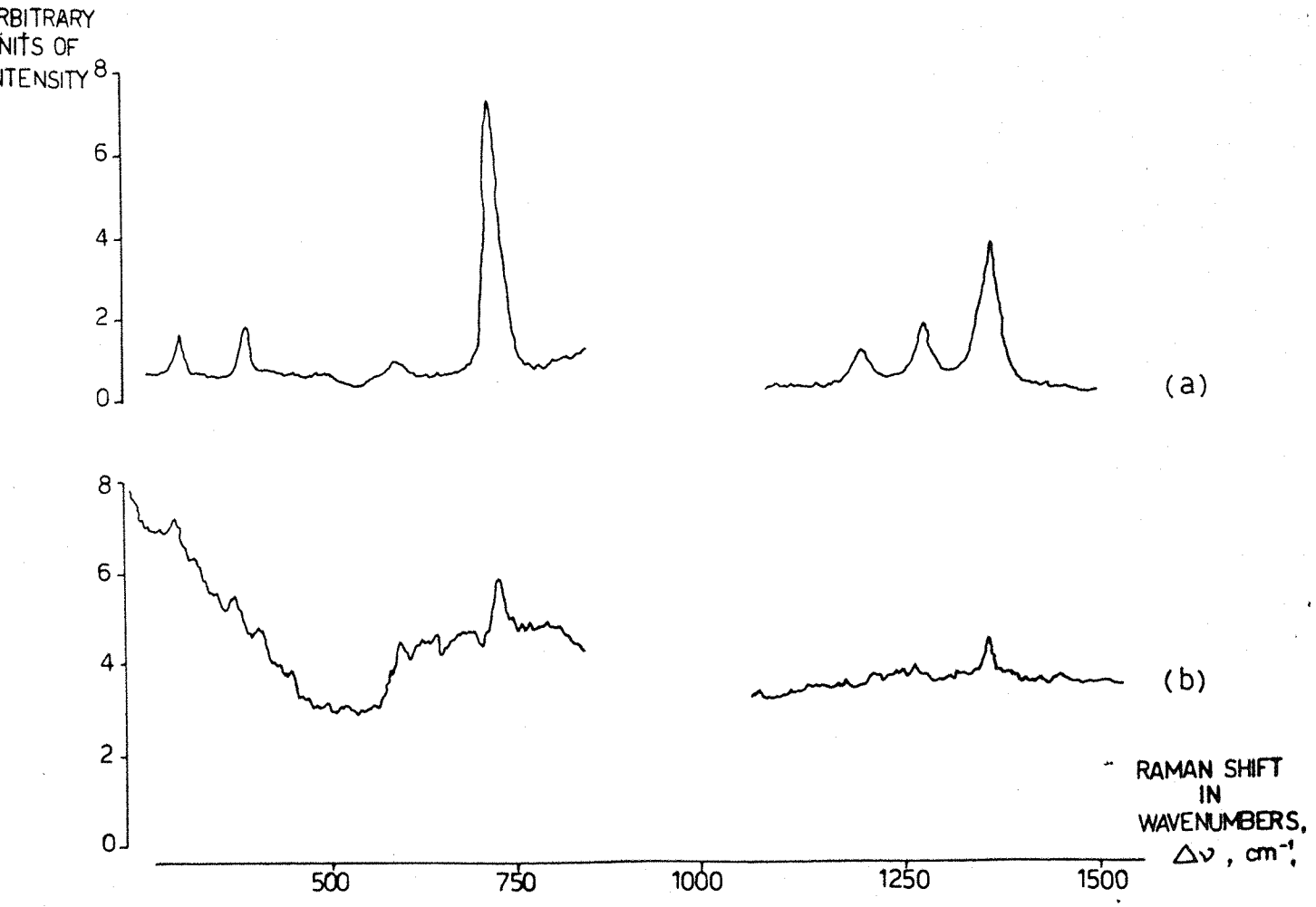

Figure 4 : Raman spectra of P.T.F.E. powder; (a) fibre optic method, (b) conventional method, recorded on the Applied Photophysics LR-36. Laser power available at sample = 100mW.

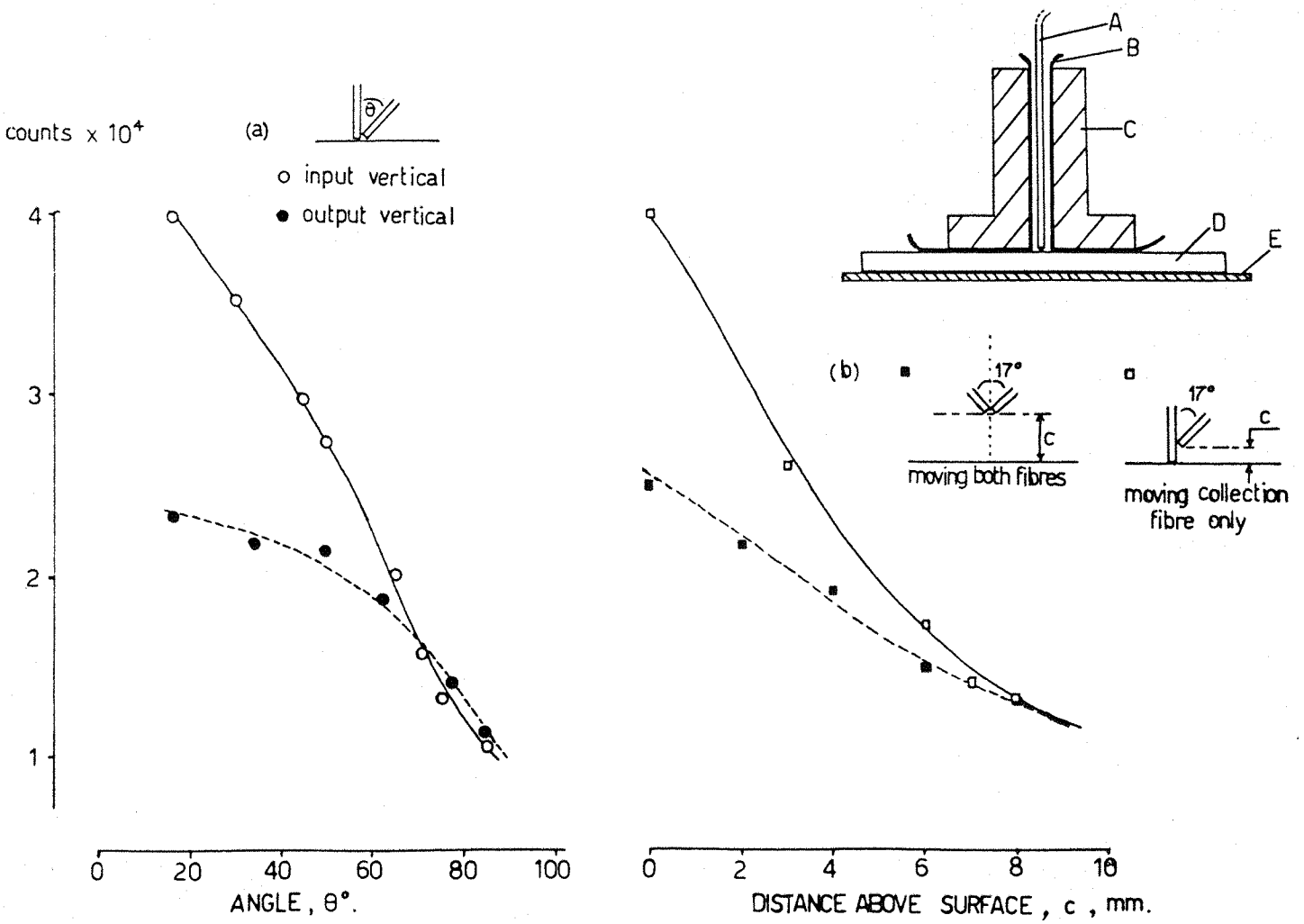

Figure 5 : Raman intensity of the $\Delta\nu = 1296 cm^{-1}$ band of polyethylene, recorded at the surface of the polymer (see inset) with (a) variation of angle between input and output fibres, and (b) variation of fibre height above the surface. A = fibre, B = aluminium foil, C = aluminium alloy blocks, D = polyethylene sheet, thickness 5mm, E = black surface.